SOVIET ATOMIC ENERGY

АТОМНАЯ ЭНЕРГИЯ

(ATOMNAYA ÉNERGIYA)

TRANSLATED FROM RUSSIAN

$\frac{c}{b}$ **CONSULTANTS BUREAU, NEW YORK**

SOVIET ATOMIC ENERGY

SOVIET ATOMIC ENERGY

CONTENTS

Engl./Russ.

CONTENTS

ARTICLES

MEASUREMENT OF RESONANCE ESCAPE PROBABILITY

L. N. Yurova, A. V. Bushuev,
and V. M. Duvanov   UDC 539.125.5.173.162.3:539.125.5.162.3

One of the most important problems in investigating the neutron cycle in a thermal reactor is the estimation of the resonance escape probability φ. In [1, 2] the value of $^{28}\varphi$ was obtained by combining some measured parameters with calculated quantities. The accuracy of the determination was low and did not satisfy an increasing number of requirements, and therefore people began to use the directly measurable parameters $^{28}\rho$, $^{28}\delta$, $^{25}\delta$, etc. instead of φ.

Now the development of experimental techniques has made it possible to determine φ rather accurately from experimental data.

Measurement Procedure. Starting from the balance equation, the probability of resonance absorption of neutrons in fuel can be written in the form

$$1-\varphi = \frac{^{28}N}{^{25}N}\frac{\langle^{28}\sigma_c\rangle}{\langle^{25}\sigma_f\rangle}\frac{\exp(\varkappa^2\bar{\tau})}{^{28}R_c^{25}v\left(1+\frac{^{28}v-1}{^{25}v}\,^{28}\delta\right)} + \frac{(1+^{25}\alpha\,\text{epi})\exp(\varkappa^2\bar{\tau})}{^{25}R_f^{25}v\left(1+\frac{^{28}v-1}{^{25}v}\,^{28}\delta\right)},\tag{1}$$

where $^{28}N/^{25}N$ is the ratio of the ^{238}U to ^{235}U concentrations in the fuel, $^{28}R_c$ and $^{28}R_f$ are the cadmium ratios for the $^{238}U(n,\gamma)$ and $^{235}U(n,f)$ reactions, $^{28}\delta$ is the ratio of ^{238}U and ^{235}U fission reactions rates in the fuel, $^{25}\alpha$ epi is the ratio of ^{235}U fission to absorption rates in the fuel for epicadmium neutron energies, ^{25}v and ^{28}v are the average numbers of neutrons per fission of ^{235}U and ^{238}U nuclei, $\langle^{28}\sigma_c\rangle/\langle^{25}\sigma_f\rangle$ is the ratio of the rates of neutron captures in ^{238}U and fissions in ^{235}U per nucleus, $\varkappa^2$ is the material buckling, $\bar{\tau}=\sum_i\tau_i\varphi_i/\sum_i\varphi_i$; τ_i is the age of neutrons with the i-th energy of the i-th resonance, φ_i is the resonance escape probability during slowing down to the i-th resonance.

It is obvious that the terms on the right-hand side of Eq. (1) represent the probability of resonance capture in ^{238}U and ^{235}U; i.e.,

$$1-^{28}\varphi = \frac{^{28}N}{^{25}N}\frac{\langle^{28}\sigma_c\rangle}{\langle^{25}\sigma_f\rangle}\frac{\exp(\varkappa^2\bar{\tau})}{^{28}R_c^{25}v\left(1+\frac{^{28}v-1}{^{25}v}\,^{28}\delta\right)};\tag{2}$$

$$1-^{25}\varphi = \frac{(1+^{25}\alpha\,\text{epi}\,(\exp\varkappa^2\bar{\tau})}{^{25}R_f^{25}v\left(1+\frac{^{28}v-1}{^{25}v}\,^{28}\delta\right)}.\tag{3}$$

TABLE 1. Errors in $\langle^{28}\sigma_c\rangle/\langle^{28}\sigma_f\rangle$, ^{28}R, and $^{28}\delta$ and Uncertainty of Nuclear Data

Parameter	Uncertainty, %	Reference
$^{28}N/^{25}N$*	0,1	[7]
$\langle^{28}\sigma_c\rangle/\langle^{25}\sigma_f\rangle$	1,5	[3]
$^{28}R_c$	1,5	[5]
$^{28}\delta$	2—3	[6]
^{25}v	0,3	[8]
^{28}v	0,7	[9]

*For natural uranium.

TABLE 2. $^{28}\varphi$ as a Function of Water Gap Thickness

Gap, mm	φ_i/φ_0	$\Delta(\varphi_i/\varphi_0)$	Gap, mm	φ_i/φ_0	$\Delta(\varphi_i/\varphi_0)$
0	1,000	—	4	1,037	0,007
2	1,030	0,006	6	1,055	0,007

TABLE 3. $^{23}\varphi$ as a Function of Lattice Pitch

V_C/V_U	φ_i/φ_0	$\Delta(\varphi_i/\varphi_0)$
38	1,000	—
76	1,092	$\pm 0,006$
152	1,142	$\pm 0,006$

TABLE 4. $^{28}I_{eff}$ as a Function of Water Gap Thickness

Gap, mm	$^{28}I_{eff}$, b (standard method [4])	$^{28}I_{eff}$, b [by Eq. (5)]	$^{28}I_{eff}$, b [by Eq. (5) taking account of anisotropy]
0	$10,6\pm0,3$	$10,57\pm0,24$	$10,57\pm0,24$
2	$10,6\pm0,3$	$10,55\pm0,23$	$10,17\pm0,23$
4	$10,3\pm0,4$	$11,36\pm0,33$	$10,52\pm0,33$
6	$10,4\pm0,4$	$11,35\pm0,32$	$10,17\pm0,32$

The accuracy with which $^{28}\varphi$ can be determined in the measurement of functionals by γ spectrometry can be estimated. As was shown in [3, 4] this method ensures high statistical accuracy with minimum systematic errors. $\langle^{28}\sigma_c\rangle/\langle^{25}\sigma_f\rangle$ and $^{28}R_c$ were measured with a Ge(Li) spectrometer and $^{28}\delta$ with a scintillation spectrometer. The ratio $\langle^{28}\sigma_c\rangle/\langle^{25}\sigma_f\rangle$ was determined by calibrating detectors in the thermal column, with the $^{238}U(n, \gamma)$ and $^{235}U(n, f)$ reaction rates being estimated by the intensities of the 278- and 293-keV radiations from ^{239}Np and ^{143}Ce, respectively. ^{28}R was measured by using a Cd cover. $^{28}\delta$ was determined by the method of two foils, recording the 1.6-MeV radiation from the fission product ^{140}La.

Table 1 shows the errors in determining these functionals and the uncertainty of the nuclear data used in Eq. (2). These indicate that the value $^{28}\varphi \approx 0.85$ may be in error by $\sim 0.5\%$.

Measurement and Results. $\langle^{28}\sigma_c\rangle/\langle^{25}\sigma_f\rangle$, $^{28}R_c$, and $^{28}\delta$ were measured in a uranium – graphite subcritical system [4] mounted on the converter of the horizontal neutron beam of the IRT-2000 reactor. The cell structure and the composition of the materials were described in [10]. The measurements were performed in systems with various graphite-to-uranium ratios (V_C/V_U = 38, 76, 152) and for various thicknesses of the water gap around the uranium slugs (0 = 6 mm). The V_C/V_U ratio was varied by changing the pitch of the lattice. Foils of natural uranium metal were used in measuring $\langle^{28}\sigma_c\rangle/\langle^{25}\sigma_f\rangle$ and $^{28}R_c$. $^{18}\delta$ was determined by using metal foils of natural uranium and uranium enriched 11 times in ^{235}U. The fuel channels of the experimental system contained separate slugs, which led to uncertainties in the axial distribution of the $^{238}U(n, \gamma)$ and the $^{235}U(n,f)$ reactions, and affected the average values of $\langle^{28}\sigma_c\rangle/\langle^{25}\sigma_f\rangle$ and $^{28}R_c$. Approximate corrections were determined experimentally and used in calculating the functionals.

$^{28}\delta$ was measured in a "dry" lattice with V_C/V_U =38, and its value was used in calculating φ for all the lattices considered. The assumption that $^{28}\delta$ is constant was based on the following facts:

1. The value of $^{28}\delta$ obtained in the lattice agrees, within the limits of experimental error, with the corresponding value for a single rod in a graphite moderator [6].

2. Surrounding a fuel slug by layers of various materials has little effect on $^{28}\delta$ [6].

3. It can be shown that the sensitivity coefficient of φ with respect to $^{28}\delta$ is small (< 0.02).

The functionals $\langle^{28}\sigma_c\rangle/\langle^{25}\sigma_f\rangle$, $^{28}R_c$, and the parameter $^{28}\delta$ averaged over the volume of a slug, and also the nuclear data ($^{25}\nu$ =2.418 ±0.008 [8], $^{28}\nu$ =2.82 ±0.2 [9]) were used to determine $^{28}\varphi$ by Eq. (2). The results obtained are shown in Tables 2 and 3. They were normalized to the value of $^{28}\varphi$ in a "dry" lattice with V_C/V_U = 38.

It was noted in some papers that the use of a Cd cover in the fuel leads to a certain overestimate of $^{28}R_f$. It was shown in [5] that the value of $^{28}R_c$ obtained by using a Cd cover, and by subtracting the epicadmium activation of ^{238}U using a 1/v detector agreed within the limits of experimental error ($\sim 2\%$). Evidently the magnitude of the effect of a Cd cover $(\Delta^{28}R_c/^{28}R_c)*$ in the measurements of $^{28}R_c$ in a lattice of the type investigated did not exceed 2%. It can be shown that it is related to the corresponding value of $(\Delta^{28}\varphi/^{28}\varphi)*$ by the expression

TABLE 5. $^{28}I_{eff}$ as a Function of V_C/V_U

V_C/V_U	$^{28}I_{eff}$, b (standard method)	$^{28}I_{eff}$, b [by Eq. (5)]
38	$10,6\pm0,3$	$10,57\pm0,24$
76	$11,9\pm0,4$	$11,18\pm0,34$
152	$13,9\pm0,5$	$13,66\pm0,41$

TABLE 6. $^{25}\varphi$ as a Function of Water Gap Thickness

Gap, mm	φ_i/φ_0	$\Delta(\varphi_i/\varphi_0)$	Gap, mm	φ_i/φ_0	$\Delta(\varphi_i/\varphi_0)$
0	1,000	—	4	1,006	0,002
2	1,006	0,002	6	1,008	0,002

$$\left(\frac{\Delta^{28}\varphi}{^{28}\varphi}\right)^* = \frac{1-^{28}\varphi}{^{28}\varphi}\left(\frac{\Delta^{28}R_c}{^{28}R_c}\right)^*. \tag{4}$$

Thus, $(\Delta^{28}\varphi/^{28}\varphi)^*$ is less than $(\Delta^{28}R/^{28}R)^*$ by a factor of four to five.

Determination of $^{28}I_{eff}$. The value of $^{28}I_{eff}$ was determined by using nuclear data from [8] in the following formula:

$$^{28}I_{eff} = -\frac{\sum_i \xi_i \sum_s^i V_i}{^{28}NV_U}\ln{^{28}\varphi}. \tag{5}$$

The slug structure of a fuel channel was taken into account in determining the volumes of water and uranium. The error in the determination was ~2.5%. Table 4 shows the relative values of $^{28}I_{eff}$ for various thicknesses of the water gap around the fuel slugs. A comparison of these data shows good agreement for water films up to 2 mm thick. For film thicknesses of 4 and 6 mm, however, the values obtained by Eq. (5) are 10% higher than those determined by the standard method. This difference is apparently related to the known effect of anisotropic scattering by hydrogen nuclei, which was not taken into account in (5). Anisotropic scattering leads to a decrease in the average number of collisions and in the average loss of energy in the water film; i.e., the water film around the fuel slugs moderates less effectively than a uniform distribution of water nuclei in the moderator. The agreement between the value of $^{28}I_{eff}$ obtained by the standard method and that calculated by Eq. (5) can be improved by introducing a correction for the effect of anisotropy.

Table 5 lists the values of $^{28}I_{eff}$ obtained by both methods in lattices with various values of V_C/V_U. They corroborate the dependence of $^{28}I_{eff}$ on V_C/V_U, which is explained by the deviation of the spectrum of epicadmium neutrons in uranium — graphite lattices from the Fermi distribution.

It should be noted that in measuring $^{28}I_{eff}$ in [4] the same cadmium covers were used as in the experiments on measuring $^{28}R_c$ to determine $^{28}\varphi$. It can be shown that the systematic error in $\Delta^{28}I_{eff}/^{28}I_{eff}$ due to the effect of the cadmium cover in determining $^{28}I_{eff}$ by the standard method is equal to $\Delta^{28}R_c/^{28}R_c$. In determining $^{28}I_{eff}$ in terms of $\ln{^{28}\varphi}$ the error in $(\Delta^{28}I_{eff}/^{28}I_{eff})^{**}$ is related to $(\Delta^{28}R_c/^{28}R_c)^*$ by the expression

$$\left(\frac{\Delta^{28}I_{eff}}{^{28}I_{eff}}\right)^{**} = \frac{1-^{28}\varphi}{^{28}\varphi\ln{^{28}\varphi}}\left(\frac{\Delta^{28}R_c}{^{28}R_c}\right)^* \simeq \left(\frac{\Delta^{28}R_c}{^{28}R_c}\right)^*. \tag{6}$$

Thus, the perturbation of the neutron distribution in the fuel by a cadmium cover has the same effect in both methods of measuring $^{28}I_{eff}$.

$^{25}\varphi$ was found from Eq. (3). The value of $^{25}\alpha$ epi, equal to 0.514 ± 0.016 [11], is weakly dependent on the type of system, particularly for slightly enriched or natural uranium, since it is determined mainly by the Fermi spectrum. $^{25}R_f$ was measured by the activation method using a cadmium cover by recording the 293 keV gamma radiation from the fission product ^{143}Ce in 90% enriched uranium foils diluted with aluminum. The results are shown in Table 6.

The authors thank V. I. Naumov for helpful comments during a discussion of the results.

LITERATURE CITED

1. M. B. Egiazarov et al., in: Proc. of Conf. Academy of Sciences of the USSR on the Peaceful Uses of Atomic Energy [in Russian], Atomizdat, Moscow (1955), p. 53.
2. Z. I. Gromova et al., At. Énerg., 2, No. 5, 411 (1957).
3. L. N. Yurova et al., At. Énerg., 32, No. 5, 412 (1972).
4. L. N. Yurova et al., At. Énerg., 38, No. 2, 95; No. 4, 245 (1975).
5. A. V. Bushuev and L. N. Yurova, At. Énerg., 27, No. 4 334 (1969).
6. C. Bigham, CRRF-1220 (1965).
7. V. I. Malyshev et al., in: Radioactive Elements in Rocks [in Russian], Pt. II, Novosibirsk (1972) p. 147.
8. Neutron Cross Sections, BNL-325 (1973).
9. M. Fleishman and H. Soodak, Nucl. Sci. and Engng., 7, 217 (1960).
10. T. V. Golashvili et al., At. Énerg., 13, No. 5, 435 (1962).
11. H. Eiland et al., Nucl. Sci. and Engng., 44, 188 (1971).

KINETICS OF ANNEALING OF RADIATION PORES IN 0Kh18N9T STAINLESS STEEL, IRRADIATED BY NEUTRONS

V. A. Pechenkin, Yu. V. Konobeev,
and V. I. Shcherbak

A study of radiation porosity in pure metals and alloys is of great scientific and practical interest in connection with the problem of creating economical fast-neutron breeder reactors with liquid metal coolant and thermonuclear reactors. In particular, a study of the behavior of assemblies of pores during annealing of the irradiated material will permit important data to be obtained about the nature of the pores, their stability, and also the efficiency of other void sinks in the material (dislocation loops, extended dislocations, grain boundaries, etc.) to be assessed under conditions of weak supersaturation of the material with voids.

At the present time, certain investigations are being undertaken, devoted to a study of the behavior of void pores in irradiated metals under annealing conditions [1, 2].

However, in these papers, the behavior of the distribution function of the cavities with respect to size as a function of the duration of annealing and the change of the dislocation structure in the material are insufficiently highlighted.
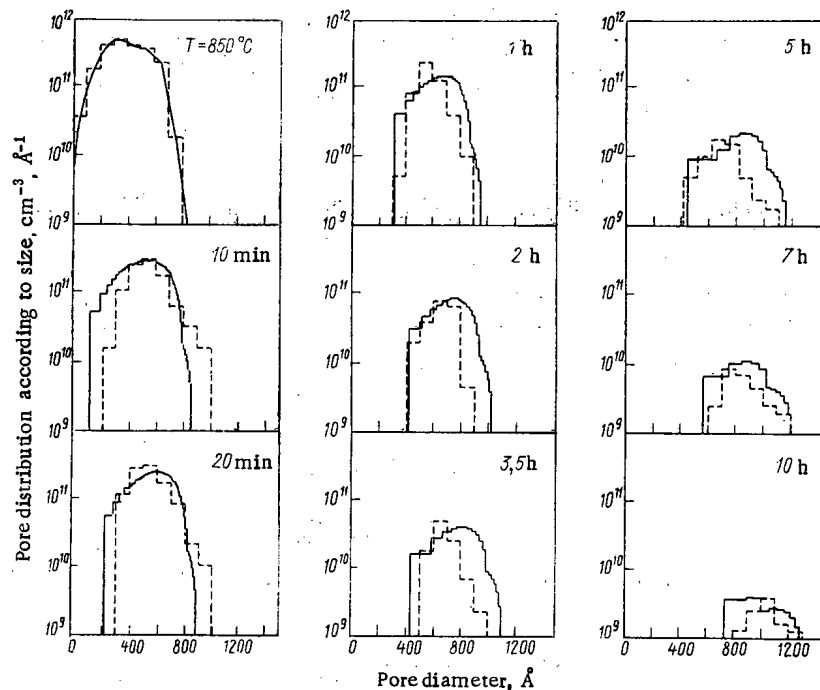
Fig. 1. Experimental (---) and theoretical (———) change of the pore distribution function according to size during annealing of 0Kh18N9T stainless steel, irradiated in Br-5 at 460°C with a flux of $4 \cdot 10^{22}$ neutrons/cm^2.
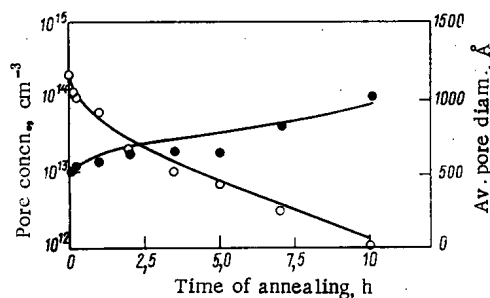
Fig. 2   Fig. 3

Fig. 2. Experimental (●, ○) and theoretical dependence of pore concentration (○) and average diameter (●) on the duration of annealing.
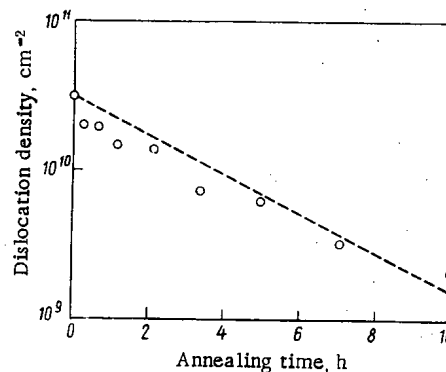
Fig. 3. Experimentally obtained (○) and used in the calculation (---) dependence of dislocation density on the duration of annealing.

In the present paper, the results are given of an experimental and theoretical study of the annealing of pores in 0Kh18N9T stainless steel, irradiated at 460°C in the BR-5 reactor with a neutron flux of $4 \cdot 10^{22}$ neutrons/cm^2 (E > 0.1 MeV).

Experimental Results. The structure of the irradiated samples was investigated by means of an electron microscope. Preparation of the samples for scanning and processing of the results was effected by a well-known procedure [3]. The dislocation density was determined by the method described in [4]. Annealing of the samples was carried out in vacuo (10^{-5} mm Hg) at a temperature of 850°C. The microstructure of the irradiated samples consisted of void pores, dislocation loops, and segments. The coarsest pores, as a rule, had an octahedral shape. In individual cases, the pores are associated with precipitations. The dislocation loops in the irradiated steel are Frank loops and, according to [5], are formed by interstitial atoms. The concentration of dislocation loops was found to be equal to $8 \cdot 10^{14}$ cm^{-3}, and their average diameter amounted to 300 Å. During annealing, the size of the loop decreased monotonically. The loops were anneled almost completely after 4 to 5 h (their concentration became less than 10^{12} cm^{-3}). The dislocation density in the irradiated steel prior to annealing according to estimate was equal to $3 \cdot 10^{10}$ cm^{-2}.

The distribution histograms of the pores according to size, calculated by the results of processing the electron-microscope photographs, for various annealing times, the concentration of pores N_V and their average diameter $\langle D \rangle$, the dislocation density N_d, and the swelling $\Delta V/V$ are plotted in Figs. 1-4. In addition to the electron-microscope investigation, the changes in linear dimensions of the samples as a result of annealing at 850°C during 0.5, 0.75, 1, and 2 h, were measured. On the assumption that the reduction of linear dimensions is due to annealing of the pores and that $\Delta l/l = {}^1/_3 \Delta V/V$, the results of the measurements of the linear dimensions are shown in Fig. 4.

Theoretical Analysis. A theoretical analysis of the kinetics of pore annealing has been carried out on the following assumptions: The pores have a void origin and possess a spherical shape; the pores and the dislocation network serve as a void sink in the material; the efficiency of the dislocations as void sinks is determined by the relation $L(t) = \varepsilon N_d$ (t), where ε is a constant factor, considered as a fitting parameter.

In [6], for the analysis of the growth kinetics of pores in irradiated metal, it was assumed that $\varepsilon = 1$, which follows from the normal diffusion approach. It will be shown later that for a theoretical description of the kinetics of pore annealing, it is necessary to assume that $\varepsilon \ll 1$.

The rate of change of diameter of a spherical pore D as a function of time has been described by the well-known equation

$$\frac{dD}{dt} = \frac{4D_c}{D} \left[\frac{C_v(t)}{C_{v0}} - \exp \frac{D_0}{D} \right],$$

(1)

where D_c is the coefficient of self-diffusion; $D_0 = 4\gamma\Omega/kT$; γ is the coefficient of surface tension; Ω is the volume per single atom of material; $C_v(t)$ is the steady-state concentration of voids at time t remote from the sinks; $C_{v0} = \exp(-E_v^f/kT)$ is the equilibrium concentration of voids in the material at the annealing temperature T. The quantity γ was calculated by the energy of formation of the voids E_v^f by means of the relation

797
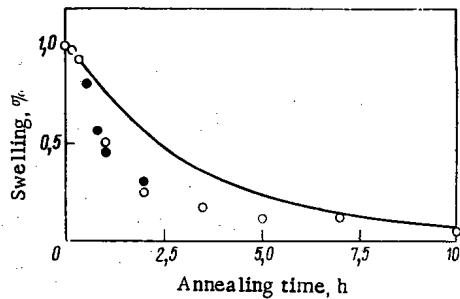
Fig. 4. Experimentally found and theoretical (——) dependence of swelling $\Delta V/V$ on the duration of annealing: O, ●) calculated by electron-microscope data and change of linear dimensions, respectively.

$$\gamma = \frac{E_v^f}{3\Omega}\left(\frac{3\Omega}{4\pi}\right)^{1/3}. \tag{2}$$

The supersaturation of the material by voids $C_v(t)/C_{v0}$, which occurs in Eq. (1), was determined from the steady-state equation of balance, describing the concurrency of the capture process of voids by pores, dislocations and thermal vaporization processes. For this, the equilibrium concentration of voids at dislocations was assumed to be equal to C_{v0}. The equation of balance has the form:

$$\frac{C_v(t)}{C_{v0}} = \frac{S_1(t) + L(t)}{S(t) + L(t)}, \tag{3}$$

where

$$S(t) = 2\pi \int_0^\infty D t(D, t)\,dD; \tag{4}$$

$$S_1(t) = 2\pi \int_0^\infty D f(D, t)\exp D_0/D\,dD, \tag{5}$$

where $f(D, t)\,dD$ is the concentration of cavities, the diameter of which at the instant t is contained in the interval from D to D + dD.

Method of Calculation. The behavior of the pore distribution function with respect to diameter during annealing was calculated on a computer by formulas (1)-(5) for various values of ε. For this, the experimental histogram of the pore distribution with respect to diameter in the irradiated sample before annealing was approximated by a broken curve (Fig. 1). The axis of the diameters was divided into equal intercepts of length 10 Å, for which a new and more detailed histogram was plotted by means of a broken curve. The variation with time of each of the initial diameters $D_j(0)$, isolated on the axis, was calculated by the method of finite differences by means of Eq. (1). At each time step (2-60 sec) the supersaturation $C_v(t)/C_{v0}$ was determined from expressions (3)-(5), and in Eqs. (4) and (5) the integrals were replaced with sums. As the number of pores included between the diameters $D_i(t)$ and $D_{i+1}(t)$ remains constant, then the histogram of the pore distribution with respect to diameter, at any instant t_i was calculated by the following formula:

$$f_i(t_j) = f_i(0)\frac{D_{i+1}(0) - D_i(0)}{D_{i+1}(t_j) - D_i(t_j)}, \tag{6}$$

where $D_i(0)$ is the pore diameter when t = 0; $f_i(0)$ is the initial histogram of the pore distribution (experimental). It was assumed for the calculation that a pore is annealed if its diameter $D_i(t_j) < 10$ Å. An estimate showed that the error carried by this approximation is quite small. The calculation was carried out for a metal, whose parameters were close to those of stainless steel.

The parameters of the metal used in the calculations are:

$$D_c = \exp(-E_v^c/kT), \text{cm}^2/\text{sec}; E_v^c = 2.95 \text{ eV};$$
$$E_v^f = E_v^c/2; \quad 1/\Omega = 10^{23} \text{ cm}^{-3}; \quad a = 2.87 \text{ Å}.$$
$$b = 1.65 \text{ Å}; \quad \nu = 0.28; \quad d = \sqrt{3}a/2\sqrt{2};$$
$$\mu = 5 \cdot 10^{11} \text{ dyne/cm}^2.$$

Results of the Calculation. The calculations for various values of $L = 10^7$-10^{10} cm^{-2}, carried out on the assumption of a constant dislocation density during the whole time of annealing, showed that for small values of L, contrary to experiment, the pore concentration N_v at the end of annealing (10 h) exceeds the experimental value by an order of magnitude. At large values of L, the pores are annealed so much more rapidly. In order to explain the behavior of the assembly of pores during annealing, it is necessary to take into account

the actual course of the dependence of the dislocation density on the time, $L(t) = \varepsilon N_d(t)$ (see Fig. 3). However, it was found that when $\varepsilon = 1$, the pores are annealed completely after 50 min. Satisfactory agreement with experiment can be achieved only by choosing $\varepsilon = 1.4 \cdot 10^{-2}$. The histograms of the pore distribution with respect to dimensions, calculated for this value of ε, their concentration, average diameter, and swelling are shown in Figs. 1, 2, and 4.

Thus, under annealing conditions, the efficiency of the dislocations as void sinks is found to be less by two orders of magnitude than the efficiency obtained on the assumption that a dislocation is an ideal sink. This coincides with the conclusion of [7], made by an analysis of the rate of climb of the dislocations in a material supersaturated by voids.

Efficiency of Dislocations as Void Sinks. The quantity ε can be estimated by an experimental function of the pore distribution with respect to dimensions. Actually, according to the parameters given above, $D_0 \simeq 30 \overset{\circ}{A}$. Taking into account that in the material investigated, the pore diameters are much larger than D_0, we find the value of the critical pore diameter from Eq. (1), by expanding $\exp D_0/D$ in series with respect to D_0/D. Assuming that the right-hand side is equal to zero, we obtain

$$D_{cr} = \langle D \rangle + \frac{L}{2\pi N_v},\qquad (7)$$

where $\langle D \rangle$ is the average diameter of the pores at time t.

When $L = 0$, D_{cr} should be equal to $\langle D \rangle$ and the asymptotic behavior of the assembly of pores should be described by the theory of coalescence of the pores in an infinite crystal, in which only the pores serve as internal void sinks [8]. Subsititution of the experimental values for $\langle D \rangle$, $L = \varepsilon N_d$ and N_v in Eq. (7), shows that when $\varepsilon = 1$, the critical pore diameter is always greater than the maximum diameter D_{max} and, consequently, the pores should be annealed after a short time, in contrast with experiment. Therefore, in order to describe the observed evolution of the pore distribution with respect to dimensions, it is necessary to assume that $L \ll N_d$ and this means $\varepsilon \ll 1$. For $t \geq 5$ h, $D_{cr} < d_{max}$, and $L/\langle D \rangle \, 2\pi N_v < (0.2\text{-}0.3)$. We find that at this stage of annealing $\varepsilon < 0.02$. However, the quantity ε should not be much less than 0.02, as in this case, according to [8], the concentration of cavities should be reduced according to the law $N_v \sim 1/t$, whereas in the experiment N_v decreases much more rapidly. An estimate of ε can be obtained also from data on the change of swelling with the annealing time. In this case, the equation has the form

$$\frac{d}{dt}\frac{\Delta V}{V} = -D_v L (C_v - C_{v0}) = -D_c D_0 2\pi N_v \frac{L}{L+S}.\qquad (8)$$

The quantity ε can be found by graphical differentiation of the experimental relation $(\Delta V/V)(t)$. In this case, ε is found to be a function of time and in the initial stage of annealing, $\varepsilon \sim 0.1$.

The constant quantity $\varepsilon = 0.014$ was chosen for the calculations, because it led to values of N_v and $\Delta V/V$ which are close to the experimentally obtained values when $t = 10$ h (Figs. 2 and 4).

In considering ε, we note that if we assume a dislocation to be an ideal diffusion sink for voids, i.e., if we enclose its capture surface in the form of a cylinder with radius equal approximately to the radius of the core of the dislocation r_0, then the diffusion flow of voids to the dislocation of length N_d, according to [7], will be equal to

$$J_v = \frac{2\pi D_v N_d}{\ln \frac{R(t)}{r_0}} (C_v - C_{v0}),\qquad (9)$$

where D_v is the coefficient of diffusion of voids in the material, $r_0 \sim b$; b is the Burgers vector; $R(t)$ is half of the average distance between dislocations. Estimates for the experimentally observed values of $R(t)$ show that $2\pi/(\ln R(t)/r_0) \sim 1$, i.e., $\varepsilon = 1$.

The low efficiency of void capture by an extended dislocation can be explained if we assume [7] that such capture occurs only at steps of the dislocation and not over its entire length. The diffusion flow of voids to a dislocation of length N_d, in the case of small saturations of the metal by voids (the cases occurring in the problem being considered) [7] is

$$J_v = 4\pi r C_j D_v [C_v - C_{v0}] N_d,\qquad (10)$$

where r is the effective radius of capture of a void by the step; C_j is the linear concentration of steps along the linear dislocation; $C_j = b^{-1} \exp(-W_j/kT)$ is the equilibrium concentration of steps in the dislocation; W_j is the energy of activation of the thermal formation process of a step.

799

Assuming that $r \approx b$, we find from formula (10)

$$\varepsilon = 4\pi \exp\left(-W_j/kT\right). \tag{11}$$

Thus, the efficiency of a dislocation as a void sink can be low if the energy of formation of the step W_j is sufficiently high. In order to estimate W_j, we use the theory of elasticity [10] and we obtain

$$W_j = \frac{\mu b^2 a_1}{4\pi(1-\nu)},$$

where μ is the shear modulus, $a_1 = \Omega/bd$; d is the distance between slip planes and ν is Poisson's coefficient.

Substituting the value of the parameters (see p. 798) we find $W_j = 0.4$ eV and $\varepsilon = 0.1$, which is greater by an order of magnitude than is necessary for coincidence between the experimental and calculated data. It is possible, however, that the theory of elasticity gives an underestimate of W_j. An increase of W_j by a factor of one-and-one-half to two would gaurantee coincidence with experiment.

The somewhat higher efficiency of dislocations as void sinks in the first stages of annealing can be explained by the effect of dislocation loops of interstitial atoms. Despite the total length of the dislocation loops before the start of annealing being less than the length of extended dislocations and when $T = 850°C$ almost all the loops are annealed after 5 h, the diffusion flow of voids to the loops can be compared with the flow of voids to the extended dislocations (or even exceeds it), as, because of the curvature of the dislocation line, the linear concentration of steps in the loop may be found to be considerably higher.

The flow of voids to a loop of radius R_l can be represented in the form

$$J_l = \left(\frac{dR_l}{dt}\right) 2\pi R_l b/\Omega.$$

We shall suppose that the loops are ideal diffusion sinks. Then, for a loop without a packing defect, the rate of change with time of its radius [11] is

$$\frac{dR_l}{dt} = \frac{A}{a} D_c \left[\exp\left(-\frac{\tau\Omega}{R_l bkT}\right) - \frac{C_v}{C_{v0}}\right], \tag{12}$$

where $A = 4\sqrt{3}/\pi$ [12]; τ is the linear energy of the dislocated loop equal to [10]

$$\tau = \frac{\mu b^2}{4\pi(1-\nu)} \ln \frac{4R_l}{\nu}, \tag{13}$$

where $\rho \sim b/8$.

Since large loops (in particular, of ideal hexagonal shape) under conditions of small supersaturation of the material by voids cannot be ideal diffusion sinks, then, in the general case we can introduce for a loop the void capture efficiency parameter $\varepsilon_l(R_l)$, by analogy with that for an extended dislocation. Then the void flow to a loop of diameter d_l is

$$J_l = \varepsilon_l \frac{4D_c d_l}{\Omega} \left[\exp\left(-\frac{l_0}{dl}\right) - \frac{C_v}{C_{v0}}\right], \tag{14}$$

where l_0 is a parameter, weakly dependent on d_l, varying from 60 Å for $d_l = 10-110$ Å and $d_l = 600$ Å.

It can be seen from a comparison of formulas (1) and (14) that simultaneous coalescence of pores and a loop of interstitial atoms is impossible, as under supersaturation conditions of a metal by voids, the rate of change of d_l with time is negative for all values of d_l. This conclusion agrees with the fact that in the experiment carried out the loops were annealed after $t \leq 5$ h. In order to estimate the effect of a loop on annealing of the pores, we consider the loops as sinks in the equation of balance, by expanding $\exp(-l_0/d_l)$ in series with respect to l_0/d_l in Eq. (14). As a result, we obtain a new expression for the critical pore diameter:

$$D_{cr} = \frac{\langle D \rangle + \langle \varepsilon_l d_l \rangle \frac{2N_l}{\pi N_v} + \varepsilon \frac{N_d}{2\pi N_v}}{1 - \frac{\langle \varepsilon_l l_0 \rangle}{D_0} \frac{2N_l}{\pi N_v}}, \tag{15}$$

where N_l is the concentration of loops at the instant t; $\langle \varepsilon_l d_l \rangle$ is the average value of the product, found by means of the loop distribution function with respect to dimensions. It follows from Eq. (15) that in the initial stages of annealing, when annealing of the loops takes place in the sample, the critical diameter of the pores may be somewhat greater than that found from Eq. (7), which leads to a larger value of ε in this equation.

However, for a more precise estimate of this effect, it is necessary to know the behavior of the distribution function of the loops with respect to dimensions and the dependence $\varepsilon_l(d_l)$.

Thus, in order to achieve coincidence between the calculated and observed processes of annealing of the assembly of pores in the material it is necessary to take account of: the lower efficiency in comparison with the usually assumed efficiency of extended dislocations as void sinks; and the change of efficiency of the dislocations during annealing, which can generate dislocation loops of interstitial atoms.

Role of the Gas. The calculations carried out and their comparison with the results of observations, permit the conclusion to be drawn that the helium formed during irradiation as a result of (n, α)-nuclear reactions, has a very slight effect on the behavior of the pores during annealing. It is shown [13] that the concentration of helium atoms in stainless steel 304, which is similar in composition to 0Kh18N9T steel, after irradiation under similar conditions can reach 10^{-3} at. %. This concentration is insufficient for the pores to be considered as gas bubbles in the first stages of annealing (when the internal pressure of the gas in a pore is balanced by the surface tensions).

We shall suppose that during irradiation, the gas simply has been stored in the matrix and its concentration has reached a value of 10^{-3} at. %. Assuming for the estimate that the energy of activation of helium diffusion in steel is equal to 2.6 eV, it can be shown that after annealing during about 15 min all the helium can be entrained by the pores. If the gas existing in the pores is not dissolved in the steel, then after prolonged annealing, equilibrium, thermally stable gas bubbles with a diameter of less than 200 Å are generated, which is not observed in the experiment. On the other hand, if the helium found in the pores is readily soluble in the metal and can be redistributed between the pores, subjected to the same equilibrium between the gas pressure in the pore and the surface tension, then coalescence of the gas pores should take place according to the law found in [14]. In this case, during coalescence of the gas pores, swelling increases according to the law $\Delta V/V \sim t^\alpha$, where $\alpha = 1/2$ (monatomic gas) or $\alpha = 2/3$ (diatomic gas), which is contrary to the data obtained.

Thus, the gas formed as a result of irradiation is not stored in the pores and later diffuses to the boundaries of grains with dislocations or is captured by impurity atoms. The question of the weak capture of gas by pores located at a distance from the grain boundaries will require a separate analysis.

CONCLUSIONS

The pores, formed in austenitic 0Kh18N9T stainless steel irradiated at 460°C with a neutron fluence of $4 \cdot 10^{22}$ neutrons/cm^2, are of a void nature and are not filled with gas as a result of 10 h annealing at 850°C.

The proposed model for describing the annealing of the pores coincides satisfactorily with experiment, if it is assumed that the efficiency of dislocations as void sinks is less by two orders of magnitude than the total length of the dislocations. This low efficiency of the dislocations can be explained by the capture of voids only at steps of the dislocations.

For a detailed description of the behavior of an assembly of void pores under annealing conditions, detailed data are necessary about the behavior of assembly of dislocation loops of interstitial atoms and dislocation networks.

The authors tender sincere thanks to V. N. Bykov for useful discussion topics.

LITERATURE CITED

1. C. Cawthorne et al., in: Proc. Reading Conf. on Voids Formed by Irradiation of Reactor Materials, BNES, Mar. 22-25 (1971), p. 35.
2. A. Jostsons et al., in: Proc. AEC Symp. "Radiation Induced Voids in Metals," New York, June 9-11 (1971) (CONF 710601), p. 363.
3. V. N. Bykov et al., At. Énerg., 35, No. 4, 235 (1973).
4. R. Ham, Philos. Mag., 6, 1183 (1961).
5. H. Brager et al., Metal. Trans., 2, 1893 (1971).
6. S. Harkness and Che-Yu-Li, Metal. Trans., 2, 1457 (1971).
7. R. Balluffi, Phys. State Solid., 31, 443 (1969).
8. I. M. Lifshits and V. V. Slezov, Zh. Éksp. Teor. Fiz., 35, 479 (1958).
9. F. Ham, J. Appl. Phys., 30, 915 (1959).
10. J. Hirth and J. Lothe, Theory of Dislocations, McGraw-Hill, New York (1968).
11. B. Eyre and D. Maher, AERE-R-6618 (1970).

12. D. Seidman and R. Balluffi, Philos. Mag., 13, 649 (1966).
13. D. Norris, Radiation Effects, 15, 1 (1972).
14. A. Markworth, Metal. Trans., 4, 2651 (1973).

EFFECT OF THE INTERACTION OF 0Kh18N9T STEEL WITH
THE COOLANT ON THE DEVELOPMENT OF POROSITY
IN THE FUEL CLUSTER SHEATH OF THE BR-5 REACTOR

V. I. Shcherbak, V. N. Bykov,
V. D. Dmitriev, S. I. Porollo,
and A. Ya. Ladygin

UDC 621.039.531

During metallographic investigations of the regular fuel clusters of the carbide zone of the BR-5 reactor, diffusion interaction was observed between the steel and the coolant, both frontally and along the grain boundaries [1]. The depth of the interaction layer depended mainly on the irradiation temperature and the residence time of the 0Kh16N15M3B and 0Kh18N9T steel in the sodium, as it is supposed that the interaction with the sodium is caused by carburization of the steel under the BR-5 reactor conditions. The change of the chemical and phase composition of the steel as a result of interaction with the sodium, obviously, must have a significant effect on the process of development of void porosity, which is very important for estimating the efficiency of the individual units of the active zone of fast reactors.

In this present paper, some results are given of an investigation of the interaction with the coolant of 0Kh18N9T steel, which is used for the manufacture of the hexahedral sheaths of the fuel clusters of BR-5 reactors, and the effect of this interaction on the swelling of the steel.

Irradiation Conditions and Investigational Procedure. For the investigation, a hexahedral sheath of a regular G-19 fuel cluster was chosen. The wall thickness of 0.3 mm remained at the center of the carbide zone of the BR-5 reactor from 1965 to 1971 and was irradiated with a neutron flux of $3.8 \cdot 10^{22}$ neutrons/cm^2 at a temperature of 430-510°C. The coolant was sodium with 0.01-0.005 wt. % O, 0.003 wt. % N, and 0.017 wt. % C [1] and was circulated through the fuel cluster from below upwards with a speed of 4 m/sec, while in the intercluster gap the flow rate of the sodium was considerably less.

Six sections of the hexahedral sheath at different heights were investigated. The temperature and the neutron flux, calculated for each section, are shown in Table 1. In addition, three further sections around

TABLE 1. Characteristics of Samples Investigated

Section No.	Distance from bottom of active zone, mm	Irradiation temperature, °C	Neutron flux, 10^{22} neutrons/cm^2	$\Delta V/V$, %
1	0	430	1,7	0,1
2	70	440	3,0	0,5
3	190	460	3,8	0,9
4	310	480	3,2	0,3
5	344	485	2,9	0,1
6	500	510	1,4	—

*The temperature of the samples investigated was assumed to be equal to the coolant temperature at the given section during the nominal operating cycle of the BR-5 reactor [1].

802
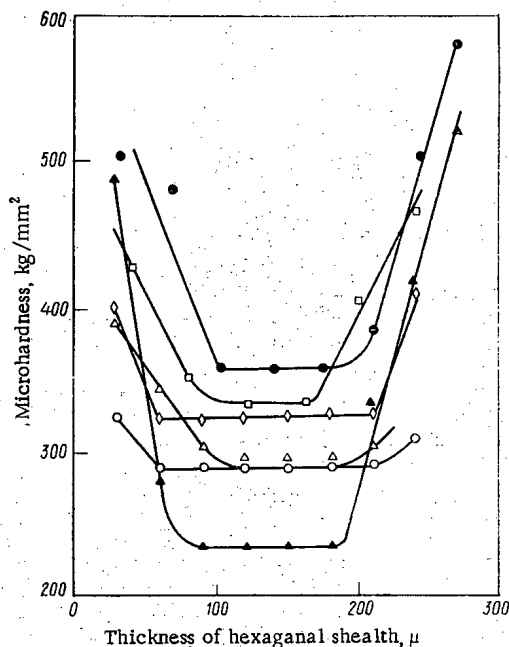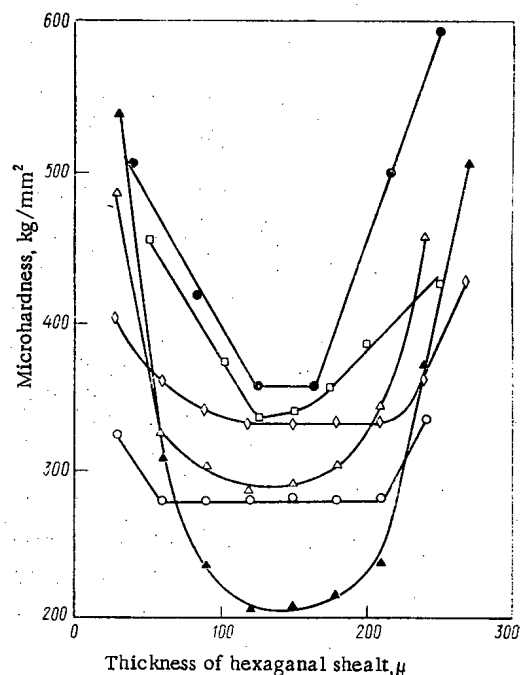
Fig. 1

Fig. 2

Fig. 1. Change of microhardness relative to the wall thickness of the hexahedral sheath at the corner of the hexahedron. The thickness is read from the outer face of the wall of the sheath. Section number (see Table 1): O) 1; ◇) 2; ●) 3; □) 4; ▲) 5; △) 6.

Fig. 2. Change of microhardness relative to the wall thickness of the hexahedral sheath for a section located at a distance of 1/4 of the width of the face from the corner (symbols the same as in Fig. 1).

the perimeter of the hexahedral sheath were investigated: at a corner of the hexahedron and at distances of 1/4 and 1/2 of the width of the face from the apex of the corner. The microhardness over these sections was measured on a PMT-3 microhardness meter.

For the electron microscopic investigation of the steel, the single-jet polishing procedure, which is usually used, was used for thinning the samples [2]. The thickness of the layer removed from the sample was measured by means of a type MVM micrometer with an accuracy of up to 10μ. The details of the preparation of the samples and the processing of the electron microscope photographs have been described previously [3, 4].

Results of the Experiment. During the metallographic investigation of the samples, cut from different sections, it was discovered that from the inner and outer sides the material of the hexahedron had been subjected to a diffusion action of the sodium. Judging by the change of microhardness, the width of the zones of interaction increases with increase of the irradiation temperature (Figs. 1 and 2), and at the corners of the hexahedron the width of the zones of interaction is somewhat less, and their microhardness is greater, than in the other sections distant from the corner at 1/2 and 1/4 of the width of the face.

According to Figs. 1 and 2 and the data of Table 1, the microhardness of the various sections with respect to height of the central part of the sheath wall, correlates well with the change of neutron flux and temperature of irradiation. The increased microhardness of the steel in section 6, obviously, is due to the interaction with sodium in the entire thickness of the sheath wall.

In the electron microscopic investigations, in that part of the sheath which was not subjected to interaction with the coolant, a microstructure was observed which is characteristic for 0Kh18N9T steel irradiated with a high neutron flux [3, 4]. The data from the total pore volume in the samples cut out from sections at different heights and at 1/4 of the face width from the corner, are shown in Table 1.

The investigations of the distribution of radiation porosity over the wall cross section of the hexahedral sheath of the fuel cluster being studied showed that the zones of interaction undergo considerably less swelling
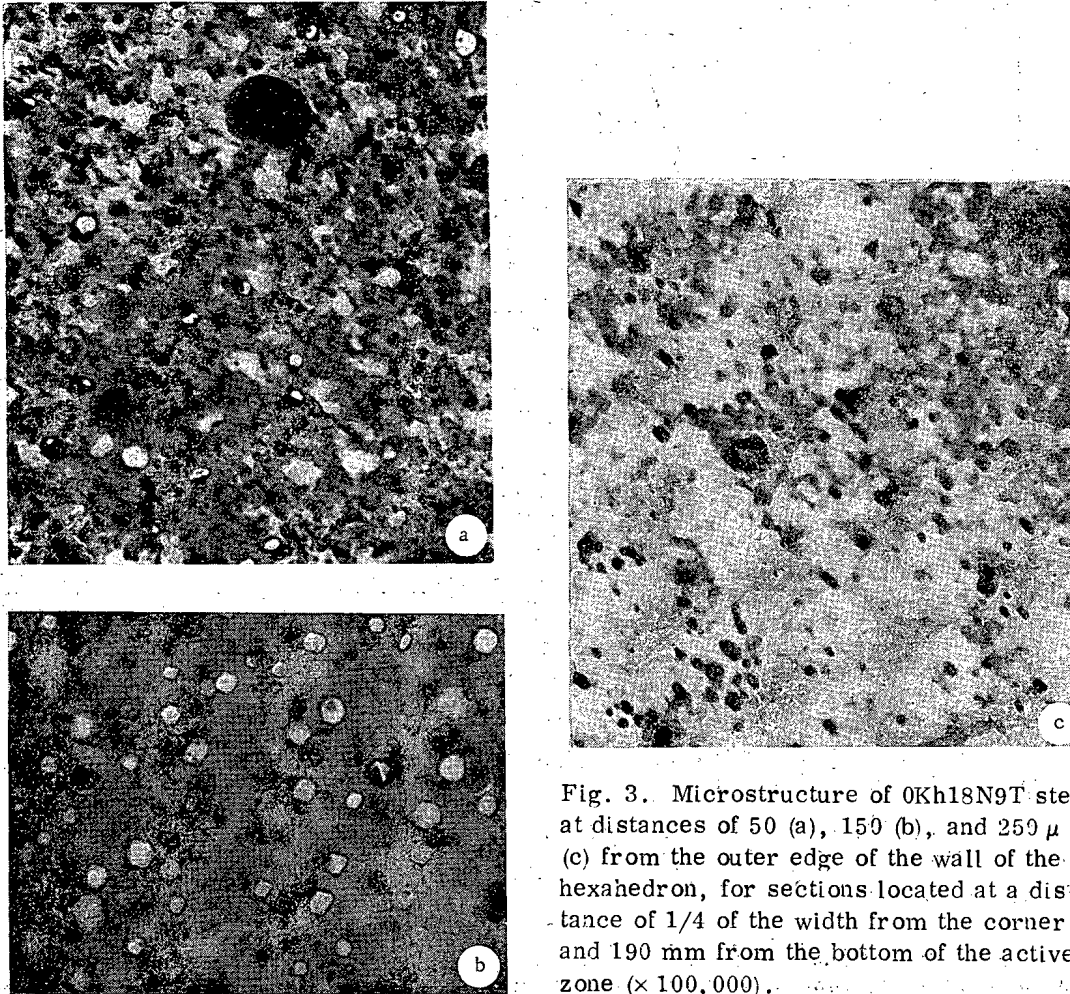
Fig. 3. Microstructure of 0Kh18N9T steel at distances of 50 (a), 150 (b), and 250 μ (c) from the outer edge of the wall of the hexahedron, for sections located at a distance of 1/4 of the width from the corner and 190 mm from the bottom of the active zone ($\times$ 100,000).

in comparison with the central section. The change of microstructure of 0Kh18N9T steel over the wall cross section of the hexahedron is shown in Fig. 3, whence it follows that the diffusion action of the coolant of the steel leads to an increased content of finely dispersed segregations in the body of the grains.

DISCUSSION

The experimental results confirm the intense interaction of the material of the hexahedral sheaths of regular fuel clusters with the coolant in the BR-5 reactor. The impurities contained in the sodium, including 0.017 wt. % C and 0.003 wt. % N, could cause carburization and nitriding of the steel [1, 5], but the action of other mechanisms cannot be excluded, in particular the penetration of sodium into the depths of the steel [6].

It follows from the data obtained that carburization suppresses the development of void porosity in the interaction zones, which promotes a nonuniform swelling of the hexahedral sheaths of regular fuel clusters not only over the height, but also over the wall thickness. As the swelling of the sheath is caused chiefly by the development of porosity in the carburized parts, the overall changes of volume of the material of the hexahedron should be less than those found by calculation, based on electron-microscopic investigations of these parts.

As already mentioned, carburization of 0Kh18N9T steel promotes an increase of the concentration of segregations in the body of the grains. These segregations might act as neutral sinks for point defects or they might retard the growth of dislocation loops, thereby reducing their capability to capture interstitial atoms, or to prevent radiation annealing of the dislocation network. These phenomena, in the final count, must lead to a reduction of the steady concentration of point defects and, consequently, to the suppression of the process of generation and growth of pores. Other explanations are possible, based in particular on the change of diffusion coefficients, surface energy, and the appearance of local stresses, as all these factors can exert a significant influence on the formation of pores.

804

LITERATURE CITED

1. A. Ya. Ladygin et al., 4th Geneva Conference, Report No. 707 [in Russian] (1974).
2. D. Norris, Rad. Effects, 14, 1 (1972).
3. V. N. Bykov et al., At. Énerg., 34, No. 4, 247 (1973).
4. V. N. Bykov et al., At. Énerg., 36, No. 1, 24 (1974).
5. B. A. Nevzorov, Corrosion of Structural Materials in Sodium [in Russian], Atomizdat, Moscow (1968).
6. K. Claxton and J. Collier, J. Brit. Nucl. Energy Soc., 12, 63 (1973).

THE p — T DIAGRAM OF THE URANIUM — CARBON SYSTEM

Yu. V. Levinskii   UDC 669.822

A detailed analysis of the phase equilibrium in the uranium — carbon system was given by Storms [1], and the most probable phase diagram of this system, consisting of a projection of the lines of maximum solubility on the temperature — composition plane, was given by Benz et al. [2].

More detailed information on equilibrium in this system is given by the p — T — x diagram or by a projection of the line of monovariant equilibrium of this system on the temperature — pressure plane (the p — T diagram). The indeterminacy in the values of the overall equilibrium pressure above most phases in the uranium — carbon system means that we can give a scheme of the p — T diagram only between 1000 and 2600°C and between 0 and 10^{-16} atm. However, even such a scheme can be very useful in constructing isobaric and isothermal cross sections of the phase diagram.

In the scheme of the p — T diagram (Fig. 1), curves 8-9 and 9-22 characterize the pressure of the vapor above solid and liquid uranium, and curves 9-24 the melting of uranium. At point 7 there are four phases in equilibrium: γ-U, UC, liquid, and gas. Through this point pass curves 7-23, 7-9, 7-6, and 7-19 of the three-phase equilibria γ-U $\rightleftharpoons$ UC $\rightleftharpoons$ l, γ-U $\rightleftharpoons$ l $\rightleftharpoons$ g, γ-U $\rightleftharpoons$ UC $\rightleftharpoons$ g, and UC $\rightleftharpoons$ l $\rightleftharpoons$ g. Curve 7-23 is vertical (T = 1117°C);
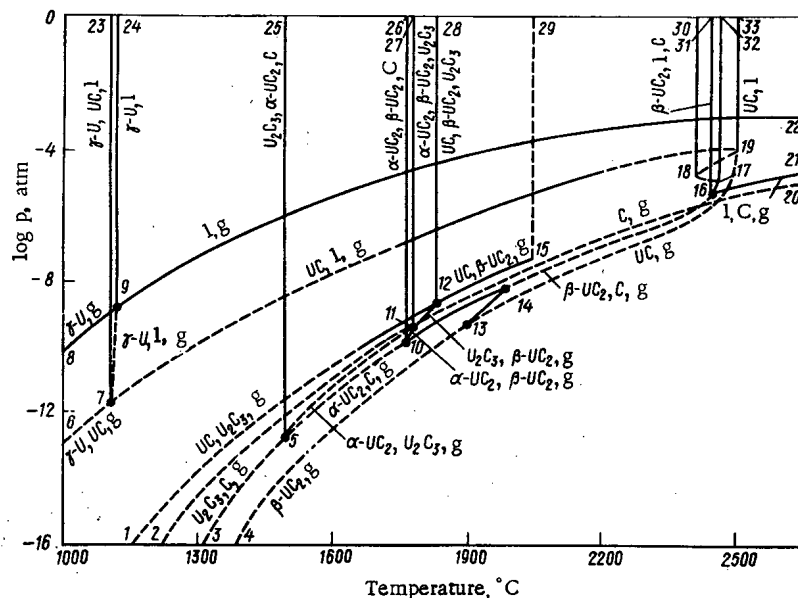
Fig. 1. p — T diagram of uranium — carbon system.
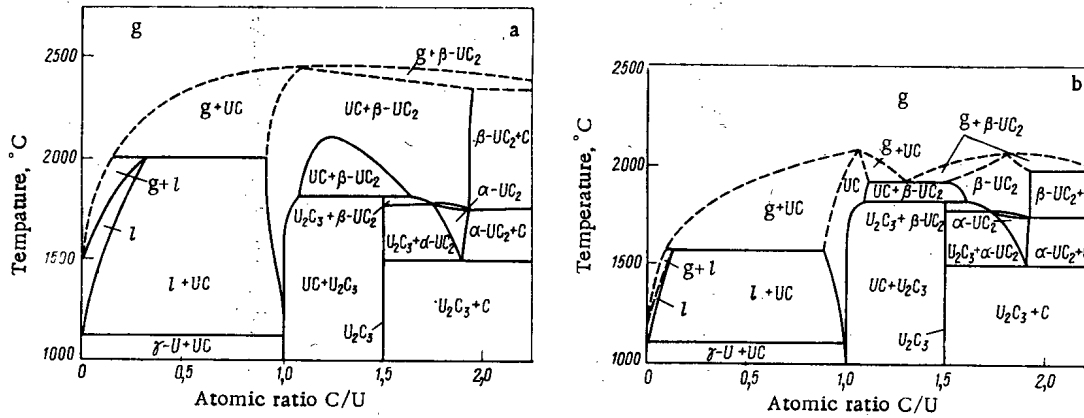
Fig. 2. Isobaric cross sections of phase diagram of uranium — carbon system at 10^{-6} atm (a) and $5 \cdot 10^{-9}$ atm (b).

between 1800 and 2100°C, curve 7-19 was constructed from the data in [1], and at lower temperatures, by extrapolation of these data, as also curve 7-6.

Curves 19-33, 17-32, and 18-30 denote congruent melting of UC, UC_2, and their solid solution. At point 16 we observe a four-phase equilibrium: β-$UC_2 \rightleftharpoons l \rightleftharpoons C \rightleftharpoons g$. This point is the start of curves 16-31, 16-21, 16-17, and 16-10 of three-phase equilibrium β-$UC_2 \rightleftharpoons C \rightleftharpoons l$, $l \rightleftharpoons C \rightleftharpoons g$, β-$UC_2 \rightleftharpoons l \rightleftharpoons g$, and β-$UC_2 \rightleftharpoons C \rightleftharpoons g$. Curve 16-31 represents the equilibrium of three condensed phases, and is vertical (T = 2430°C); curves 16-21 and 17-16 are drawn provisionally; between 1800 and 2100°C, curve 6-10 was constructed with the aid of the data in [1] on the assumption that the total gas pressure above the mixture β-UC_2 + C corresponds to the partial pressure of uranium.

The four-phase equilibrium α-$UC_2 \rightleftharpoons \beta$-$UC_2 \rightleftharpoons C \rightleftharpoons g$ is marked by point 10 (T = 1765°C, p = 10^{-10} atm); this point is the start not only of curve 10-16 but also of curves 10-26, 10-11, and 10-5 of the three-phase equilibria α-$UC_2 \rightleftharpoons \beta$-$UC_2 \rightleftharpoons C$, α-$UC_2 \rightleftharpoons \beta$-$UC_2 \rightleftharpoons g$, and α-$UC_2 \rightleftharpoons C \rightleftharpoons g$. This last curve was obtained by extrapolation of curve 10-16. At point 5 there is equilibrium between the phases U_2C_3, α-UC_2, C, and gas. The three-phase reactions $U_2C_3 \rightleftharpoons \alpha$-$UC_2 \rightleftharpoons g$, $U_2C_3 \rightleftharpoons C \rightleftharpoons g$, and $U_2C_3 \rightleftharpoons \alpha$-$UC_2 \rightleftharpoons C$ correspond to curves 5-11, 5-3, and 5-25. Curves 5-11 and 5-3 are drawn provisionally, and curve 5-25 is vertical (T = 1514°C). The four-phase equilibrium α-$UC_2 \rightleftharpoons U_2C_3 \rightleftharpoons \beta$-$UC_2 \rightleftharpoons g$ is marked by point 11 (T ≈ 1775°C, p = 10^{-10} atm). Curves 11-27 and 11-12 of the three-phase equilibria β-$UC_2 \rightleftharpoons U_2C_3 \rightleftharpoons \alpha$-$UC_2$ and $U_2C_2 \rightleftharpoons \beta$-$UC_2 \rightleftharpoons g$ are drawn provisionally.

At point 12 (T = 1780°C, p = $5 \cdot 10^{-10}$ atm) four phases are in equilibrium: UC, β-UC_2, U_2C_3, and gas. Curve 12-28 of the three-phase equilibrium $UC \rightleftharpoons \beta$-$UC_2 \rightleftharpoons \alpha$-$U_2C_3$ is vertical, and curve 12-15 of the three-phase equilibrium $UC \rightleftharpoons \beta$-$UC_2 \rightleftharpoons g$ is constructed with the aid of the data in [1]. The critical point 15 has the following coordinates: T = 2100°C, p = $2 \cdot 10^{-7}$ atm. We can suppose that the critical curve 15-29 is practically vertical in the pressure range plotted in Fig. 1.
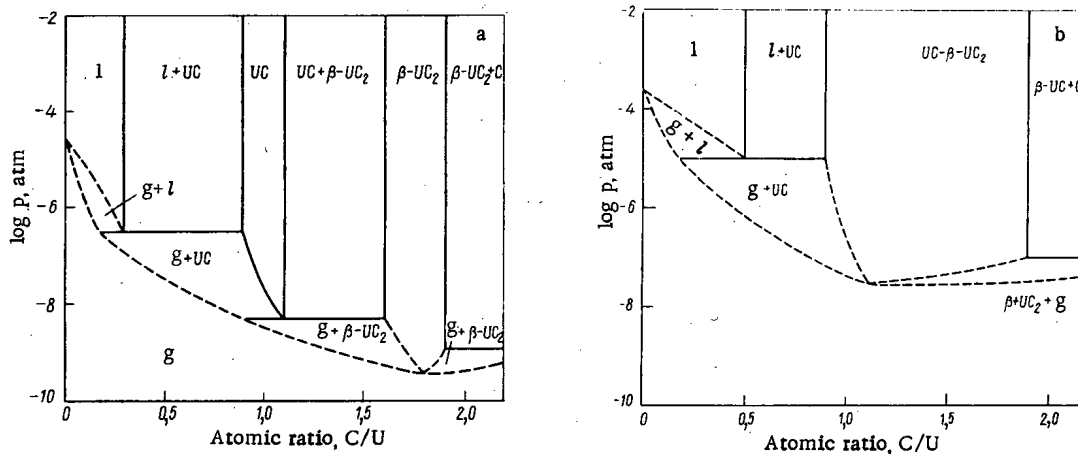
Fig. 3. Isothermal cross sections of phase diagram of uranium — carbon system at 1900°C (a) and 2200°C (b).

806

It was established that from the melting point to about 1960°C the congruently melting uranium carbide has the composition $UC_{1.1}$; in a narrow range of temperatures near 1960°C two carbides melt congruently, $UC_{1.1}$ and $UC_{1.8}$; and at lower temperatures only $UC_{1.8}$ melts congruently [1]. In this connection, the curve of congruent evaporation of uranium monocarbide starts at point 19 where UC melts and ends at about 1900°C at point 13 lying on the curve of congruent evaporation of uranium dicarbide. The latter takes its origin at point 14 on curve 10-16 and continues to the low-temperature region. There are no precise data on the position of the curves of congruent evaporation of the uranium carbides; it is merely clear that they must lie below the curves of three-phase equilibria involving UC and UC_2.

The published information concerning the equilibrium gas pressure above pure carbon is very contradictory and at a given temperature there can be discrepancies of three or four orders of magnitude [3]. Therefore in Fig. 1 curve 2-20 for the evaporation of carbon is drawn provisionally. At temperatures above the melting point of uranium monocarbide the gas pressure above carbon must be a minimum for the entire uranium — carbon system; at lower temperatures this pressure can be either higher or lower than the equilibrium pressure of the gas above various two-phase mixtures. In view of the indeterminacy of the position of curve 2-20, we shall not give further consideration to the equilibrium involving pure carbon in isobaric and isothermal conditions.

It is easy to verify that at pressures above 10^{-2} atm the isobaric cross sections of the phase diagram of the uranium — carbon system in the temperature range in question is wholly identical with the projection of the line of maximum solubility [2], because in these conditions the system does not have a gas phase. At lower pressures this identity is no longer observed [2] (Fig. 2).

As the temperature rises, the isobar at $p = 10^{-6}$ atm intersects the following curves: 7-23, 9-24, 9-22, 5-25, 10-26, 11-27, 12-28, 7-19, 15-29, 10-16, and 13-19. The transitions corresponding to these points of intersection are shown in the isobaric cross section in Fig. 2a. A characteristic feature of this isobaric cross section is congruent evaporation, and not melting of uranium monocarbide and appearance of a number of two-phase regions involving the gas phase. The lower boundary of the region of homogeneity of uranium monocarbide is shifted towards carbon, because the composition of the congruently evaporating phase is $UC_{1.1}$.

The isobar at $p = 5 \cdot 10^{-9}$ atm intersects the curves: 7-23, 9-24, 9-22, 7-19, 10-26, 11-27, 12-28, 12-15, 10-16, 13-14, and 13-19. Seven of these represent three-phase equilibria, and therefore in Fig. 2b there are seven horizontal three-phase reactions. The region of liquid solutions of carbon in uranium is narrow, and the composition of carbon-saturated liquid is $UC_{0.15}$ at 1600°C at which the liquid decomposes into gas containing mainly uranium and monocarbide of the composition $UC_{0.9}$. Uranium monocarbide $UC_{1.1}$ and uranium dicarbide $UC_{1.8}$ evaporate congruently at $5 \cdot 10^{-9}$ atm. The phases UC and β-UC_2 do not form continuous solid solutions, but occupy isolated fields on the diagram separated by the two-phase region UC + β-UC_2. The composition of carbon-saturated monocarbide is $UC_{1.13}$, and that of uranium-saturated dicarbide is $UC_{1.47}$. In the remaining regions the isobaric cross sections coincide (Fig. 2a-b).

The isothermal cross sections of the phase diagram of the uranium — carbon system at 1900 and 2200°C are shown in Fig. 3. The isotherm at T = 1900°C intersects curves 9-22, 7-19, 12-15, 10-16, and 4-13. Three points of intersection correspond to horizontals (Fig. 3a) and the rest to congruent evaporation of uranium dicarbide. Three-phase equilibrium at about $5 \cdot 10^{-7}$ atm involves gas rich in uranium, liquid with the composition $UC_{0.3}$, and uranium monocarbide of the composition $UC_{0.9}$. At about $5 \cdot 10^{-9}$ atm the monocarbide with the composition $UC_{1.1}$ decomposes to form gas and dicarbide with the composition $UC_{1.6}$. The composition of congruently evaporating dicarbide is $UC_{1.8}$.

The isotherm at T = 2200°C intersects curves 9-22, 7-19, 10-16, and 13-19. Only two of these are three-phase equilibria. In conformity with this, on the isothermal cross section (Fig. 3b) at 10^{-5} atm the liquid with composition $UC_{0.5}$ decomposes to gas and carbide with the composition $UC_{0.9}$, while at 10^{-7} atm the uranium dicarbide with composition $UC_{1.9}$ decomposes to gas and carbon. The composition of the congruently evaporating carbide is $UC_{1.1}$.

The p — T diagram can be used to estimate the behavior of uranium carbides in vacuum or in a medium with low partial pressures of uranium and carbon.

LITERATURE CITED

1. E. Storms, Refractory Carbides, Academic Press, New York (1967).
2. R. Benz, C. Hoffman, and G. Rupert, High Temp. Sci., 1, 342 (1969).
3. A. N. Nesmeyanov, The Vapor Pressures of the Chemical Elements [in Russian], Izd-vo Akad. Nauk SSSR, Moscow (1961).

THERMAL CROSS SECTIONS AND RESONANCE INTEGRALS

OF FISSION AND CAPTURE OF ^{241}Am, ^{243}Am, ^{245}Cm, ^{249}Bk, AND ^{249}Cf

V. D. Gavrilov, V. A. Goncharov,
V. V. Ivanenko, V. N. Kustov,
and V. P. Smirnov

UDC 539.172.4

In order to optimize the accumulation of transplutonium elements in reactors, one must know the cross sections of the interaction of neutrons with the nuclei of all isotopes participating in the accumulation process. The method of cadmium differences is used in the present work to measure the thermal cross sections and the resonance integrals of capture and fission of ^{241}Am, ^{243}Am, ^{245}Cm, ^{249}Bk, and ^{249}Cf. The cadmium shield had a thickness of 1 mm. ^{197}Au and ^{59}Co samples were used as monitors of the neutron flux ($\sigma = 98.8$ and 37.5 b and $I = 1558$ and 70 b, respectively) [1]. The induced γ activity of the irradiated monitors was measured with a γ-spectrometer equipped with a Ge(Li) semiconductor detector. The efficiency of the γ quantum recording was determined from spectrometric reference sources of γ radiation which had been prepared with errors of 3-5%.

Fission Cross Sections. The fission cross sections were measured at the output of the horizontal channel of an SM-2 reactor. Solid-state track detectors made from mica and photosensitive glass were used for recording fission events. The detectors had a sufficiently high efficiency for recording fission fragments and were practically insensitive to α, β, γ, and neutron radiation [2]. The small dimensions of the detectors made it possible to reduce or to eliminate the influence of neutron flux disturbances.

The initial number of nuclei of the isotopes to be investigated was determined from the α activity of the targets. The isotopes to be investigated were applied as solution onto aluminum substrates and measured with a 2π proportional flow counter. The samples were irradiated in the form of sandwiches consisting of the target and the detector. The amount of the substance under investigation and the irradiation time of the targets were chosen so that the number of tracks in the detector was kept in the range $(0.8-1.5) \cdot 10^{-3}$. Phonon-induced tracks were taken into consideration by preliminary etching of the detectors before the irradiation.

The efficiency with which the fission fragments were recorded by the track detectors was determined in tests made with the ^{252}Cf and ^{244}Cm isotopes which undergo spontaneous fission. The following efficiency figures were obtained by evaluating the results of four measurement series made with 10 ^{252}Cf and seven ^{244}Cm targets:
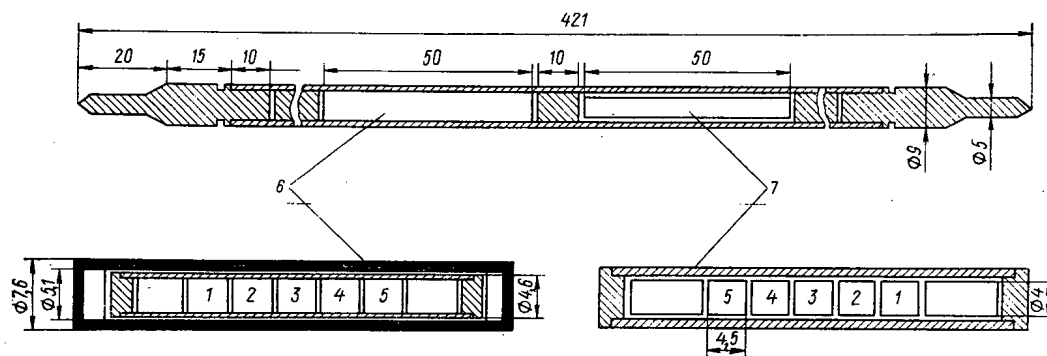
Fig. 1. Sealed tube: 1-5) samples to be investigated; 6) capsules in cadmium shield; 7) aluminum capsules.
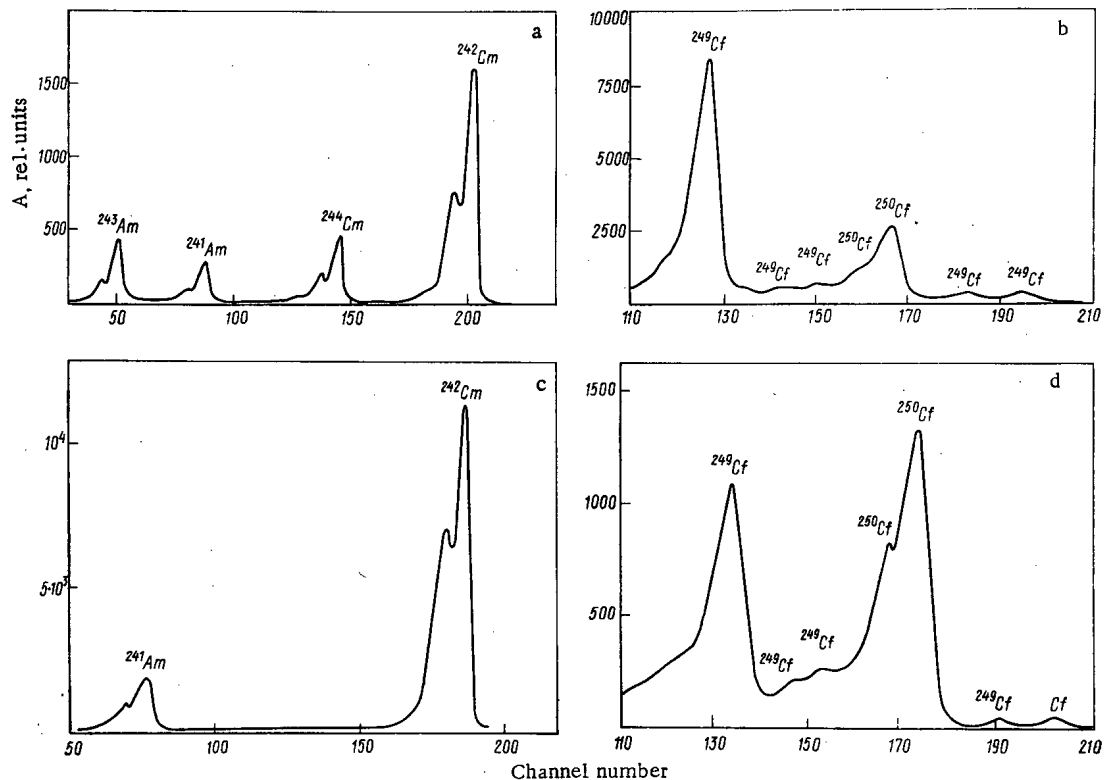
Fig. 2. α spectra of samples irradiated with the full neutron spectrum (A denotes the number of pulses per analyzer channel): a) ^{243}Am; b) ^{249}Cf; c) ^{241}Am; d) ^{249}Bk.

for the glass $\varepsilon_1 = 0.396 \pm 0.004$ and for the mica $\varepsilon_2 = 0.812 \pm 0.010$. The ratios of the rates of α decay and spontaneous fission measured in [3, 4] were used to determine the efficiency.

Three series in which the fission cross section of ^{239}Pu was measured were made to check the method. 1.5-mm-thick sheets were used as fission fragment detectors in two series. The resonance integral measured in those series was much larger than the recommended values (I = 327 ± 13 b) [5]. In the third measurement series, $1.5 \cdot 10^{-2}$-mm-thick mica sheets were used as fission fragment detectors; the result of the measurements (I = 320 ± 19 b) was in good agreement with the assumed value. The excessive resonance integral in the first measurement series can be explained by the fact that neutrons with an energy in excess of 0.5 eV, which passed through the cadmium shield, lost part of their energy by scattering at the substrate material and at the detector (d = 1.5 mm) and fell into the region of the first ^{239}Pu resonance ($E_0 = 0.296$ eV). Since the thickness of the detector was reduced by two orders of magnitude in the third series of measurements, the influence of the neutron scattering was substantially reduced and did not affect the value of the resonance integral.

Both mica and the photosensitive glass were used as detectors of fragments when the fission cross sections of ^{241}Am were determined. The values which were obtained for the resonance integral of fission with the aid of the two types of detectors are in good agreement (22.2 and 22.8 b for glass and mica, respectively).

Only mica detectors were used when the fission cross sections of ^{243}Am, ^{245}Cm, and ^{249}Cf were measured. An α-spectrometric analysis of ^{243}Am revealed that ^{242}Cm is present; the amount of ^{242}Cm was used to determine the ^{242m}Am concentration (Table 1). The thermal cross section figure 7200 b [6] and the resonance integral 1570 b [6] were used to take into account the rates of the fission reactions resulting from ^{242m}Am. The

TABLE 1. Initial Composition of the Samples under Inspection

Isotope	Composition (%) of nonirradiated samples			
^{241}Am	97,84 ^{241}Am	2,0 ^{237}Np	0,16 ^{239}Pu	—
^{249}Bk	65,46 ^{249}Bk	34,54 ^{249}Cf	—	10^{-3} ^{252}Cf
^{249}Cf	—	100 ^{249}Cf	—	$2,85 \cdot 10^{-2}$ ^{252}Cf
^{243}Am	96,63 ^{243}Am	3,37 ^{241}Am	$7,85 \cdot 10^{-3}$ ^{242m}Am	$2,37 \cdot 10^{-5}$ ^{242}Cm; $1,89 \cdot 10^{-4}$ ^{244}Cm
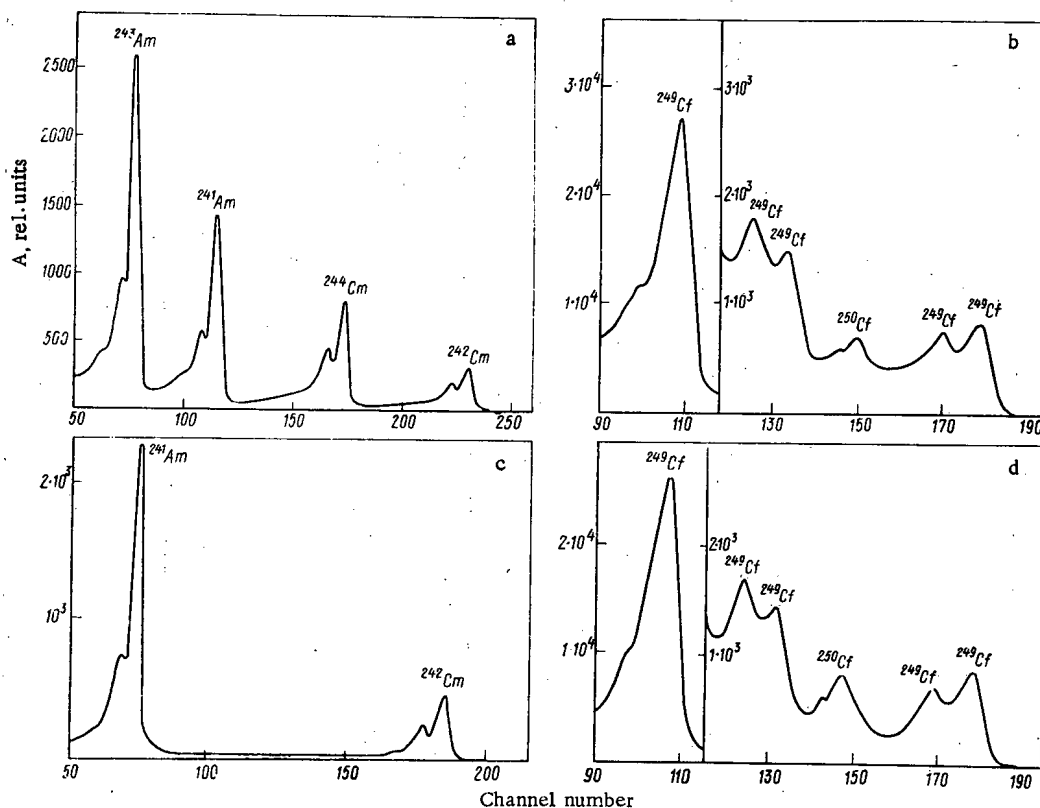
Fig. 3. α spectra of samples irradiated with the epithermal neutron spectrum
(notation as in Fig. 1).

presence of even a very small admixture of ^{242m}Am substantially reduced the accuracy with which the thermal cross section of ^{243}Am was determined. But this did not influence the value of the resonance integral and the accuracy of its determination. The results of the measurements are listed in Table 2.

Capture Cross Sections. We measured in our work the cross sections of the radiative capture of neutrons by ^{241}Am, ^{243}Am, ^{249}Bk, and ^{249}Cf nuclei. The samples were irradiated in the No. 9 channel of the SM-2 reactor. Two capsules, one of which was enclosed by the cadmium shield (Fig. 1), were irradiated. Four samples and four monitors of the neutron flux had been inserted into each of the capsules.

Targets (5-6 targets of each isotope under investigation) were prepared from the irradiated and nonirradiated samples. Measurements on the targets were thereafter made in the α spectrometer. The α spectra (resolution ~25 keV) of all isotopes inspected are shown in Figs. 2 and 3.

The thermal cross sections and the resonance integrals of capture were determined from the accumulation of the daughter products formed by the capture of neutrons by the nuclei of the isotopes under investigation.

TABLE 2. Fission Cross Sections

Isotope	Present work		Published data	
	$\sigma_0\ (v = 2200\ \text{m/sec},\ b$	I, b	$\sigma_0\ (v = 2200\ \text{m/sec},\ b$	I, b
^{239}Pu	739±46	320±19	741,6±3,1 [5]	327±13 [5]
^{241}Am	2,80±0,25	22,5±1,7	3,15±0,10 [7]	21±2 [7]
			3,13±0,15 [8]	
^{243}Am	0,20±0,11	17,1±1,3	0,07 [8]	—
^{245}Cm	1900±100	850±60	2020±37 [9]	772±40 [9]
			1920±180 [10]	1140±100 [10]
			2040±80 [11]	750±150 [12]
^{249}Cf	1610±110	1800±200	1670±80]13]	2110±70 [13]
			1690±160 [10]	2900±270 [10]
				1800 [12]

TABLE 3. Nuclear Constants Which Were
Used in Calculating the Cross Sections in the
Isotopes under Inspection

Isotope	$T_{1/2}$	E, MeV	Y,* %
^{241}Am	432,7 yr	5,486	85,5
^{243}Am	7370 yr	5,275	87,5
^{242}Cm	163 day	6,114	73,8
^{244}Cm	18,1 yr	5,806	76,5
^{249}Bk	310 day	—	—
^{249}Cf	352 yr	5,812	83,7
^{250}Cf	13,08 yr	6,031	83,0

*Yield of the α line of the indicated energy per de-
cay event.

The (n, γ) capture reaction involving ^{241}Am nuclei leads to ^{242}Am in both the ground state and the excited state. ^{242}Am nuclei with a half-life of 16.1 h are converted into ^{242}Cm via β decay (83.6%). The ^{242}Cm concentration of the irradiated samples was determined from the intensity ratio of the α lines of ^{242}Cm and ^{241}Am.

The ^{242m}Am concentration of the irradiated samples was determined with the aid of the solid-state track detectors. The irradiated and nonirradiated ^{241}Am samples were used to prepare targets from which sandwiches were made with mica sheets; the targets were irradiated with the neutron flux of the CM-2 reactor. The ^{242m}Am concentration was determined from the difference of the fission reaction rates in irradiated and nonirradiated samples per initial ^{241}Am nucleus. The thermal ^{242m}Am fission cross section σ_γ = 7200 b and its resonance integral I = 1570 b were used in the calculations. The results of [6] must be considered the most reliable data, because the americium target examined had a high ^{242m}Am concentration (~19.7%).

As in the case of ^{241}Am, the (n, γ) neutron capture reaction in the irradiation of ^{243}Am leads to ^{244}Am in both the ground state and the metastable state. ^{244g}Am nuclei with a half-life of 26 min and ^{244m}Am nuclei with a half-life of 10.1 h are converted into ^{244}Cm nuclei via β decay.

The ^{244}Cm concentration of the irradiated samples was determined with the aid of α spectrometry.

The accumulation of ^{250}Cf in irradiated ^{249}Bk and ^{249}Cf samples was determined by measuring the intensity of the α lines of ^{250}Cf and ^{249}Cf.

The concentration of the accumulated curium isotopes was determined with an error of 1-2%, but the integral flux of the epithermal neutrons did not suffice for irradiating the ^{241}Am and ^{249}Cf isotopes. This substantially increased the error made in the determination of the ^{250}Cf and ^{242m}Am concentrations and increased the time used for the α spectrometric measurements of the cadmium-enclosed samples.

The results of measurements of the isotope composition of irradiated and nonirradiated samples, the irradiation times, and the neutron fluxes were brought into account when the thermal cross sections and the resonance integrals of capture were calculated for the isotopes under consideration (Table 3). The cross sections of radiative capture (Table 4) were calculated with the equations obtained from the condition of equilibrium between the parent element and the daughter elements:

$$I_\gamma = \frac{\left(\frac{N_d}{N_i}\right)_{Cd} e^{\left(\frac{\ln 2}{T_d} t_2\right)} \ln 2}{\Phi_{epi} T_d \left[1 - e^{\left(\frac{\ln 2}{T_d} t_1\right)}\right]} ; \qquad (1)$$

$$\sigma_\gamma = \frac{\left[\left(\frac{N_d}{N_i}\right) - \left(\frac{N_d}{N_i}\right)_{Cd} F_{Cd}\right] e^{\left(\frac{\ln 2}{T_d} t_2\right)} \ln 2}{\Phi_{th} g(T) T_d \left[1 - e^{\left(\frac{\ln 2}{T_d} t_1\right)}\right]} , \qquad (2)$$

where N_d/N_i and $(N_d/N_i)_{Cd}$ denote the ratio of the nuclei of the daughter element and the parent element in the samples irradiated with the total neutron spectrum and the epithermal neutron spectrum, respectively; Φ_{th} and Φ_{epi} denote the densities of the thermal neutrons and the epithermal neutrons, respectively; T_d denotes the half-life of the daughter element; t_1 and t_2 denote the sample irradiation time and the sample storage time, respectively; F_{Cd} denotes the cadmium correction (E_{Cd} = 0.68 eV) [18]; and g(T) denotes the correction for the deviation of the cross section from 1/v in the range of thermal neutrons (T = 65°C).

811

TABLE 4. Cross Sections of Radiative Capture

Isotope	Present work		Published data	
	$\sigma\,(v = 2200\ \text{m/sec})$ b	I, b	$\sigma\,(v = 2200\ \text{m/sec})$, b	I, b
^{241}Am	780±50 *	1570±10 *	748±20 [13] 670±60 [7]	1440±120 [12] 1330±117 [13]
^{241}Am	73±14 †	230±80 †	83,8±2,6 [13] 70±5 [7]	250±50 [12] 208± [13]
^{243}Am	83±6	2200±150	79,3±2,6 [1] 75±6 [7]	2340± [14] 2250 [15] 1820±70 [1]
^{249}Bk	1800±100	1100±100 1300±300	1700 [15] 1300±300 [1] 1100±300 [16]	1100 [12] 1850 [13]
^{249}Cf	530±33	720±120	465±25 [17] 270±100 [15]	1030 [12] 765±35 [1]

*Cross section of the reaction ^{241}Am $(n, \gamma) \rightarrow \ ^{242g}$Am.
†Cross section of the reaction ^{241}Am $(n, \gamma) \rightarrow \ ^{242m}$Am.

By comparing the results listed in Tables 2 and 4, we can conclude that the data obtained in our work on the cross sections of radiative capture and fission are in rather good agreement with the results obtained by other scientists. In some papers the capture cross sections were determined from the accumulation of products obtained by long-lasting neutron irradiation, though these products are far from the initial nuclei; the results of the present work, however, were obtained for conversion chains comprising two links only. This substantially reduces the experimental error and increases the reliability of the results. We note that in the experiment under consideration, samples in which the concentration of the indicator amounts of the isotopes examined were less than 1 μg were irradiated; therefore the self-shielding of the samples could be minimized. In our opinion, self-shielding is one of the main reasons for the spread of the experimental data concerning the resonance integrals of capture and fission.

The errors which were made in the measurements of the capture and fission cross sections originate mainly from the errors made in the determination of the neutron fluxes, because the efficiency of recording the γ quanta with the spectrometer was determined from spectrometric reference sources of gamma radiation, i.e., from sources which had been prepared with an accuracy of 3-5%. It will be possible to improve the thermal cross section data and the resonance integrals of capture and fission when experiments are made with single-isotope targets and when the accuracy with which the neutron fluxes are determined is increased.

LITERATURE CITED

1. BNL-325, 3rd edition, Vol. 1 (1973).
2. A. Kapustsik et al., Pribory i Tekh. Éksperim., 1, 43 (1968).
3. B. M. Aleksandrov et al., At. Énerg., 28, No. 4, 361 (1970).
4. D. Metta et al., J. Inorg. and Nucl. Chem., 27, 33 (1935).
5. M. Cabell, in: Proc. IAEA Symp. "Nuclear Data for Reactors — 1966," Vol. 2, Paris, Oct. 17-21 (1966).
6. K. Woefsberg et al., J. Nucl. Energy, 20, 558 (1966).
7. M. A. Bak et al., At. Énerg., 23, No. 4, 316 (1967).
8. E. Hulett, Phys. Rev., 107, 1294 (1957).
9. R. Benjamin, Nucl. Sci. and Engng., 47, No. 2, 203 (1972).
10. J. Halperin et al., ORNL-4581 (1970).
11. H. Diamond, J. Inorg. and Nucl. Chem., 30, No. 9, 2553 (1968).
12. A. Eberle, KFK-1544 (1972).
13. R. Harbour, Nucl. Sci. and Engng., 50, No. 3, 364 (1973).
14. J. Butler, Canad. J. Phys., 35, 147 (1957).
15. V. Kon'shin, Vestnik Akad. Nauk BSSR, No. 3, 26 (1972).
16. A. Harvey, Phys. Rev., 95, No. 7, 581 (1954).
17. R. Benjamin et al., in: Proc. 3rd Conf. on Neutron Cross Sections and Technology, Knoxville, March 15-16, 1971, p. 116.
18. R. D. Vasil'ev, Principles of the Metrology of Neutron Radiation [in Russian], Atomizdat, Moscow (1972).

USING PYROELECTRIC DETECTORS FOR THE
DOSIMETRY OF PULSED γ RADIATION

L. S. Kremenchugskii and R. Ya. Strakovskaya   UDC 621.384.326.22.536

In recent years pyroelectric radiation detectors for the measurement of radiation in the optical range have been intensively developed and investigated [1, 2]. Reports have appeared on the successful utilization of pyroelectric radiation detectors for measuring ionizing radiation [3-5]. The low inertia of these detectors makes it possible to use them for pulse measurements; the high radiation stability of ceramic pyroactive materials [6] and the wide dynamic range of the measurements allow the utilization of these detectors for the dosimetry of powerful sources of ionizing radiation. In [4] the quasiadiabatic absorption of γ radiation energy was considered; the considerations apply also to short radiation pulses.

The present paper reports on the results of an investigation of pyroelectric radiation detectors used for the dosimetry of γ radiation in a more general case. The principle of operation of pyroelectric radiation detectors is based on the fact that the absorption of the radiation energy increases the temperature of the pyroactive crystal, and this implies a change of the polarization. The result is that free electric charges appear on the detector plates and a current is generated in the circuit (pyroelectric effect). The pyroelectric origin of the signal in polarized Seignette-electric crystals exposed to ionizing radiation was considered in [3] and confirmed in our research work.

When compared with radiation measurements in the optical range, the operation of pyroelectric radiation detectors used to detect γ radiation is characterized by the following properties.

1. Since the γ radiation is practically uniformly absorbed by the bulk of the detector, the diffusion time constant is close to zero and the operation of the pyroelectric radiation detectors can be described by a system with lumped parameters.

2. Since pyroelectric radiation detectors respond to the energy (power) absorbed by the detector, the detector should be considered a meter of absorbed dose or dose rate. Therefore, in the equation of the thermal balance of the γ radiation detector, the time-dependent temperature changes of the detector and the absorbed dose rate should be related. When operated in the optical wavelength range, pyroelectric radiation detectors function as pickups of the incident radiation flux and therefore the incident energy (power) practically coincides with the energy (power) absorbed by the detector, provided that black coatings are used.

3. Pyroelectric radiation detectors respond only to changes in the radiation flux and therefore the radiation flux must be modulated for measurements in the optical wavelength range. When measurements are made on stationary fluxes of γ radiation, it is difficult to use modulators because the penetration power of the γ quanta is high. Other solutions must be used to obtain a modulated signal from the detector.

4. In order to reach a sensitivity which is close to the maximum sensitivity of pyroelectric radiation detectors recording γ radiation, the selection of the optimal geometrical dimensions of the detector must take into consideration the input capacity of the amplifier, whereas the maximum sensitivity in the optical range is reached with the smallest possible dimensions of the sensitive element of pyroelectric radiation detectors.

When we consider below the response of a pyroelectric radiation detector to γ radiation, we will restrict our considerations to the thermal influence upon the detector. This makes it possible to consider the response of a pyroelectric radiation detector to γ radiation in terms of the theory of pyroelectricity. We show below that this approach is justified.

Let us write down the equation of the thermal balance for a pyroelectric radiation detector upon which a γ radiation pulse acts. When we use the equation of the thermal balance for a pyroelectric radiation detector

---
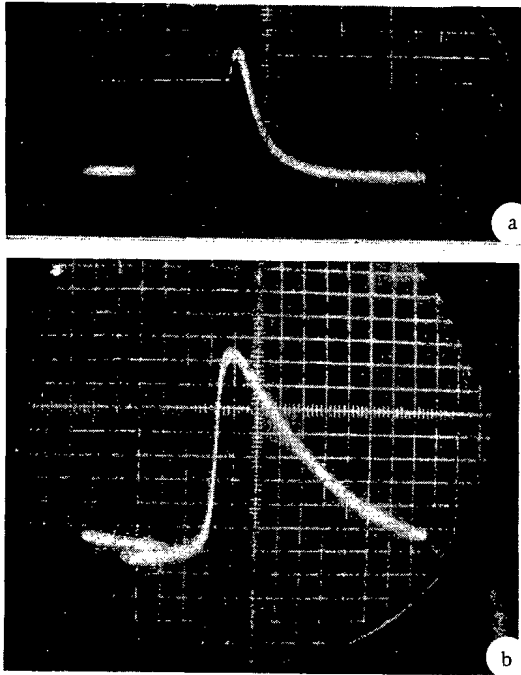
Fig. 1. Oscillograms of the pulses of pyroelectric radiation detectors exposed to γ radiation; a) recording of the dose rate and b) recording of the dose; scales: 1 and 10 mV/scale division and 0.5 and 1 sec/scale division, respectively.

operated in the optical range [1, 2] and when we replace the heat capacity of the crystal by the specific heat c and the mass g and, furthermore, when we assume that the absorbed radiation energy referred to unit mass is the dose rate, we can state the equation of the thermal balance of the pyroelectric radiation detector for the absorbed dose rate P(t) in the form

$$\frac{dT}{dt} + \tau_t^{-1}(T - T_0) = \frac{P(t)}{c} 10^{-5}, \tag{1}$$

where T denotes the temperature which the sample reaches under the influence of the γ radiation; T_0 denotes the temperature of the medium; τ_t denotes the thermal time constant of the crystal; P(t) denotes the dose rate in a γ radiation pulse; c denotes the specific heat [J/(g · deg)] of the pyroactive material; and 10^{-5} is the coefficient which matches the units of the measurements (rad and Joule to gram).

When the pyroelectric radiation detector is considered a capacitor C_0 and a current generator with the load R_0, the equation of [2] applies to the output voltage:

$$\frac{dU}{dt} + \frac{U}{\tau_e} = \frac{A\gamma}{c_0} \frac{d}{dt} \left\{ 10^{-5} \frac{\exp(-t/\tau_t)}{c} \int_0^t \exp(\theta/\tau_t) P(\theta) \, d\theta \right\}, \tag{2}$$

where the term in the brackets results from the integration of Eq. (1) with the conventional initial conditions (T − T_0 = 0 for t = 0); $\tau_e = R_0 C_0$ and denotes the time constant of the electric circuit; A denotes the detector area; and γ denotes the pyroelectric coefficient. By integrating Eq. (2) with the initial conditions t = 0, U = 0, we obtain

$$U(t) = \frac{A\gamma}{C_0 c} 10^{-5} \left\{ \frac{\tau_t}{\tau_t - \tau_e} \exp(-t/\tau_e) \int_0^t P(\theta) \exp(\theta/\tau_e) \, d\theta - \right.$$

$$\left. - \frac{\tau_e}{\tau_t - \tau_e} \exp(-t/\tau_t) \int P(\theta) \exp(\theta/\tau_t) \, d\theta \right\}. \tag{3}$$

This equation can be solved only when the form of the function P(θ) is given. We consider the case in which P(θ) is a discontinuous function which is equal to zero for t < 0 and equal to P_0 for t ≥ 0. Then for t ≥ 0 the solution of Eq. (3) can be represented in the form

$$U(t) = \frac{A\gamma}{C_0 c} 10^{-5} P_0 \frac{\tau_t \tau_e}{\tau_t - \tau_e} [\exp(-t/\tau_t) - \exp(-t/\tau_e)]. \tag{4}$$

If $\tau_e < \tau_t$, the difference between the two exponentials f(t) renders a pulse of positive polarity. By setting the first derivative equal to zero, we can determine the value of the argument t_0 at which f(t) reaches the maximum and we can also determine the maximum f_0(t). For $\tau_e \ll \tau_t$ we have

814

$$\tau_0 \approx -\tau_e \ln \tau_e/\tau_t; \qquad (5)$$

$$f_0 \approx \frac{\tau_t - \tau_e}{\tau_t}. \qquad (6)$$

After substituting the f_0 value from Eq. (6) into Eq. (4), we obtain the amplitude of the signal:

$$U_0 = \frac{A\gamma R_0}{c} 10^{-5} P_0. \qquad (7)$$

After reaching the maximum, the signal decays in the form of an exponential which is given by the time constant τ_t. Finally, we obtain

$$U(t) = \frac{A\gamma R_0}{c} 10^{-5} P_0 \exp(-t/\tau_t), \qquad (8)$$

where U(t) is the response of the detector to the front of a sudden change of magnitude P_0 of the dose rate. We realize that the signal amplitude is proportional to P_0.

When the dose rate does not change suddenly but when the change takes place with some front t_f, where $\tau_e \ll t_f$ but $\tau_t \gg t_f$, the first term in the brackets of Eq. (3) is a quantity almost equal to $\tau_e P(t)$, whereas the second term, which describes the drop of the signal owing to the thermal time constant, is small relative to the first term. Integration of Eq. (3) from 0 to t_f renders the signal

$$U(t) = \frac{A\gamma R_0}{c} 10^{-5} \frac{\tau_t \tau_e}{\tau_t - \tau_e} P(t) [1 - \exp(-t/\tau_e)] \approx \frac{A\gamma R_0}{c} 10^{-5} P(t), \qquad (9)$$

which indicates that the form of the front of the signal reproduces the form of the front of the pulse P(t). When the dose rate does not change after having reached the maximum, the signal decays exponentially by virtue of τ_t, in analogy to Eq. (8).

Thus, a pulse signal develops when a sudden radiation change acts upon a pyroelectric radiation detector. If $t_f \ll \tau_e$, the signal front is given by τ_e. If $t_f \gg \tau_e$, the signal front reproduces the form of the radiation front. The signal decay at a stationary radiation level is given by the value of τ_t.

When a short radiation pulse occurs and when $P(\theta)$ changes much faster than $\exp(t/\tau_t)$ and $\exp(t/\tau_e)$, or if $t_{imp} \ll \tau_t$ and $t_{imp} \ll \tau_e$, then

$$U(t) = \frac{A\gamma}{C_0 c} 10^{-5} \int_0^t P(\theta) d\theta = \frac{A\gamma}{C_0 c} 10^{-5} D(t). \qquad (10)$$

The maximum of the signal is proportional to the dose D in the radiation pulse:

$$U_0 = \frac{A\gamma}{C_0 c} 10^{-5} D. \qquad (11)$$

In order to determine the shape of the signal after termination of the radiation pulse, one must consider the response of the detector to a negative radiation change. According to Eq. (4), when a sudden change $-P_0$ occurs, the signal is equal to the difference of the two exponentials $[\exp(-t/\tau_e) - \exp(-t/\tau_t)]$. If $\tau_e \gg t_t$, the drop of the signal depends upon τ_e. If $\tau_e \ll \tau_t$, a negative change occurs and the subsequent signal drop takes place with the time constant τ_t.

The formulas obtained for the signal amplitude in the case of exposure to γ radiation allow the determination of the sensitivity of a pyroelectric radiation detector.

The voltage sensitivity S_{dr}^V (expressed in units V/rad/sec) for dose rate measurments can be obtained from Eq. (8)

$$S_{dr}^V = \frac{U(t)}{P(t)} = \frac{A\gamma R_0}{c} 10^{-5} \exp(-t/\tau_t). \qquad (12)$$

The current sensitivity S_{dr}^A (expressed in units A/rad/sec) is accordingly under these conditions

$$S_{dr}^A = \frac{A\gamma}{c} 10^{-5} \exp(-t/\tau_t). \qquad (13)$$

The maximum of the voltage sensitivity S_d^V (expressed in units V/rad) in the case of dose measurements can be obtained from Eq. (10):

$$S_d^V = \frac{U(t)}{D(t)} = \frac{A\gamma}{C_0 c} 10^{-5}, \qquad (14)$$

815

and the corresponding Coulomb-rad sensitivity S_d^C (expressed in units C/rad) is

$$S_d^C = \frac{A\gamma}{c} 10^{-5}. \tag{15}$$

The maximum of the Coulomb-rad sensitivity per unit irradiated surface area depends only upon the pyroelectric coefficient and the specific heat of the pyroactive material of a pyroelectric radiation detector and is therefore the basic sensitivity characteristic of such a detector. This sensitivity is given by the principle of operation of the detector and is independent of the circuit in which the detector is used.

The threshold sensitivity of pyroelectric radiation detectors depends upon the noise of the R_0C_0 circuit, provided that the noise of the measuring circuit and the temperature-induced noise can be ignored [1]. Accoding to [2], the integral noise in the entire frequency range is

$$\sqrt{\overline{u^2}} = \sqrt{kT/c_0}, \tag{16}$$

where k denotes the Boltzmann constant.

The threshold sensitivity which was obtained from Eqs. (12) and (15) for the dose rate is

$$\Pi_{dr} = \frac{\sqrt{\overline{u^2}}}{S_{dr}^V} = \frac{\sqrt{kTC_0}}{\tau_e} \frac{c}{A\gamma} 10^5 \exp(t/\tau_t). \tag{17}$$

Since the selection of τ_e depends upon the duration of the signals to be measured, Π_{dr} depends also upon the pulse duration. Therefore, the threshold sensitivity for the dose, which with formulas (14) and (16) can be represented in the form

$$\Pi_d = \frac{\sqrt{\overline{u^2}}}{S_d^V} = \frac{\sqrt{kTC_0}}{A\gamma} c\, 10^5 = \sqrt{\frac{kT\varepsilon\varepsilon_0}{Al}} \frac{c}{\gamma} 10^5 \tag{18}$$

is a universally valid characteristic of pyroelectric radiation detectors. The Π_d value depends upon the property of the pyroelectric material and the geometrical dimensions of the detector. The threshold sensitivity decreases with increasing detector volume (Al). This relation holds as long as the capacity of the pyroelectric radiation detector is not comparable with the input capacity of the circuit. For a selected area A, the optimal detector length is given by the condition that the detector capacitance C_{det} must be equal to the input capacitance of the circuit, C_c:

$$l_{opt} = \frac{\varepsilon\varepsilon_0 A}{C_c}. \tag{19}$$

A dose-related threshold sensitivity close to the minimum is then obtained. It also follows from Eq. (18) that the threshold sensitivity of a detector having a fixed volume does not depend upon whether the detector is a longitudinal or transverse pickup element. Pyroelectric radiation detectors have a uniform angular sensitivity, i.e., they are isotropic detectors.

Let us determine from the signal duration and the signal power the range in which measurements can be made with pyroelectric radiation detectors. Though an analysis using a model system with lumped parameters does not allow the determination of the inertia of pyroelectric radiation detectors (the inertia is given by the rate at which spontaneous polarization is established), investigations of laser pulses have shown that the limit inertia is of the order of 10^{-10} sec [7]. Since the γ radiation is absorbed by the bulk of the detector, an extremely fast response can be expected in this case from pyroelectric radiation detectors.

The upper limit of the durations which still can be detected is given by the time constant τ_t, which amounts to several seconds.

The lower limit of the range of dose rates which can be measured is given by the threshold sensitivity of the pyroelectric radiation detector. In the case of a 1-cm^3 barium titanate pyroelectric radiation detector, the dose sensitivity is 10^{-1} rad. The upper limit is given by the nonlinearity of the characteristics of the pyroelectric radiation detector, i.e., by the pyrocoefficient and the dielectric constant when overheating occurs and when the detector temperature approaches the Curie point. In the case of barium titanate ceramics, constant characteristics are observed up to approximately 60°C and the tolerable overheating can amount to 40°C. By solving the equation (1) of thermal conductivity, one can determine the maximum dose corresponding to a 40°C temperature increase: The dose amounts to about $2 \cdot 10^6$ rad.

Thus, the range in which doses can be measured with pyroelectric radiation detectors encompasses seven orders of magnitude. The range of the dose rates which can be measured depends upon the range of dose measurements and the pulse duration. The range of dose rates which can be measured in a pulse is extremely wide: It ranges from 10^{-1} to 10^{15} rad/sec.

Pyroelectric radiation detectors have been used to measure a γ-radiation pulse which increased within about 1 sec to the 95% value and had a dose rate of up to 1300 rad/sec. The measurements were made in dose-rate recording operation and in a mode of operation in which the total of the dose accumulated during the pulse time was determined. Figure 1 shows oscillograms of the signals recorded. The Coulomb-rad sensitivity was obtained when a dose of $2 \cdot 10^{-13}$ C/rad was recorded with a detector capacitance of $2 \cdot 10^{-9}$ F. The sensitivity value corresponds to that calculated with formula (15), and this attests to the pyroelectric origin of the signal measured.

The type of detector considered opens new possibilities of measuring ionizing radiation. It will be possible to determine both dose and dose rate, and the duration of γ radiation pulses.

LITERATURE CITED

1. L. S. Kremenchugskii, Seignette-Electric Radiation Detectors [in Russian], Naukova Dumka, Kiev (1971).
2. L. S. Kremenchugskii, Pyroelectric Detectors [in Russian], Preprint In-ta Fiz. Akad. Nauk UkrSSR, Kiev (1972).
3. D. Hester, D. Glower, and L. Overton, IEEE Trans. Nucl. Sci., 11, 145 (1964).
4. D. Glower and D. Hester, Trans. Amer. Nucl. Soc., 8, 66 (1965).
5. D. Hester and D. Glower, Nucl. Appl., 2, 41 (1936).
6. S. P. Solov'ev and I. I. Kuz'min, Izv. Akad. Nauk SSSR, Ser. Fiz., 34, No. 12, 2604 (1970).
7. C. Roundy et al., Opt. Commun., 10, No. 4, 374 (1974).

DEPOSITED ARTICLES

CHOICE OF OPTIMAL DIMENSIONS FOR A SYNCHROTRON
BREMSSTRAHLUNG TARGET

V. A. Vizir', B. N. Kalinin,   UDC 539.121.8
V. M. Kuznetsov, and P. P. Krasnonosen'kikh

The present article proposes some methods for raising the efficiency of an electron synchrotron when used for obtaining several simultaneously operating bremsstrahlung beams.

Bremsstrahlung beams are produced in a synchrotron by decelerating electrons on internal targets, set at various azimuths. Targets of thickness 0.1-0.2 rad units are usually employed, and the electrons pass through the target only once. Under real conditions, the ouput of collimated photons does not increase appreciably when the target thickness is increased. It is a very complicated matter to arrange for the simultaneous operation of two targets, since the division of the beam between them depends very critically on the radial positioning of the targets, and, moreover, the targets must be set at specific azimuths, which is not always possible, given the way the equipment itself is arranged.

Use of thin (~0.01 rad units) targets enables us to achieve multiple passage of the electrons. For filament targets of diameter d, comparable with the rotation step h_c of the electrons on account of the synchrotron radiation, the probability of electrons encountering the target is

$$P = q \sum_{0}^{n} (1-q)^n,$$

where $q = (1 - \nu_r) d/n_c$; $n = (0-[\nu_r/(1 - \nu_r)])$; ν_r is the frequency of radial betatron oscillations.

By applying a combination of thin or filament targets we can obtain several simultaneously operating bremsstrahlung beams with intensities which can be well regulated. The total intensity, however, will not be greater than from a single thick target (~0.1-0.2 rad units).

The combined operation of a diamond (thin) and a thick target enables us to obtain a coherent photon beam (from the diamond) and at the same time a beam from the amorphous target. In this case the electrons are first incident on the diamond target, and, after further rotation, on the thick target. Moreover, the overall output of bremsstrahlung radiation is increased by 30-50%.

The proposed methods have been tested experimentally, and are in use in the Tomsk synchrotron. This has allowed us to increase the efficiency of the synchrotron by 40-50%.

(No. 865/8274. Paper submitted April 7, 1975.
Complete text 0.35 Author's Folios, 3 Figures, 3 References.)

THE ROLE OF NUCLEAR CASCADES IN THE FORMATION
OF NEUTRONS IN Pb, Cd, Fe, Al AND FISSION OF LEAD
NUCLEI BY THE ACTION OF COSMIC RADIATION AT
VARIOUS DEPTHS BELOW THE EARTH

V. A. Zyabkin and R. M. Yakov'lev

UDC 539.591.550.35

The paper considers the rate of formation of neutrons in Pb, Cd, Fe, Al and the rate of fission of lead nuclei by the action of cosmic radiation over a range of depths from sea level to 1000 m of water equivalent (m.w.e). In the calculations, the nuclear-active components of the cosmic radiation are assumed to be high-energy μ mesons and slow μ^- mesons. The processes leading to the formation of neutrons and the fission of
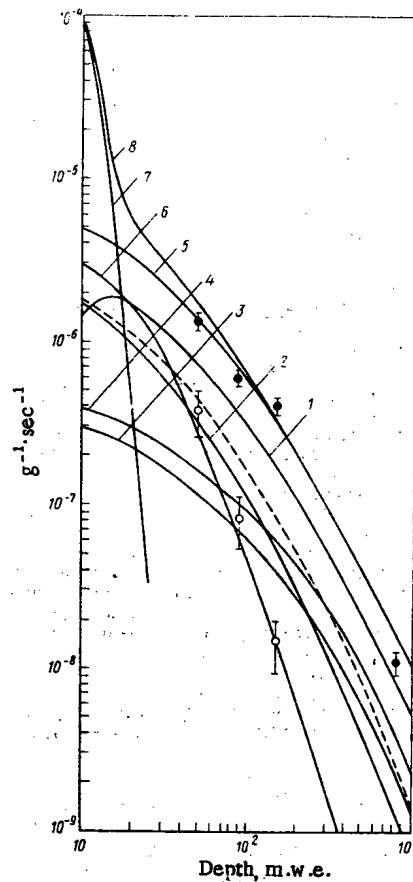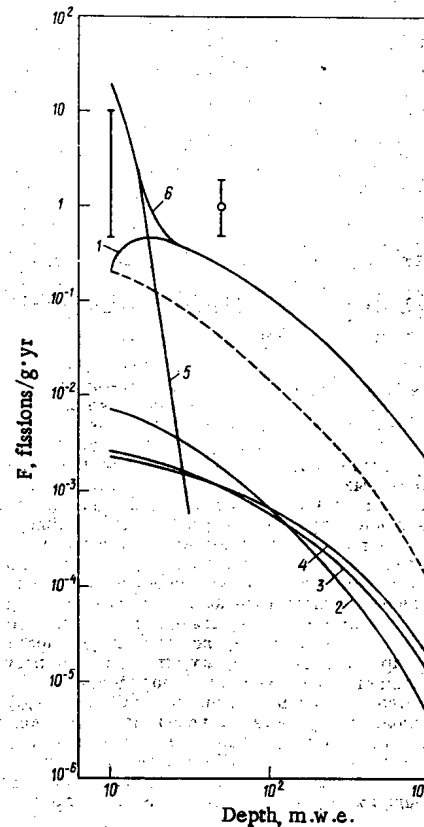
Fig. 1   Fig. 2

Fig. 1. Rate of formation of neutrons in lead as a result of various processes (sea level is assumed to be at 10 m.w.e.): 1) Direct interaction (---- calculation without taking account of nuclear cascades [2]); 2) δ electrons; 3) pairs; 4) bremsstrahlung; 5) total rate of formation by the action of high-energy μ mesons; 6) slow μ^- mesons; 7) nuclear-active component; 8) total rate of formation by the action of cosmic rays; ●, ○) rate of formation by the action of high-energy μ mesons and slow μ^- mesons, respectively [3-5].

Fig. 2. Rate of fission of lead, as a result of various processes: 1) direct interaction (---- calculation without taking account of nuclear cascades [5]); 2) δ electrons; 3) bremsstrahlung; 4) pairs; 5) nucleon component; 6) total rate of fission by the action of cosmic rays, ○) results of [6, 7].

819

nuclei by the action of high-energy μ mesons include the direct interaction of the electromagnetic field of the μ meson with the nucleus, the formation of δ electrons, bremsstrahlung radiation of μ mesons and pair formation. The calculation of the direct interaction is carried out by Hand's model [1], taking into account secondary nuclear-cascade processes. The results of the calculations are compared with experimental data (Figs. 1 and 2).

The conclusion is drawn that at underground locations, positioned at a depth of more than 100 m.w.e., cosmic radiation as a source of the neutron background is insignificant in comparison with the neutron radiation due to natural radioactivity of the surrounding rocks of the granite type.

LITERATURE CITED

1. L. Hand, Phys. Rev., 129, 1834 (1963).
2. G. V. Gorshkov and V. A. Zyabkin, At. Énerg., 34, No. 3, 210 (1973).
3. G. V. Gorshkov and V. A. Zyabkin, Yad. Fiz., 7, 770 (1968).
4. G. V. Gorshkov and V. A. Zyabkin, Yad. Fiz., 12, 340 (1970).
5. G. V. Gorshkov, V. A. Zyabkin, and R. M. Yakovlev, Yad. Fiz., 13, 791 (1971).
6. G. N. Flerov et al., Preprint JINR D6-4554, Dubna (1968).
7. G. N. Flerov and V. P. Perelygin, At. Énerg., 26, No. 6, 520 (1969).

EFFECT OF THERMOMECHANICAL PROCESSING ON THE
AMPLITUDE-DEPENDENT INTERNAL FRICTION OF URANIUM

A. I. Stukalov, G. S. Gaidamachenko,
and A. V. Azarenko

The effect of thermomechanical processing on the parameters of the dislocation structure of uranium in two compositions (0.8 at. % Fe + 0.13 at. % Si and 0.06 at. % Fe + 0.18 at. % Si) having approximately identical content of other impurities, was investigated by means of the method of amplitude-dependent internal friction. The internal friction was measured on a modified apparatus, the construction of which has been described previously [1]. The results were processed by means of the theory introduced by Granato and Lücke [2].

It is shown that the annealing of uranium at 820°C over 10 h, with subsequent quenching in water, leads to a reduction of the dislocation density by a factor of 10 approximately and to an increase of the lengths of dislocation segments by 30% approximately. With subsequent induction β-quenching of uranium (740°C) in water, as well as deformation at room temperature, the dislocation density is increased and the length of the dislocation segments is decreased. Annealing at 620°C over 2 h reduces the dislocation density to $8 \cdot 10^8$ and $7 \cdot 10^9$ cm^{-2} in uranium of the first and second composition, respectively.

The paper shows the dependencies of the internal friction on the deformation amplitude and the logarithm of the product of the amplitude-dependent part of the internal friction; the deformation amplitudes on the reciprocal of the deformation amplitude, and also the dependence of the dislocation density and the lengths of dislocation segments on the parameters of the treatments used. Analysis of these dependences permits the conclusion to be drawn that the silicon atoms fix the dislocations in uranium to a greater degree than the iron atoms. Therefore, processes of dislocation multiplication (during quenching and deformation) and their disappearance (during annealing) in uranium of the second composition, take place more intensely than in uranium of the first composition.

LITERATURE CITED

1. V. E. Ivanov, B. I. Shapoval, and V. M. Amonenko, Fiz. Met. Metalloved., 11, No. 1, 52 (1961).
2. A. Granato and K. Lücke, J. Appl. Phys., 27, 583, 789 (1956).

TWO METHODS OF DETERMINING FUEL
BURNUP BY γ SPECTROMETRY

L. I. Golubev, L. I. Gorobtsov,
V. D. Simonov, and M. A. Sunchugashev

Fuel burnup in the fuel elements of the first and second assemblies of the NVAÉS was determined by measuring the absolute activities of ^{137}Cs and ^{106}Ru by semiconductor γ spectrometry. The error of the method was ~±10%.

Experiment showed that the amount of ^{137}Cs formed is directly proportional to the fuel burnup, but the amounts of ^{106}Ru and ^{134}Cs are nonlinear functions of burnup. For example, the amount of ^{134}Cs formed depends quadratically on the fuel burnup, and in the present measuring this dependence can be described by the expression $n(^{134}Cs) = 5.41 \cdot 10^{-15} \rho^2$, cm^{-3}. In addition the amount of ^{106}Ru formed depends on the fuel enrichment.

Thus, the ratio of the ^{134}Cs and ^{137}Cs activities is also directly proportional to the fuel burnup; i.e., $\rho = (16.6 \pm 0.9)\eta$ kg/ton of U, where η is the ratio of the ^{134}Cs and ^{137}Cs activities. This expression is valid for burnups of 5-26 kg/ton of U in fuel which is enriched in ^{235}U (Fig. 1).

The experimental points for fuel assembly 3 are shifted parallel to the horizontal axis. This can evidently be accounted for by the fact that during the burnup of fuel which is more than 30-40% enriched and is irradiated more than 3 yr (assembly 3 was irradiated more than 5 yr) the rate of formation of ^{137}Cs as a result of the depletion of fissionable isotopes decreases, while the buildup of ^{134}Cs continues at the original rate due to inleakage of neutrons from neutrons from neighboring assemblies where the burnup is smaller.

Fuel burnup can be determined more accurately by the method of isotopic ratios since it does not use fission product yields, decay constants, or γ intensities with their attendant errors. In addition, the areas of the photopeaks, the corrections for the decay and burnup of fission products, and γ self-absorption factors in the fuel are used as ratios.

The error of the method can be reduced to ±5%, but calibrations using the absolute activities of ^{137}Cs and ^{106}Ru or destructive methods are required.
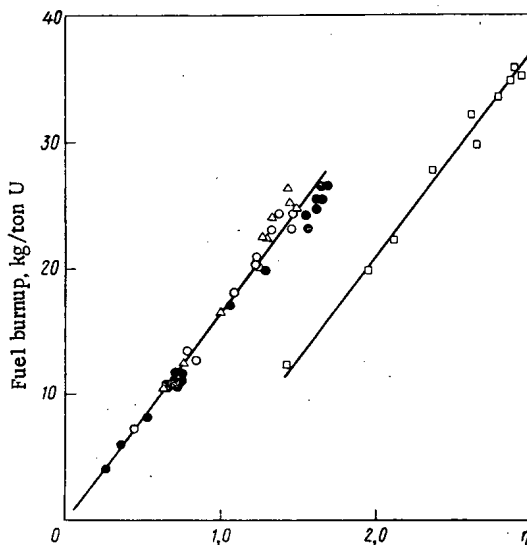

Fig. 1. Fuel burnup as a function of the ratio of the ^{134}Cs and ^{137}Cs activities in various fuel assemblies: O) 1; Δ) 2; □) 3; ●) 4, 5.

SINGULAR EQUATIONS AND CONDITIONS OF SOLVABILITY
OF BOUNDARY PROBLEMS IN THE THEORY OF NEUTRON TRANSFER

B. D. Abramov

The process of neutron transfer in a bounded volume V is considered; the process is described by a multigroup transfer equation, taking into account scattering anisotropy [1]

$$\Omega \nabla \psi + \Sigma \psi = \sum_{l=0}^{M} \frac{2l+1}{4\pi} A_l \int d\Omega' P_l (\mu_0) \psi (x, \Omega') + h,$$

(1)

where Σ and A_l are quadratic matrices; $\psi(x, \Omega)$ is a column vector, the components of which (neutron fluxes) in the corresponding energy groups at the point $x = \{x_1, x_2, x_3\}$ are directed along $\Omega = \{\Omega_1, \Omega_2, \Omega_3\}$; $h(x, \Omega)$ is some given vector with absolutely integrable components. It is assumed that the volume V consists of a finite number of sections (within the limits of each, the matrices of coefficients Σ and A_l are constant) bounded by piecewise-smooth surfaces of the class $C^{(1)}$ [2].

The solution of Eq. (1) is sought in the class of vector functions $\psi(x, \Omega)$ which are absolutely integrable on $V \times V_\Omega$ and which, for almost all values of x, $\Omega \in \overline{V} \times V_\Omega$, satisfy the following boundary condition at the external surface Γ of the volume V

$$\psi (x, \Omega) = f(x, \Omega), \quad \Omega n(x) < 0, \quad x \in \Gamma$$

(2)

and the condition of flux continuity at the boundaries between the sections. Here V_Ω is the set of directions Ω; $n(x)$ is the unit vector along the external normal to Γ; $f(x, \Omega)$ is a given vector function with absolutely integrable components. In the case of a concave volume, the "leaking" neutrons are included when determining $f(x, \Omega)$ in the usual manner.

It is shown that the solvability of the boundary problem in Eqs. (1)-(2) in the given class of vector functions is equivalent to the solvability of a specified system of singular integral equations with additional conditions relating the values of the flux at the section boundaries and at the external surface.

For example, if the scattering is isotropic, the volume is homogeneous and convex, and the problem involves only a single velocity ($\Sigma = 1$, $A_0 = c > 0$, $c \neq 1$, $h = 0$), the equation obtained is as follows

$$\lambda (\Omega s) g (s, \Omega s, \Omega) + (\Omega s) \frac{c}{4\pi} \int d\Omega' \frac{g (s, \Omega s, \Omega')}{(\Omega - \Omega') s} = 0,$$

(3)

where

$$s = \{s_1, s_2, s_3\}, \quad |s| = 1; \quad \Omega s = \Omega_1 s_1 + \Omega_2 s_2 + \Omega_3 s_3;$$

$$\lambda (\omega) = 1 - \frac{c\omega}{2} \int_{-1}^{1} \frac{d\mu}{\omega - \mu};$$

$$g (s, \omega, \Omega) = - \int_{\Gamma} d\gamma \Omega n (x) e^{sx/\omega} \psi (x, \Omega);$$

$d\gamma$ is an element of the surface Γ. The necessary and sufficient condition for the solvability of the boundary problem considered in this example is that, for each s and all $\Omega s \neq 0$, Eq. (3) be solvable under the following conditions:

a) $g(s, \Omega s, \Omega)$ is a holomorphic function of the variable $\Omega s \neq 0$ for all s, and depends only on s and Ωs;

b) if $\pm \omega_0$ are zeros of the function $\lambda(\omega)$, then

$$\int d\Omega \frac{g (s, \pm \omega_0, \Omega)}{\pm \omega_0 - \Omega s} = 0.$$

The relations obtained may be used to develop numerical methods for calculations in nuclear reactors. They are derived without formulating any solutions of the transfer equation itself.

LITERATURE CITED

1. G. I. Marchuk, Methods for Nuclear-Reactor Calculations [in Russian], Gosatomizdat, Moscow (1961).
2. V. S. Vladimirov, "Mathematical problems of single-velocity theory of particle transfer," in: Proceedings of the V. A. Steklov Mathematical Institute [in Russian], Vol. 61, Izv. Akad. Nauk SSSR, Moscow (1961).

LETTERS TO THE EDITOR

INTERPRETATION OF INSTRUMENT LINES OF AN IONIZATION PULSE SPECTROMETER SUITABLE FOR MICRODOSIMETRY

V. A. Pitkevich and V. G. Videnskii

UDC 539.125.5.164.07

The statistical distribution function of the radiation energy absorbed in the volume of a tissue-equivalent material of dimensions 10-100 nm is measured by means of a tissue-equivalent proportional counter [1-3]. Here, the mean energy of ion-pair formation is used for energy calibration [4, 5]. This procedure is incorrect since it involves the use of a mean value for the measurement of the statistical distribution and, in addition, the mean energy of ion formation depends on the energy and type of the charged particles falling in the sensitive volume of the counter [6, 7]. A more satisfactory procedure, especially when the volume of the material has dimensions 10 nm and, accordingly, the number of ionizations is low, is to obtain from the equipment spectrum not the distribution of the absorbed energy but the distribution function for the number of ion pairs formed in the sensitive volume of the counter.

The proposed method of interpretation employs the ideas of a characteristic function of random quantities and of the response function of the spectrometer to one ion pair $\varphi_1(u)$. We write the pulse amplitude of the instrument spectrum as $f_\Delta(u)$. There is a probability $f_1(u)$ that a voltage pulse in the range $(u, u + du)$ will appear at the spectrometer output when a single pair of ions is formed in the detector. The response function depends on the fluctuations of the gas-amplification coefficient of the proportional counter and the noise properties of the spectrometer, and incorporates all these factors. In the conditions being considered, the avalanche discharges from each ionization may be regarded as statistically independent. In this case, the pulse amplitude at the spectrometer output when k ionizations occur in the counter will be equal to the sum of the pulse amplitudes of each ionization. Here it is necessary to take into account that the spectrometer response function for k pairs of ions may be written in the form of a k-fold packet of the response function $\varphi_1(u)$.

We wish to find the quantity P_k, the discrete distribution of the probability of formation of k pairs of ions. The instrument spectrum of the ionization spectrometer can be written in the form

$$f_\Delta(u) = P_0 \delta(u) + \sum_{k=1}^{\infty} P_k \varphi_1^{*(k)}(u). \tag{1}$$

Using the Fourier transform for Eq. (1), we obtain the following expression for the characteristic function $\chi_\Delta(t)$ of the random quantity $\tilde{u}$ ($\tilde{u}$ is the pulse amplitude at the spectrometer output when an arbitrary number of ion pairs is formed in the detector)

$$\chi_\Delta(t) = P_0 + \sum_{k=1}^{\infty} P_k \int_0^\infty e^{itu} \varphi_1(u)^{*(k)} du = P_0 + \sum_{k=1}^{\infty} P_k \xi_1^k(t), \tag{2}$$

where $\xi_1(t)$ is the characteristic function of a random quantity; $\tilde{u}_1$ is the pulse amplitude for one ion pair.

Taking into account that the number of ionizations is small, the series in Eq. (2) may be cut off at the m-th term, where m is easily determined from the mean energy of ion formation. Then we use the relation between the initial moments of the random quantities and the values of the derivative of the characteristic function for $t = 0$. We obtain

$$\chi_\Delta^{(i)}(t)|_{t=0} \approx \sum_{k=1}^{m} P_k [\xi_1^k(t)]^{(i)}|_{t=0}; \quad i = 0, 1, \ldots, m. \tag{3}$$

Equation (3) represents an m-th order system of linear equations in P_k. The matrix of the system depends on the initial moments β_r of the random quantity $\tilde{u}_1$. Therefore it may be calculated in advance from the known spectrometer response function for one ion pair, and serves as a basic characteristic of the spectrometer.

824

TABLE 1. Error Matrix of System

Case No. *	Error, %				
	Matrix elements				
1	0,184	0,184	0,184	0,184	0,184
2	0,279	0,279	0,279	0,279	0,279
1	0,295	0,047	0,066	0,131	0,172
2	1,38	1,07	0,932	0,852	0,800
1	3,63	1,65	0,889	0,501	0,271
2	6,01	3,56	2,62	2,14	1,86
1	15,0	6,58	3,66	2,29	1,52
2	20,1	10,0	6,49	4,83	3,90
1	43,2	17,9	9,71	6,07	4,11
2	52,9	23,7	14,2	9,86	7,53
	Independent terms				
1	0,153	0,182	1,15	6,17	17,3
2	0,588	1,64	4,20	9,67	19.4

*For case No. 1, $\lambda = 0.4$; for case No. 2, $\lambda = 1$.

TABLE 2. Solution of System of Linear Equations for Interpretation of Instrument Spectrum

Case No. *	k					
	0	1	2	3	4	5
	Calculational error, %					
1	0,22	3,1	29	190	850	2330
2	0,50	1,8	3,4	1,5	23	55
	Probability, %					
1	67,0	26,8	5,36	0,72	0,07	0,006
2	36,8	36,8	18,4	6,1	1,5	0,3

*For case No. 1, $\lambda = 0.4$; for case No. 2, $\lambda = 1$.

The independent terms in Eq. (3) are the initial moments α_r of the equipment spectrum. Since the general expressions for the elements are complicated, we give, as an example, only the result for m = 5

$$a_{0k} = 1; \quad a_{1k} = k_0\beta_1; \quad a_{2k} = k_0\beta_2 + k_1\beta_1^2;$$
$$k = 0, 1, \ldots, 5;$$
$$a_{3k} = k_0\beta_3 + 3k_1\beta_1\beta_2 + k_2\beta_1^3;$$
$$a_{4k} = k_0\beta_4 + 3k_1\beta_2^2 + 4k_1\beta_1\beta_3 + 6k_2\beta_1^2\beta_2 + k_3\beta_1^4;$$
$$a_{5k} = k_0\beta_5 + 5k_1\beta_1\beta_4 + 10k_1\beta_2\beta_3 + 10k_2\beta_1^2\beta_3 + 15k_2\beta_1\beta_2^2 + 10k_3\beta_1^3\beta_2 + k_4\beta_1^5;$$
$$k_s = k(k-1)(k-2)\ldots(k-s); \quad s = 0, 1, \ldots, 4.$$

(4)

In order to interpret the equipment spectrum, the process by which it is formed was modelled on a computer using the Monte Carlo method. The initial moments β_r and α_r were obtained directly from a realization of the random quantities $\tilde{u}_1$ and $\tilde{u}$. The values of u_1 were chosen in accordance with $\varphi_1(u_1)$:

$$\varphi_1(u_1) = \frac{2}{\sqrt{\pi}} \sqrt{\bar{u}_1} \exp(-u_1).$$

(5)

The random quantity $\tilde{u}$ was realized according to the expression

$$\tilde{u} = \tilde{u}_{10} + \tilde{u}_{11} + \tilde{u}_{12} + \ldots + \tilde{u}_{1k},$$

(6)

where $\tilde{k}$ is a random quantity obeying the Poisson distribution (say) with mean values $\lambda = 0.4$ and 1 (so that the number of terms in the sum does not exceed 5). To confirm that the terms of the matrices of the system in Eq. (3) and the initial moments of the equipment spectrum had been accurately determined, theoretical values of β_r and α_r were also calculated. The results of the calculation are shown in Table 1. Table 2 shows the error in calculating the probability P_k and, in the lower part, theoretical values of P_k. As is evident from Table 2, the accuracy of determining P_0, P_1, and P_2 is entirely acceptable (the history number is 10^5). The probabilities P_3, P_4, and P_5 are determined with a large error (for $\lambda = 0.4$). This is entirely to be expected, since the larger values of k give the maximum contribution to the higher moments, which in our case are calculated with poor accuracy. This becomes clear if we consider that for a history number 10^5 the numbers of events with k = 3, 4, and 5 are fairly small (720, 70, and 6, respectively). Therefore, if the probability P_k (for some value of k) is very small, the higher moments must be calculated fairly accurately. For $\lambda = 1$, the accuracy of determining P_k is completely acceptable even when the basic higher moments are not very accurately calculated. This can be explained in that, in this case, the probabilities P_k do not differ by too much.

In our opinion, the results given for the interpretation of the instrument spectrum ("measured" by computer) show that the method is very effective.

Thus, we may conclude that, in order to determine the discrete distribution of the probability that a definite number of ion pairs will be formed in the sensitive volume of a proportional counter, it is sufficient to know the initial moments of the equipment spectrum and the spectrometer response function for a single ion pair. In this case, a matrix composed of combinations of the moments of the response function may serve as a basic characteristic of the spectrometer with the proportional counter.

LITERATURE CITED

1. H. Rossi and W. Rosenzweig, Radiology, 64, 404 (1955).
2. D. Srdoć, Radiation Research, 43, 302 (1970).
3. P. N. Belonogii, V. I. Ivanov, and V. A. Pitkevich, in: Problems of Microdosimetry. Proceedings of the 1st All-Union Conference on Microdosimetry [in Russian], Atomizdat, Moscow (1973), p. 72.
4. V. G. Videnskii, V. A. Pitkevich, and V. V. Farnakeev, Med. Radiologiya, 4, 75 (1972).
5. P. N. Belonogii, Candidate's Dissertation [in Russian], Moscow Engineering-Physics Institute, Moscow (1974).
6. W. Stone and L. Cochran, Phys. Rev., 107, No. 3, 702 (1957).
7. A. Cole, Radiation Research, 38, 7 (1969).

PLANNING THE RECONSTRUCTION OF THE ACTIVE
ZONE OF A VVR-M REACTOR

P. M. Verkhovykh, V. S. Zvezdkin,
G. A. Kirsanov, K. A. Kolosov,
K. A. Konoplev, Yu. P. Saikov,
V. N. Sukhovei, T. A. Chernova,
and Zh. A. Shishkina

UDC 621.039.53

The greatest reserve factor available for increasing the power of the VVR-M type of reactor lies in developing the heat-emitting surface area of the fuel elements per unit volume of the active zone. This may be done by reducing the thickness of the fuel elements and the hydraulic diameter of the channels in the heat-emitting (fuel element) assemblies (FEA); however, if the pressure loss in the active zone is to remain intact, this involves worsening the heat-transfer conditions. The increase in the reactor power will not in this case be proportional to the increase in the heat-emitting surface of the fuel elements; hence in determining the reserves it will be essential to take account of all factors associated with the geometrical parameters of the FEA.

Considering that the active zone of the reactor consists of parallel plates of thickness a and height l lying at a distance b from each other, the optimization problem may be reduced to one of finding the geometrical parameters of the FEA corresponding to the maximum value of the functional
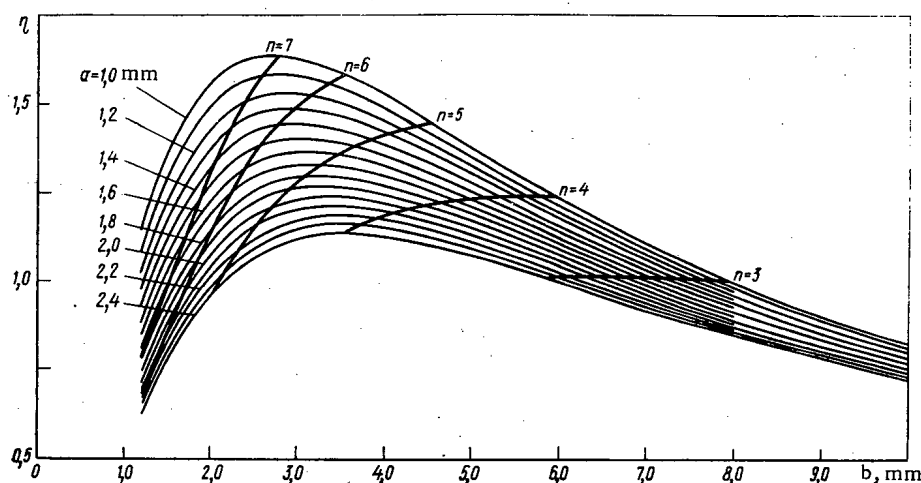

Fig. 1. Relative increase in the power of the VVR-M reactor η as a function of the gap between the fuel elements b for various thicknesses of the fuel elements a.
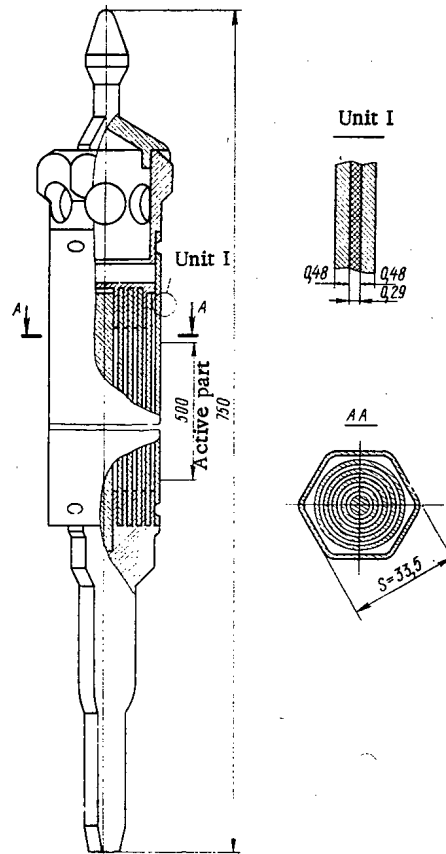
826

Fig. 2. Fuel-element assembly of
the VVR-M3 type.

$$\bar{q}_v = \frac{2q_0}{(a+b)l} \int_0^l f(z)\,dz, \tag{1}$$

constituting the height-averaged volumetric density of energy evolution in the actual thermally stressed channel. Here q_0 is the maximum permissible thermal flux density; $f(z)$ is the known distribution function of energy evolution over the height of the active zone.

The greatest permissible thermal flux density in the reactor may be determined from the conditions of its safe operation. For example, the minimum difference between the saturation temperature t_S and the fuel element wall temperature t_w should be no less than a certain specified quantity Δt:

$$(t_s - t_w)\text{mm} \geqslant \Delta t. \tag{2}$$

In general the difference $t_S(z) - t_w(z)$ in the actual thermally stressed channel is a function of the longitudinal coordinate z, and if this distance reaches a minimum in the cross section with coordinate $z = z_0$ then from condition (2) and the condition for the existence of an extremum we obtain the following equations:

$$\Delta t = t_s(z)\,|_{z=z_0} - t_e - \frac{2q_0}{V\rho cb} \int_0^{z_0} f(z)\,dz - \frac{q_0 f(z)\,|_{z=z_0}}{\alpha}; \tag{3}$$

$$\frac{\partial t_s(z)}{\partial z}\bigg|_{z=z_0} - \frac{2q_0}{V\rho cb} f(z)\,|_{z=z_0} - \frac{q_0}{\alpha} \frac{\partial f(z)}{\partial z}\bigg|_{z=z_0} = 0 \tag{4}$$

where t_e is the temperature of the coolant at the entrance into the active zone; V is the velocity of the coolant in the channels of the FEA; ρ and c are the density and specific heat of the coolant respectively; α is the heat-transfer coefficient.

Equations (3) and (4) enable us to determine the coordinate of the dangerous cross section z_0 and the maximum thermal flux q_0.

The velocity of the coolant was determined from the equation of pressure loss in the active zone

$$\Delta P_{AZ} = \frac{\rho V^2}{2}\left[\xi_{in}+\xi_{fr}\,l/2b+\xi_{out}+\xi_{lat}\,\frac{1}{(1+a/b)^2}\right],$$

where ΔP_{AZ} are the pressure losses in the active zone; ξ_{in} and ξ_{out} are the local resistance coefficients at the FEA inlet and outlet respectively; ξ_{fr} and ξ_{lat} are the resistances associated with friction and the reactor lattices.

The $t_s(z)$ relationship was determined from the known relationship between the saturation temperature and the pressure (itself depending on the coordinate), viz, $t_s[P(z)]$, where

$$P(z)=P_0+\rho g\,(H_0+z)-\frac{\rho V^2}{2}\,(\xi_{in}+\xi_{fr}\,z/2b+1).$$

Here g is the gravitational acceleration; P_0 is the atmospheric pressure; H_0 is the depth of reactor pool. Equations (3) and (4) were solved and $\bar{q}_v$ determined from Eq. (1) with the aid of an electronic computer.

Since the functional relationships for the thermal and hydraulic processes in annular gaps and plane-parallel slots are identical, the results of calculations carried out for plane fuel elements are also valid for the VVR-M reactor fuel elements of tubular construction.

Figure 1 shows the dependence of the relative increment in the power of the VVR-M reactor on the geometrical parameters of the fuel elements:

$$\eta = \bar{q}_v/\bar{q}_{v0},$$

where $\bar{q}_{v0}$ is the volumetric density of energy evolution (averaged with respect to height in the actual thermally stressed channel) for an FEA of the VVR-M2 type [1] as at present used in the VVR-M reactor.

The calculations were carried out for a water temperature of 50°C at the entrance into the active zone, in the absence of rarefaction between the reactor lattices and on the assumption that the maximum wall temperature of the fuel element equalled the water saturation temperature.

Of the whole set of possible tube thicknesses and intertube gaps in the VVR-M reactor we may only choose those which ensure conservation of the unit cell dimensions of the active zone as determined by the construction of the reflector and the step of the reactor lattices. Subject to this condition, for a specified number of tubes in the assembly the relationship between the tube thickness and the gap is uniquely determined from geometrical considerations. Figure 1 contains a set of lines corresponding to fuel elements with different numbers of coaxial tubes in the set (n).

It follows from Fig. 1 that the greatest gain in reactor power is obtained by rising six-tube FEA with a fuel-element thickness of 1.2-1.4 mm. We accordingly made some new six-element assemblies of the VVR-M3 (Fig. 2) and VVR-M4 types consisting of an outer fuel element (a hexagonal tube with a gauge diameter of 33.5 mm), four tubular fuel elements with outer diameters of 11.1, 16.7, 22.3, and 27.9 mm, and a central rod-type fuel element of diameter 5.5 mm. The diameter of the fuel in the rod was 1.8 mm.

The VVR-M4 type of assembly only differs from the VVR-M3 by having a break of 100 mm in the fuel in the middle section of the fuel elements in order to increase the flux density of the thermal neutrons in the region of the individual horizontal channels. As fuel we used a uranium—aluminum alloy with a uranium content of 23.5 wt. %. The can material was aluminum alloy SAV-1. The following table gives the comparative characteristics of the VVR-M2 and VVR-M3 types of FEA respectively.

Thickness of tubular fuel element walls, mm	2.5; 1.25
Thickness of cladding layer, mm	0.9; 0.48
Thickness of active layer, mm	0.7; 0.29
Length of active layer, mm	500; 500
Hydraulic diameter, mm	6; 3.1
Heat take-off surface area per unit volume of the active zone, cm^{-1}	3.62; 6.6
Metal/water ratio	0.816; 0.728
Amount of ^{235}U in active zone, g/liter	61.2; 67.9
Amount of ^{235}U per unit heat take-off surface, g/m^2	166; 103
Enrichment with ^{235}U, %	36; 90
Year of initiation	1963; 1972 (experimental part)

The hydraulic characteristics of the VVR-M3 type of FEA were measured in a hydraulic test-bed using the method of [2]. The average hydraulic resistance of the set of new FEA for a water velocity of 2.5-3.0 m/sec was 6.85 ± 0.10, which was 1.57 times greater than that of the VVR-M2 type of FEA [2].

Thermal calculations based on the experimental results confirm the possibility of reconstructing the VVR-M reactor, with its power increased to 30 MW, by using the new FEA and increasing the power of the heat exchangers and cooling systems; they also show the possibility of installing the new FEA in the active zone of the reactor together with FEA of the VVR-M2 type.

The efficiency of the new (especially thin-walled) fuel elements is primarily determined by the hermetic state of the cans. For the VVR-M2 fuel elements the contribution of surface contamination to the activity of the coolant is negligibly small ($\sim 3\%$), which corresponds to an equivalent amount of ^{235}U per unit surface of $(3 \pm 1) \cdot 10^{-10} \text{ g/cm}^2$ [3]. The increase in ^{235}U enrichment by a factor of 2.5 in the new fuel elements increases the contribution of the surface contamination by a factor of four as compared with the VVR-M2 fuel elements. The equivalent ^{235}U content per unit surface of the new fuel elements was determined from the rate of entry of fission fragments into the coolant of a loop channel of fuel elements with zero burn-up; it amounted to $(7 \pm 2) \cdot 10^{-10} \text{ g/cm}^2$.

The main contribution to the fragment activity of the coolant arose from the worsening of the hermeticity of the fuel elements as burn-up proceeded. Three batches of fuel elements made at different times were tested. Those of the VVR-M3 and VVR-M4 types were tested in the active zone of the VVR-M reactor together with VVR-M2 fuel ements at a reactor power of 16 MW. Although 19 FEA were placed in the zone.

An analysis of the systematic monitoring of the hermeticity of the fuel elements in the active zone of the reactor over the whole period of use of the new fuel elements showed that, on placing VVR-M3 and VVR-M4 assemblies in the active zone to the extent of 8.7% of the total number of assemblies, the fission activity of the coolant did not increase at all but remained at the usual level (10^{-6} Ci/liter with respect to ^{85m}Kr, ^{87}Kr, ^{88}Kr, ^{135}Xe, ^{138}Xe) for fuel burn-ups of 0-70% in the new elements. Defining the nonhermeticity β as the ratio of the fragment leak rate to the rate of fragment formation, we may estimate the upper limit for the new fuel elements by considering the rate of entry of the fragments into the reactor coolant at the instant at which the maximum number of new fuel elements occurs in the active zone, allowing for errors committed in measuring this rate (2σ).

By considering the iodine isotopes we find that, if only one assembly is leaking, then $\beta = 40 \cdot 10^{-7}$; if all are leaking to the same extent the value is $2 \cdot 10^{-7}$. In the case of four assemblies we traced the changes in nonhermeticity during the period of burn-up by periodically removing the elements from the active zone and testing in the loop channel. The results convinced us that the nonhermeticity of the new elements was at the same level as that of the VVR-M2 type.

Experimental service of the VVR-M3 and VVR-M4 fuel elements in the reactor confirmed their high efficiency up to the maximum burn-up achieved (78%), which corresponds to a fission density in the interior of the fuel composite of $1.45 \cdot 10^{21} \text{ cm}^{-3}$. The successful reactor tests create a realistic basis for modernizing the VVR-M reactor by using the new fuel elements and increasing the reactor power to 30 MW.

The authors wish to thank D. M. Kaminker for constant support and also Yu. P. Semenov and B. S. Razov for constant help in the execution of this work.

LITERATURE CITED

1. D. M. Kaminker and K. A. Konoplev, 3rd Geneva Conference, Paper No. 235 (1964).
2. G. A. Kirsanov et al., At. Énerg., 39, No. 5, 320 (1975).
3. N. G. Badanina, K. A. Konoplev, and Yu. P. Saikov, At. Énerg., 32, No. 4, 316 (1972).

ANALYSIS OF ON — OFF ZONAL REACTOR CONTROL SYSTEMS

E . V . Filipchuk, V . T . Neboyan,
and P . T . Potapenko

UDC 621.039.562:621.039.512.45

Constant-speed servodrives are predominantly used in automatic control systems of power distribution in reactor cores. Speed control is usually hampered by the fact that the servodrive operates under fundamentally different conditions when moving the rods up than when moving them down. For example, all rods of the RBMK reactor have a constant-speed drive. Thus, technical realization of the required control necessitates the design of multidimensional on — off systems.

Here we describe an engineering design method for systems with specified quality characteristics in reactors with stable power distribution. The system consists of n identical on — off controllers evenly spaced in the core region where power is uniformly distributed (in the control region). The detectors and control rods of local controllers are placed at the nodes of a square or triangular lattice. According to the adiabatic approximation, the relation between the vector and neutron flux deviations from the specified values (settings) $n = (n_1, n_2, \ldots, n_m)^T$ as sensed by the detectors, and the vector of external effects produced by the rods $\Delta k = (\Delta k_1, \Delta k_2, \ldots, \Delta k_m)^T$ is given by the equation

$$n = H(p) \Delta k,$$

(1)

where H (p) is the reactor transfer matrix

$$H(p) = W_0(p) A.$$

(2)

The transfer function of a point reactor $W_0(p)$ and the static matrix A are found either experimentally or calculated.

The analysis of the system in a power distribution stabilization mode can be considerably simplified considering the limited interaction of local on — off regulators. Accordingly, local reactivity perturbations, caused for example by overloading or by the introduction of various instruments into the core, are assumed to be taken care of only by local controllers adjacent to the point of perturbation. In this case, the number of interacting controllers is five for a square lattice and seven for a triangular lattice.

Such an assumption is valid for the following reasons. For nuclear safety reasons the number of simultaneously shifted rods is restricted by appropriate interlocking. The deformation of the neutron field caused by a local reactivity perturbation decays with distance from the perturbation point. Because of the presence of a dead zone, distant local controllers do not take part in control. Thus, the synthesis of the entire system is reduced to calculating a small number of interacting controllers with central symmetry.

Let the subscript 1 denote the center controller. The, considering the symmetry and uniformity of the neutron field in the control zone, we have from Eq. (1):

$$n = C(p) \Delta k,$$
$$\text{where } n = (n_1, n_2)^T; \quad \Delta k = (\Delta k_1, \Delta k_2)^T;$$
$$C(p) = \begin{pmatrix} C_{11}(p) & C_{12}(p) \\ C_{21}(p) & C_{22}(p) \end{pmatrix} = \begin{pmatrix} a_{11} & a_{12}(m-1) \\ a_{21} & a_{22}+2a_{23} \end{pmatrix} W_0(p).$$

(3)

Figure 1 shows an equivalent block diagram of a control system based on Eqs. (3), where $D_{1,2}(p)$, $R_{1,2}(p)$, and $B_{1,2}(p)$ are transfer functions of the detector, the controller, and the drive with control rod. If the matrix elements of the linear section of the system have filtering properties, the nonlinear elements F_1 and F_2 can be harmonically linearized for transient fluctuations [2]. In consequence, the characteristic equation of the system becomes
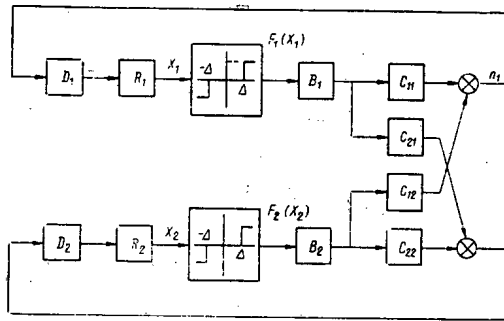
Fig. 1. Equivalent block diagram of control
system.

$$1 + D_1(p) R_1(p) \left\{ B_1(p) C_{11}(p) q(A_1) + \right.$$

$$+ B_2(p) q(A_2) D_2(p) R_2(p) \times \left[\frac{C_{22}(p)}{D_1(p) R_1(p)} + \right.$$

$$\left. \left. + q(A_1) B_1(p) \left(C_{11}(p) C_{22}(p) - C_{12}(p) C_{21}(p) \right) \right] \right\} = 0, \tag{4}$$

where $q(A_1)$ and $q(A_2)$ are the equivalent transfer constants of the nonlinear elements.

Damped "sinusoidal" fluctuations correspond to the complex roots of the characteristic equation. Thus, to find the attenuation index $\xi(A)$ and the frequency $\omega(A)$ let us substitute $p = \xi + j\omega$. An expression relating the fluctuation amplitudes in the center and peripheral channels, A_1 and A_2, can be obtained from the equation of a harmonically linearized system, taking into account that ξ and ω change little with time:

$$A_2 = A_1 \left| \frac{D_2(p) R_2(p) C_{22}(p)}{D_1(p) R_1(p) C_{12}(p)} + \right.$$

$$\left. + D_2(p) R_2(p) B_1(p) \frac{C_{22}(p) C_{11}(p) - C_{12}(p) C_{21}(p)}{C_{12}(p)} q(A_1) \right|. \tag{5}$$

Equations (4) and (5) completely define the quality characteristics $\xi = \xi(A)$ and $\omega = \omega(A)$ as functions of amplitude. These equations can be used to plot quality diagrams that are very useful in the design of such systems.

The design technique is quite general. In particular, the technique is applicable to a control system containing an integral-power controller and several local controllers symmetrically positioned around the circumference of a circle of one radius.

It is evident that the complete scheme of controller arrangement is similar to the scheme of interacting controllers discussed above. Thus, the above design technique can be applied in practice to many variants of this scheme. The validity of assumptions and of the entire technique has been confirmed by the results of analog simulation. If the filtering properties of the system are limited to integrating networks, the result of the synthesis can be regarded as a first approximation which can be corrected, e.g., by digital simulation.

LITERATURE CITED

1. E. V. Filipchuk, P. T. Potapenko, and A. N. Kosilov, At. Énerg., 35, No. 5, 317 (1973).
2. E. P. Popov, Applied Theory of Control Processes in Nonlinear Systems [in Russian], Nauka, Moscow (1973).

EFFICIENCY OF DETECTION OF FISSION FRAGMENTS
BY SOLID TRACK DETECTORS

A. P. Malykhin, I. V. Zhuk,
O. I. Yaroshevich, and L. P. Roginets

UDC 539.107:621.039.564

The absolute and relative efficiency of detection of fission fragments by various solid track detectors must be known for absolute measurement of fission and neutron flux densities, and for comparing the data published by different authors.

The few published data refer mainly to the detection of fission fragments escaping from thin sources, i.e., from sources with a width much less than the mean free path of the fragments $\bar{R}$ in the source material. Practically no data are available for fragments escaping a thick source ($d \gg \bar{R}$).

Accordingly, we have measured the relative detection efficiencies of various track detectors for a thin and thick source and calculated their absolute values. Thick sources used for this purpose are polished natural uranium foils 0.1 mm thick and 5.2 mm in diameter exposed to free air for two weeks. Thin layers were prepared by vacuum deposition of an ~80 μg/cm^2 layer of uranium with a 90% enrichment of ^{235}U. All thin layers were calibrated against the thick sources using fluorophlogopite as a detectors most convenient for counting.

The sources were then formed into two kinds of sandwiches for thick- and thin-source measurements. One type of sandwich consisted of a thick source placed between the studied detector and fluorophlogopite. After exposure and chemical processing of the detectors, the ratio of track densities on the detectors in each sandwich and the obtained values were normalized with respect to macrofol-E taken as unity. The second type of sandwich consisted of a thin source in contact with the studied detector and fluorophlogopite monitor. According to the readings of monitors all track densities were referred to a single flux and normalized as before with reference to macrofol-E track density.

TABLE 1. Detection Efficiency of Fission Fragments by Various Track Detectors

| Detector | Chemical treatment | Thin source | | | Thick source |
		relative detection efficiency	absolute detection efficiency	data of other authors	relative detection efficiency
Macrofol-E	6,25N NaOH; 60° C; 50 min	1	95,2±0,53	(95,2±0,53)%; 6,5N NaOH; 20° C; 50hr[1]	1
Polycarbonate film	6,25N NaOH; 60° C; 50 min	1,01±0,02	96±2	—	1,06±0,01
Natural (capacitor) mica	6,8% HF; 60° C; 120 min	0,89±0,01	85±2	—	0,96±0,01
Synthetic mica (fluorophlogopite)	6,8% HF; 60° C; 20 min	0,91±0,01	87±1	83%; 20%HF; 20° C; 10 min [2]	0,888±0,007
Cover glass (GOST 6672-59)	2% HF; 21° C; 30 min	0,43±0,01	40,9±0,9	(42±6)%; 41% HF; 21° C; 10 min [3] (42±4)%; 2,5%HF; 19° C; 23 min [2] (41±2)%; 2,5%HF; 19° C; 30 min [4]	0,527±0,006
Dacron	6,25N NaOH; 60° C; 60 min	—	—	—	1,03±0,01

The sandwiches were irradiated in a rotating plastic disk in the water reflector of one of critical assemblies at the Institute of Nuclear Power Engineering of the Academy of Science of the BelorussianSSR. After chemical processing the central parts of the detectors were photographed under a microscope; the tracks were counted from photographs with the aid of a marking pen and an electric counter.

The obtained results and the absolute fragments detection efficiency for a thin source, based on the accepted value $\varepsilon = (95.20 \pm 0.53)\%$ for macrofol-E [1] are listed in Table 1. The values of ε for glass and fluorophlogopite thus calculated are in quite good agreement with the results of other authors.

Because of the lack of accurate data on absolute detection efficiency of fragments escaping thick sources, the conversion of measured relative values into absolute is based on the so-called sensitivity constant [5] $k = T/\Phi\bar{\sigma}_f$, where T is the track density on the detector irradiated in contact with a thick source, tracks/cm^2; Φ is the neutron flux, neutrons/cm^2; and $\bar{\sigma}_f$ is the average fission cross section for the given neutron spectrum, cm^2. According to [5], $k = 1.16 \cdot 10^{19}$ tracks/neutron $\cdot$ cm^2 with an error $\pm 3\%$ is valid over a wide range of neutron energies for various thick sources (including pure ^{235}U and ^{238}U) and detectors (lexan, mylar, etc.).

Comparing the above expression with the one derived in [6] for track density on a detector, we find that for a thick source $k = 0.5\,\rho\bar{R}\varepsilon$, where ρ is the source nuclear density, cm^{-3}; and ε is the detector efficiency. For $\bar{R} = 10.25$ mg/cm^2 for ^{235}U [7], corresponding for $\gamma = 18.6$-19.05 g/cm^3 to a linear path of $\sim 5.5\,\mu$, and for $\rho = 4.8 \cdot 10^{22}$, the detection efficiency of fission fragments of the detector used in [5] (lexan) was about 88%. Since lexan and macrofol-E have the same chemical composition and to within 1% the same efficiencies for thin sources [3], the sensitivity constants and absolute efficiencies of our detectors can be evaluated assuming $\varepsilon_{lex} = \varepsilon_{mac-E} = 88\%$. Then, for polycarbonate film (of macrofol type), natural (capacitor) mica, fluorophlogopite, cover glass, and Dacron we get $\varepsilon = 93$, 84, 78, 46, 91% and $k = (1.23, 1.1, 1.03, 0.61, 1.2) \cdot 10^{-5}$ tracks/neutron $\cdot$ b, respectively.

As might be expected, the efficiency of most detectors is lower for thick than thin sources. An exception is cover glass whose efficiency after such normalization increases slightly. Such anomalous behavior of silica glass with changing fragment energy is to a certain degree confirmed by data obtained in [8]. However, it should be noted first that in [8] the detection efficiency is taken to be the quantity (here denoted as $\varepsilon_{[8]}$) T/n, where T is the track density on the detector and n is the surface fission density in a source layer with a thickness d if $d \leq \bar{R}$, and $\bar{R}$ if $d > \bar{R}$. In our work efficiency is defined as $\varepsilon = T/2n\mu$, i.e., the ratio of the number of detected fragments to the number of fragments hitting the detector. Here 2n is the number of fragments formed, and μ is the fraction of fragments hitting the detector so that for $0 \leq d \leq \bar{R}$, $\mu = 0.5\,[1 - d/2\bar{R}]$ [6]. Hence, $\varepsilon \to \varepsilon_{[8]}$ when $d \to 0$ and $\varepsilon = 2\varepsilon_{[8]}$ if $d = \bar{R}$. Thus, the twofold (2.0 ± 0.1) reduction of efficiency of glass when changing from a thin to thick detector, observed in [8], is associated with fragment absorption within the source proper and agrees with the unchanging (in our definition) detector efficiency. In this case, the value $\varepsilon = 40.9\%$ for glass in contact with a thin source should be valid also for a thick source. The values obtained for our set of detectors are respectively (in the order of listing in Table 1) equal to 77.5, 82.1, 74.2, 68.9, 40.9, and 80.0%, i.e., are approximately 12% lower than when normalized in terms of the sensitivity constant. The standard error of such calibration is about 6%.

LITERATURE CITED

1. R. Gold and R. Armani, Nucl. Sci. and Engng, 34, 13 (1968).
2. A. Kapustsik et al., Pribory i Tekh. Éksperim., No. 5, 72 (1964).
3. H. Khan, Nucl. Instrum. and Methods, 98, 229 (1972).
4. M. N. Kondrat'ko et al., At. Énerg., 27, No. 6, 544 (1969).
5. S. Pretre, E. Tochilin, and N. Goldstein, USNRDL-TR-1098, Oct. 1966.
6. A. P. Malykhin et al., Izv. Akad. Nauk BSSR, Ser. Fiz. Énerg. Nauk, No. 2, 16.
7. I. Niday, Phys. Rev., 121, No. 5, 147 (1961).
8. S. N. Kraitor and T. V. Kuznetsova, in: Metrology of Neutron Radiation in Reactors and Accelerators [in Russian], Proc. of the 2nd All-Union Conference, Oct. 14-17, 1974, Vol. 1, Izd. TsNIIatominform, Moscow (1974), p. 146.

LIMITS OF APPLICABILITY OF WEAK-ENRICHMENT APPROXIMATION FOR CASCADE SEPARATION OF TWO-COMPONENT MIXTURES

N. I. Laguntsov, B. I. Nikolaev,
G. A. Sulaberidze, and A. P. Todosiev

The development of new methods, and the elaboration and improvement of existing methods, for the separation of stable isotopic and molecular mixtures, together with the search for means of intensifying the technological processes occurring in the separating equipment, has led to the creation of apparatus with a satisfactorily high separation coefficient. For example, when mass-diffusion elements are used to separate isotopes of a number of low-mass elements (neon, argon) and mixtures of molecular gases (fine screening of substances), the separation coefficient for each element exceeds $\alpha_0 = 1.1$ [1].

Because of the increase in the separation achieved in the elements, it is no longer possible to assume that the enrichment at each stage is small, and this is the assumption which lies at the basis of the known methods for calculations of cascade equipment [2, 3]. As a result, the use of the so-called weak-enrichment approximation for cascade calculations leads to the accumulation of systematic errors both in determining the number of stages and in calculating the efficiency of the equipment. Therefore, it is of fundamental importance to choose the correct calculation procedure, appropriate to the degree of enrichment at each stage.

The theory of cascade calculations for arbitrary enrichment at each stage is now sufficiently well developed [4, 7]. The region of values of α_0 in which the theory of arbitrary enrichment should be used can be determined by comparing results obtained in the weak-enrichment approximation and by the arbitrary-enrichment method. To this end, we analyze a series of calculations for cascades with a given number of stages S, for
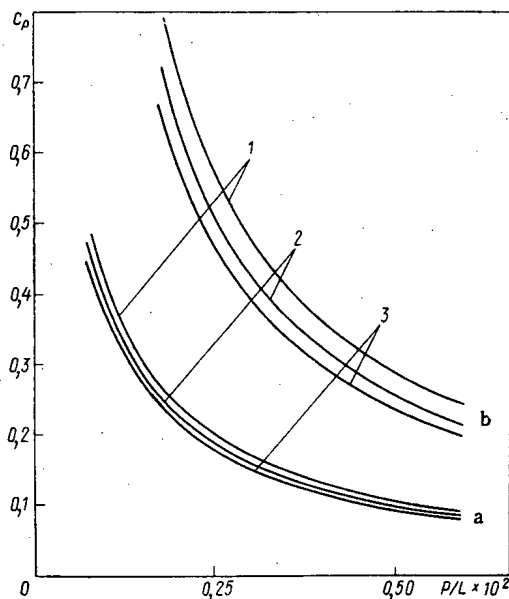

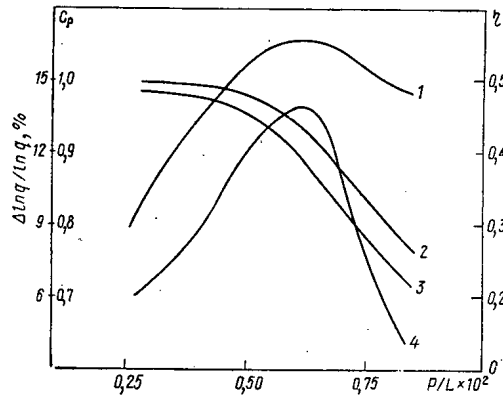Fig. 1. Concentration in outflow as a function of P/L.

834

Fig. 2

Fig. 3

Fig. 2.   Cascade parameters η (1), c_p (2, 3), and $\Delta \ln q / \ln q$ (4) as a function of P/L.
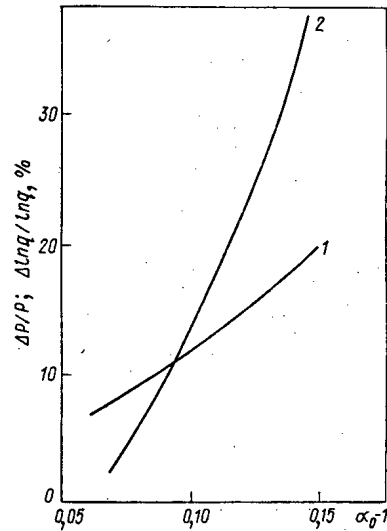
Fig. 3.   Relative deviation of outflow (1) and separation factor (2) as a function of α_0.

different values of α_0 and the ratio of the outflow to the flow entering the stage, P/L. This approach allows us to consider only the simplest case, a cascade of constant width without a waste section.

In the weak-enrichment approximation, the transfer equation in the cascade for the concentration of the light component c can be written in the form [2]

$$\frac{dc}{ds} = \delta - \frac{2P}{L} (c_P - c),$$
(1)

where

$$\delta = \varepsilon c (1 - c)$$
(2)

is the enrichment function; c_p is the concentration in the outflow.

For stages in which separation takes place along a channel (for example, a mass-diffusion separating element), the enrichment coefficient ε is related to the static separation coefficient α_0 and the flux division coefficient θ by the following expression [3]

$$\varepsilon = (\alpha_0 - 1) \frac{1}{\theta} \ln \frac{1}{1 - \theta}.$$

Denoting by c_F the concentration in the feeder reservoir, we write Eq. (1) in the form [2]

$$S = \frac{2}{\varepsilon \varphi} \operatorname{arcth} \frac{(c_P - c_F) \varphi}{(c_P + c_F) \left(1 + \frac{2P}{\varepsilon L}\right) - 2c_P c_F - 4c_P \frac{P}{\varepsilon L}},$$
(3)

where $\varphi \sqrt{1 + 4P/\varepsilon L (1 - 2c_P) + 4P^2/\varepsilon^2 L^2}$.

For known values of the parameters S, θ, α_0, P/L, and c_F, Eq. (3) may be regarded as the equation determining the concentration in the outflow.

For the calculation of the cascade using the method of arbitrary enrichment, the differential equation in Eq. (3) must be replaced by the difference equation [4]

$$c_s - c_{s-1} = \frac{L_{s-1} \theta_{s-1}}{L_s (1 - \theta_s)} \delta_{s-1}^+ + \delta_s^- - \frac{P(c_P - c_{s-1})}{L_s (1 - \theta_s)},$$
(4)

where the enrichment function for the case of separation along a channel $\delta = \delta^-/\theta = \delta^+/1 - 0$ has the form [6]

$$(1-\theta)^{\alpha_0-1}\left(1+\frac{\delta^-}{1-c}\right)^{\alpha_0}=\left(1-\frac{\delta^-}{c}\right).$$
(5)

To solve Eq. (4) by computer, an iterative procedure for the determination of c_P was composed, using the balance equation in a cascade cross section between the feeder reservoir and the first stage of the cacade.

Calculations were carried out in the weak-enrichment approximation and by the method of arbitrary enrichment for several different cascades with various numbers of stages. The value of α_0 was varied in the range 1.07-1.2. In Figs. 1-3, results are shown for a 60-stage cascade separating a mixture with an initial concentration of the valuable component $c_F = 0.01$.

In Fig. 1, the concentration in the outflow is shown as a function of P/L and $\alpha_0 = 1.07$ (a) and 1.2 (b). It is evident that increase in α_0 is accompanied by a marked rise in the difference between the values of c_P given by the method of arbitrary enrichment (curve 3) and the weak-enrichment approximation (curve 1). Also in Fig. 1, results obtained for the cascade using Eq. (4) and an approximate enrichment function are shown (curve 2). Curve 2 permits an analysis of the errors arising in the transition from a difference equation to a differential equation and the use of the approximate enrichment function in Eq. (2). Thus, the effect on the calculated results of passing from an accurate finite difference equation — Eq. (4) -- to an approximate differential equation — Eq. (1) — is evident from a comparison of curves 1 and 2. The difference in the calculated results due to the use of different enrichment functions — passing from the accurate function in Eq. (5) to the approximate function in Eq. (2) — is shown by the relative positions of curves 3 and 2.

It is interesting to note that the divergence of the curves and hence the error in determining the calculated values of the outflow depend on the value of P/L. Therefore it is worthwhile to compare cascades operating in conditions optimal in P/L. As the criterion of optimal operation, we may use the efficiency of the mode, which can be determined in our case as the ratio of the total fluxes of an ideal cascade and a real cascade when producing the same product. For a cascade with a given number of stages, the dependence of the mode efficiency on the parameter P/L is found to have a maximum. Physically, this may be interpreted in the following manner. In conditions of no outflow (P/L = 0), as is known, $\eta = 0$. With increase in outflow, η also rises. However, at a sufficiently large outflow, when the concentration gradient becomes small, the conditions of separation deteriorate, and the efficiency begins to fall. Thus, for a cascade with a given number of stages, the dependence $\eta = f$ (P/L) should have a maximum.

Dependences of the mode efficiency η and the concentration in the outflow c_P calculated by the various methods for $\alpha_0 = 1.1$ are shown in Fig. 2, together with the dependence of the deviation of the separation factor $\Delta\ln q/\ln q$, the value of which is proportional to the error in determining the number of stages. It is interesting that the maximum of the curve for the mode efficiency coincides with the maximum of $\Delta\ln q/\ln q$. From Fig. 2 it is apparent that for $\alpha_0 = 1.1$ the use of the weak-enrichment approximation (curve 2) leads to considerable error in determining the outflow and the number of stages.

In Fig. 3, it is shown that, with change in α_0, the errors $\Delta\ln q/\ln q$ and $\Delta P/P$ increase according to a quadratic law; this is evidently associated with the effect in this region of terms $\sim(\alpha_0 - 1)^2$, which are neglected in the approximate method. The curves are drawn for values of P/L corresponding to maximum mode efficiency.

Thus, it is expedient in cascade calculations to use the theory of arbitrary enrichment. Use of the weak-enrichment approximation is satisfactory only for small values of the static separation coefficient $(\alpha_0 -- 1 \ll 0.1)$, when the systematic error is small. The suggested approximation allows the necessary machine time to be reduced.

LITERATURE CITED

1. I. G. Gverdtsiteli and V. K. Tskhakaya, in: Extraction of Isotopes. Proceedings of All-Union Conference on the Use of Isotopes [in Russian], Izd. Akad. Nauk SSSR, Moscow (1958), p. 113.
2. A. Selecki, Rozdzielanie Izotopow Naturalnych, Warsaw (1965).
3. M. Benedict and T. Pigford, Nuclear Chemical Engineering, McGraw-Hill New York (1959).
4. N. A. Kolokol'tsov and N. I. Laguntsov, At. Énerg., 27, No. 6, 560 (1969).
5. N. A. Kolokol'tsov and N. I. Laguntsov, At. Énerg., 29, No. 4, 300 (1970).
6. N. A. Kolokol'tsov, N. I. Laguntsov, and G. A. Sulaberidze, At. Énerg., 34, No. 4, 259 (1973).
7. N. I. Laguntsov, At. Énerg., 35, No. 3, 205 (1973).

NEUTRON DETECTION WITH HYDROGENOUS DETECTORS

E. A. Kramer-Ageev, A. G. Parkhomov,   UDC 539.1.074.88
V. S. Troshin, and M. I. Shubtsov

One of the important characteristics of the radiation field from a reactor is the spectra of fast and intermediate neutrons. The use of fission and activation detectors provides a measurement of reactor neutron spectrum in the energy region up to 26 keV and above 0.6 MeV. Methods for the measurement of the neutron spectrum in the range 26 keV to 0.6 MeV are either extremely difficult or insufficiently developed [1, 2].

This paper considers the possibility of using double chambers (polyethylene and graphite walls, ethylene and carbon dioxide as the respective gases) or calorimeters (polyethylene — graphite) which, as threshold detectors, measure the absorbed neutron dose in hydrogen. A set of detectors with various effective energy thresholds, including a hydrogenous detector, makes possible a determination of the integral neutron spectrum and subsequently the calculation of the differential spectrum [3]. To calculate the effective threshold cross section by the Grundl — Usner method, [4], a set of test spectra was used that covered practically all the various types: fission spectrum, beam spectra from the BR-5 reactor and from the experimental channels of the IRT-2000 and VVR reactors, the neutron leakage spectrum from a heavy-water and graphite assembly, and the spectrum from the Fermi reactor.

The energy dependence on the maximum deviation of the absorbed neutron dose normalized to the fluence of neutrons with energies above a selected threshold is shown in Fig. 1 for these spectra. Independence of the type of spectrum with an error of less than 10% is ensured by the selection of a detection threshold of 300 keV. The absorbed neutron dose in polyethylene normalized to fluence (threshold, 300 keV) is $4.4 \cdot 10^{-9}$ rad·cm^2/ neutron.

The total absorbed dose from reactor radiation can be measured with an error of 2-5%. The error in the determination of the neutron component of the dose in hydrogen does not exceed 12% when the ratio of the doses in graphite and polyethylene varies from 0.1 to 0.7 [5]. If these errors are considered independent, the accuracy of the determination of fluence or flux density of neutrons with energies above 0.3 MeV will be ~16%.
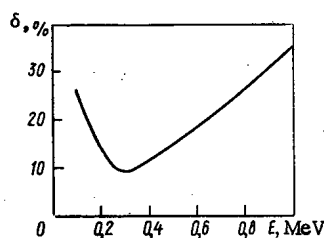

Fig. 1. Dependence of the maximum error in the determination of neutron flux density on effective threshold for various reactor spectra.

LITERATURE CITED

1. V. V. Grechko, E. A. Kramer-Ageev, and V. S. Troshin, in: Neutron Radiation Metrology at Reactors and Accelerators [in Russian], Vol. 1, Izd. TsNILatominform, Moscow (1974), p. 76.
2. K. K. Koshaeva, S. N. Kraitor, and L. B. Pikel'ner, At. Énerg., 32, 68 (1972).
3. V. S. Troshin and E. A. Kramer-Ageev, At. Énerg., 29, 37 (1970).
4. J. Grundl and A. Usner, Nucl. Sci. and Engng., 8, 598 (1960).
5. F. A. Makhlis and I. M. Kolpakov, At. Énerg., 18, 48 (1965).

ADDITIVITY DEVIATIONS IN THE THERMAL AND RADIATION-INDUCED EMBRITTLEMENT OF STEEL UNDER NEUTRON IRRADIATION

V. I. Badanin and V. A. Nikolaev

UDC 621.039.531

The vessels in power-station reactors are to be calculated [1] on the basis of brittle-failure resistance. The most important parameter here is T_c, which increases during operation on account of the neutron irradiation, thermal aging, and cyclic loading. These factors are [1] to be taken as additive and allowed for in accordance with measurements.

The basis for this approach is, in particular, that irradiation tests are usually accelerated by using high neutron flux densities in research reactors, in order that the limiting radiation dose can be obtained in a comparatively short period. Under working conditions, the material operates at an elevated temperature for an extremely long period ($100 \cdot 10^3$ h or so), and it is quite possible for thermal embrittlement to occur in that period. This is considered as an independent process, and its contribution is considered as raising T_c above the value caused by the radiation damage. This is based on the data of [2], which indicate that steel previously embrittled by a combination of cold deformation and subsequent exposure to 260 and 340°C shows after irradiation virtually the same rise in T_c as does steel in the initial state. However. the ageing effect in such tests cannot be identified with thermal embrittlement. On existing views [4], deformation ageing is the result of interaction between dislocations produced during work-hardening and atoms of elements forming interstitial solutions in iron (N and C).

The thermal embrittlement arising on prolonged exposure of undeformed steel to 300-500°C is a consequence of the formation of grain-boundary segregations of elements such as P, Sb, and As [4]. The latter also play an important part in the radiation embrittlement of steel [5, 6]. Further, there is a correlation between the tendencies to radiation embrittlement and thermal embrittlement [6], so one supposes that the phenomena are related, and therefore their effects are not additive.

In order to test this, we have compared the radiation embrittlement for several types of steel irradiated not only in the state after typical thermal treatment (quenching and high annealing) but also after additional aging. The latter was performed at 500°C in order to reduce the time required. We examined the commercial steel 15Kh3MFA (cast state) and also 15Kh2NMFA (sheet thickness 200-330 mm), as well as a laboratory batch of carbon steel (0.17% C) and 15Kh2 steel in the form of sheet of thickness 16 mm. The phosphorus content of the commercial steel was 0.013-0.014%, while that of the laboratory steel was 0.04%.

The materials were irradiated in a VVR-M reactor at 220-290 and 300-350°C; the tendency to embrittlement was evaluated by constructing a series of impact-viscosity curves from tests performed on specimens in accordance with GOST 9454-60, type IV. As T_c we took the temperature at which the impact viscosity fell to half the maximum value.

Figure 1 shows data for 15Kh2NMFA. It is clear that ageing for 500 h increases T_c by 40°. After irradiation with a flux of $1.3 \cdot 10^{20}$ or $2.1 \cdot 10^{21}$ neutrons/cm² (E above 0.5 MeV), T_c for steel in the initial state was virtually the same as that in the aged state, the result being independent of the initial value. Therefore, the rise in T_c after irradiation for aged steel is less than that for the initial material by an amount coincident with the shift in T_c consequent on the ageing. Similar results were obtained for other materials (Table 1). For the carbon steel, in which ageing for 140 hr did not alter T_c, we found a shift of 100° for the initial material and for material after annealing, in both cases in the irradiated state.
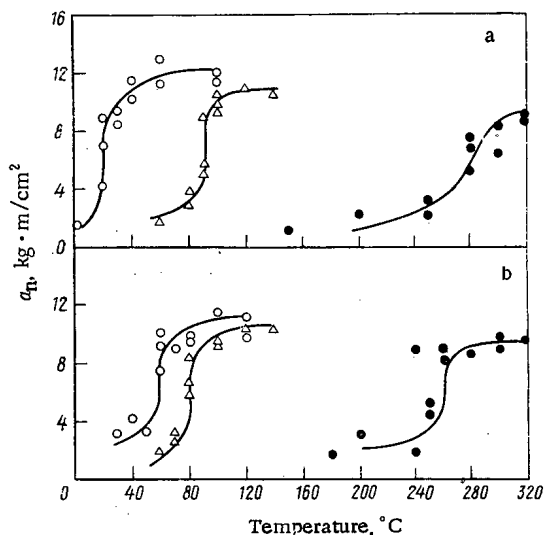
838

Fig. 1. Embrittlement of 15Kh2NMFA steel by irradiation: a) as supplied; b) after ageing; ○) initial state (200 mm sheet); △ and ●) after exposure to fluences of $1.3 \cdot 10^{20}$ and $2.1 \cdot 10^{21}$ neutrons/cm^2, respectively, at 300–350 and 220–290°C.

TABLE 1. Effect of Previous Ageing of the Embrittlement of Ferrite — Perlite Steel after Exposure to a Fluence of about 10^{20} neutrons/cm^2 at 300-350°C

Material	State	Tc, °K	
		before	after
15Kh2N MFA (sheet 330 mm)	Quenched-annealed	0	60
	The same + ageing 550°C, 500 h	50	70
15Kh3MFA (cast)	Quenched-annealed	20	60
	The same + ageing 500°C, 140 h	40	60
Carbon steel (laboratory batch)	Quenched + annealed	−30	70
	The same + ageing 500°C, 140 h	−30	70
15 ×2 (laboratory batch)	Quenched-annealed	−40	100
	The same + ageing 500°C, 140 h	0	100

These tests show that there is no need to sum the effects of embrittlement from radiation and thermal sources in calculating the change in properties in the pressure vessels of water — water power reactors. The thermal embrittlement makes itself felt in increasing the measured radiation shift Tc and thus is incorporated indirectly in the irradiation experiments.

Leaving aside details, the cause of the above appears to be as follows. Radiation-stimulated diffusion in the steel goes in parallel with the production of radiation defects to redistribute the impurities (phosphorus, antimony, and so on), which tend to segregate, i.e., one gets processes similar to those in thermal and reversible annealing. Impurity segregations before irradiation should reduce the corresponding radiation effect, since the solid solution is already depleted in the impurity elements. One supposes that the capacity for embrittlement under irradiation (at about 300°C) or prolonged heat exposure (at 300-500°C) is a function of the supersaturation of the solid solution, while the final value of T_c is independent to a large extent of the redistribution mechanism.

LITERATURE CITED

1. Standards for Strength Calculations on Components of Reactors, Steam Generators, Pressure Vessels, and Pipelines in Nuclear Power Stations and in Experimental and Research Reactors and Systems [in Russian], Metallurgiya, Moscow (1973).
2. M. Grounes and H. Myers, Nature, 193, No. 4814, 468 (1962).
3. Ya. S. Umanskii et al., Physical Metallography [in Russian], Metallurgizdat, Moscow (1955).
4. L. M. Utevskii, Annealing Embrittlement of Steel [in Russian], Metallurgizdat, Moscow (1961).
5. U. Potapovs and J. Hawthorne, Nucl. Appl., 6, No. 1, 27 (1961).
6. V. A. Nikolaev and V. I. Badanin, Metally, No. 2, 126 (1975).

THE TRANSIENT RESPONSE IN THE emf OF A THERMOCOUPLE UNDER REACTOR CONDITIONS

M. N. Korotenko, S. O. Slesarevskii, and S. S. Stel'makh

UDC 621.039.531

Irradiation of a thermocouple in a reactor produces transient shifts in the thermal emf that are dependent on the radiation flux density, and which vanish on stopping the irradiation. The effects have been estimated [1-4] as 0.5-5% of the thermal emf. Various explanations have been offered for the physical essence of the effect. In [1], free-electron theory was applied; in [2], the large changes in thermal emf were ascribed to changes in the Fermi levels of the materials, and in [3] the changes were ascribed to local heating of the working junction by the γ rays.

In most of the published experiments, the change in the thermal emf was determined by the normal metrological techniques used in calibrating thermocouples from the melting or solidification points of metals. This means that careful examination is required when this method is applied under conditions of irradiation, since the heat is produced throughout the reference, insulating, and electrode materials, which differ in the exact magnitude of the volume heat production rate q_V.

Here we leave aside the possible mechanisms for this effect, and merely present some results from comparative determination of the transient shifts in the thermal emf for couples calibrated in various ways whose working junctions were known to be at identical temperatures. For this purpose, three or four electrodes were compared in one working junction, whose size was 0.4-1.5 mm, in accordance with the wire size used (Fig. 1). Calculations indicated that the maximum temperature difference at the working junction under these conditions or irradiation was $\Delta t' \approx 0.2°C$. Table 1 gives for comparison the thermocouple resistance R, the thermal emf E, and the corresponding temperature level for six couples obtained by welding four wires of diameter 0.5 mm into one working junction (in this case, two Chromel ones Ch_1 and Ch_2, Alumel A, and Copel C). The thermal emf for each couple was also found as the algebraic sum of the thermal emf for two other couples:

$$E_{Ch_1-A} = E_{Ch_1-C} - E_{A-C} .$$

In the absence of the radiation flux, the temperatures $t_2 = t_3 = \ldots = t_6$ were virtually the same for all couples; when the VVR-M reactor was run up to a nominal power of 10 MW ($\varphi_{th} \approx 1 \cdot 10^{14}$ neutrons/cm^2 · sec, $\varphi_f \approx 4 \cdot 10^{13}$ in the same units), we had $D_\gamma \approx 2 \cdot 10^5$ rad/sec, and the temperatures derived from the readings E of the couples differed substantially. A notable point is that no additional signal disturbance was observed for wires of the same type.

TABLE 1. Temperature Measurement with a Four-Electrode Thermocouple

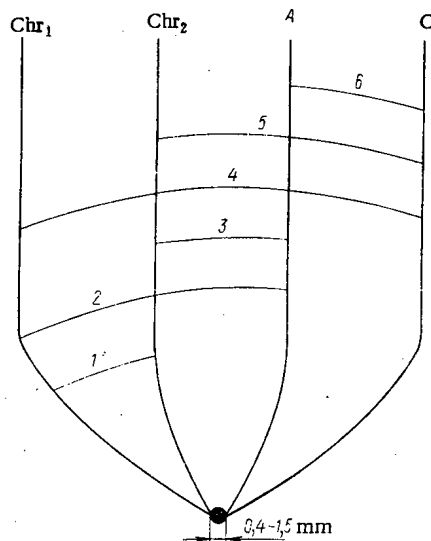| Couple No.	Type	Before irrad.			During irrad.	
		R, Ω	E, mV	t, °C	E, mV	t, °C
1	Ch_1—Ch_2	79,7	0,0012	—	0,0017	—
2	Ch_1—A	56,0	4,9512	120,1	5,0671	123,5
3	Ch_2—A	56,3	4,9523	120,1	5,0699	123,6
4	Ch_1—C	61,1	8,4648	120,1	8,8826	126,1
5	Ch_2—C	61,8	8,4693	120,2	8,8842	126,1
6	A—C	39,1	3,5161	120,3	3,8163	130,7

840

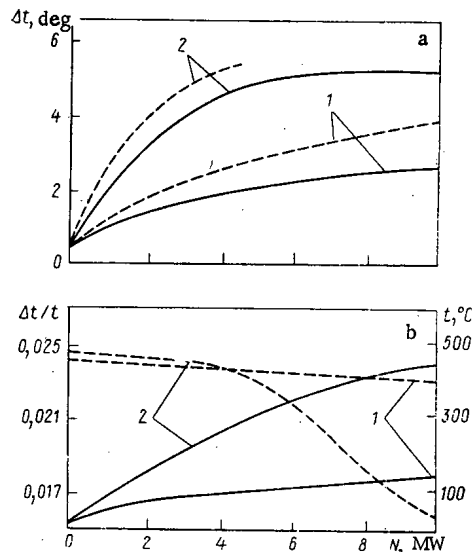Fig. 1   Fig. 2

Fig. 1. The four-electrode thermocouple.

Fig. 2. Deviations $\Delta t/t$ in readings of Chromel — Copel and Chromel — Alumel thermocouples in relation to reactor power level: 1) low-temperature irradiation; 2) high-temperature irradiation.

Figure 2a shows the temperature difference Δt in relation to reactor power (radiation flux density) derived from this compound junction for wires of diameter 0.5 mm. Figure 2b shows the shift in the existing temperature level and in the ratio of $\Delta t = t_{Ch_{1,2} - C} - t_{Ch_{1,2} - A}$ to the mean temperature for the working junction (broken line), also as a function of reactor power.

To estimate the effects of temperature on Δt we performed the irradiation at various temperature levels; Fig. 2a shows that Δt increases with the irradiation temperature under otherwise equal conditions. Also, the shape of the relationship alters. Appropriate combination of radiation flux, temperature, and wire diameter results in a saturation effect. Any further increase in temperature or flux density does not increase the error in the thermal emf. Also, Δt increases with the wire diameter.

Figure 2a shows Δt for couples screened by a layer of cadmium of thickness δ about 0.7 mm (broken line). The cadmium absorbs the thermal neutrons (by n, γ reaction), which produces a considerable number of secondary γ rays, which means a local increase in the γ ray flux at the working junction and consequently an increase in Δt. The reactor has a considerable γ background, which explains why the difference in the readings between the Chromel — Copel and Chromel — Alumel thermocouples was $\Delta t \approx 0.3$-$0.7°C$ for $N = 0$.

No effect from the integral neutron flux was observed, and satisfactory agreement between the $\Delta t = t_{Ch-C} - t_{Ch-A}$ was obtained for thermocouples exposed to thermal-neutron fluences of from $1 \cdot 10^{18}$ to about $4 \cdot 10^{20}$ neutron/cm^2.

LITERATURE CITED

1.   J. Leonard, Nucl. Appl., 6, No. 3,202 (1969).
2.   N. V. Markina, B. V. Samsonov, and V. A. Tsykanov, Fiz. Met. Metalloved., 32, No. 4, 747 (1971).
3.   G. Dau, R. Bourassa, and S. Keeton, Nucl. Appl., 5, No. 5, 322 (1968).
4.   G. Blanchi and S. Moretti, Energia Nucl., 11, No. 8, 426 (1964).

841

MEASUREMENT OF THE ENRICHMENT FACTOR IN
RELATION TO FLOW DISTRIBUTION IN A SEPARATION SYSTEM

V. A. Kaminskii, O. G. Sarishvili,
G. A. Sulaberidze, V. A. Chuzhinov,
and B. Sh. Dzhandzhgaba

UDC 621.039.3

It has been shown in serveral papers on the theory of isotope separation that the separation factor θ for a gas flow should have a marked effect on the operation of a separating element [1, 2], and the dependence of the enrichment factor on θ for elements providing Rayleigh distillation (gas diffusion, mass diffusion) takes the form

$$\varepsilon = \varepsilon_0 \frac{1}{\theta} \ln \frac{1}{1-\theta},$$

(1)

where ε_0 is expressed in terms of parameters that characterize the primary effect in the particular separation method. Although this relationship is important for the theory of multistage separators, it has not yet been confirmed by experiment.

We have tested this relationship by using mass diffusion; it has been shown [3] that the enrichment factor for such an element can be represented with sufficient accuracy by

$$\varepsilon = \frac{\Delta D}{D} \frac{q \ln q}{q-1} \frac{1}{\theta} \ln \frac{1}{1-\theta},$$

(2)

where D is the diffusion coefficient for the light component in the vapor and ln q is the Peclet diffusion number. It is clear that in this case

$$\varepsilon = \frac{\Delta D}{D} \frac{q \ln q}{q-1}.$$

It is also possible to vary θ for an element by means of transfer pumps, but this method is not used on account of the difficulties of analyzing small concentration changes at the outputs, as well as effects from this method of separating the flows on the internal operation. Another way of adjusting θ is to cascade the elements in an unsymmetrical fashion.

If the enriched flow from element i is passed to the input of the next element i + k, while the depleted flow is passed to the input of the preceding element i — (p — 1), then it is found [4] that the value of θ given by the following formula is automatically established for such a stage containing the basic number of elements:

$$\theta = \frac{p-1}{k+p-1}.$$

TABLE 1. Types of Experiment Stage

System	κ	$p-1$	θ	System	κ	$p-1$	θ
1	3	1	1/4	3	1	1	1/2
2	2	1	1/3	4	1	2	2/3
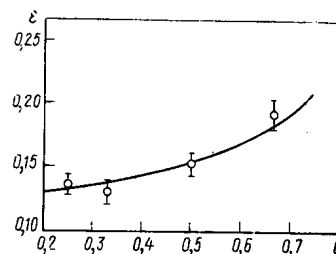
Fig. 1. The θ dependence of ε:
———) calculation, ○) experiment.

In that case, θ can be varied by changing k and p $-$ 1. To determine ε in this case we need to use the transport equation for an unsymmetrical cascade:

$$\frac{dc}{ds} = \frac{2\theta}{p-1} \varepsilon c (1-c) - \frac{2P}{k(p-1)L}(c_P - c).$$

(3)

Then we readily get an expression for ε for the case where no material is lost by sampling:

$$\varepsilon = \frac{1}{2} \frac{p-1}{\theta S} \ln \frac{c_e(1-c_s)}{c_s(1-c_e)},$$

(4)

where S is the number of elements in the working section (a part with constant θ), while c_s and c_e are the concentrations at the start and end of the part.

The apparatus consisted of a cascade of 10 steel mass-diffusion elements operating with mercury. The elements had cylindrical diaphragms of working area in each case 270 cm^2 and diffusion resistance 1.27 cm. There were 11 holes of diameter 0.3 mm per cm^2 of surface. The gap between the diaphragm and the wall of the condenser system was 3 mm. The elements were linked up in an unsymmetrical fashion with the parameters given in Table 1.

The systems with $\theta < 1/4$ and $\theta > 2/3$ are not considered, on account of the considerable complexity involved and the fact that such conditions are of little practical value. For each θ, the working section of the cascade consisted of six average elements. The concentration of the heavy fraction at the output was measured. In all runs, the elements operated under conditions giving identical $\ln q = 2.1$, the value being determined by measuring the heat taken up by the main and additional condensers in conjunction with calculation of the amount of vapor passing through the diaphragm. The θ dependence of ε was determined for the separation of neon isotopes. The working pressure in the cascade was 70 mm Hg. Figure 1 shows the results together with the theoretical curve derived from (2) for the case $\ln q = 2.1$; the agreement is clearly good.

We are indebted to B. I. Nikolaev and N. I. Laguntsov for a discussion of the paper and valuable comments.

LITERATURE CITED

1. K. Cohen, The Theory of Isotope Separation, McGraw-Hill, New York (1951).
2. N. A. Kolokol'tsov, N. I. Lagunov, and G. A. Sulaberidze, At. Énerg., 34, No. 4, 259 (1973).
3. V. A. Chuzhinov et al., At. Énerg., 40, No. 6, 471 (1976).
4. N. A. Kolokol'tsov, At. Énerg., 27, No. 1, 9 (1969).

CHARACTERISTICS OF NEUTRON RADIATION
REFLECTED FROM CONCRETE

V. A. Klimanov, A. S. Makhon'kov,
and V. P. Mashkovich

UDC 621.039.58

Concrete is widely used in the shielding of nuclear installations. However, there is no information in the literature on the differential characteristics of the albedo of neutrons in all energy groups for concrete. In the present paper, systematic information was obtained by calculation of the differential characteristics of the current number albedo for neutrons from a point monodirectional source with energies above 1 MeV reflected from a flat concrete reflector and a semiempirical formula is proposed to describe this information.

The calculations were made with the KUPOL program [1]. Its algorithm is based on the Monte Carlo method using a multigroup system of constants averaged by means of the program OBRAZ [2]. Concrete of ordinary chemical composition was chosen for the computation; composition is given in atom/cm^3: H, $6.023 \cdot 10^{21}$; C, $7.07 \cdot 10^{21}$; O, $44.7 \cdot 10^{21}$; Mg, $0.251 \cdot 10^{21}$; Al, $0.402 \cdot 10^{21}$; Si, $7.57 \cdot 10^{21}$; S, $0.169 \cdot 10^{21}$; Ca, $9.02 \cdot 10^{21}$; Fe, $0.13 \cdot 10^{21}$. The angles of incidence of the neutron beam were 0, 60, 75, and 85°. The energies of the incident neutrons were assigned in the form of energy groups ΔE_0, the boundaries of which are given in Table 1.

Use of information on differential characteristics of albedo in tabular form is associated with considerable difficulty because of the limitations of the auxiliary storage of modern computers. At the present time, various semiempirical formulas are widely used for a description of the differential characteristics of neutron albedo; they are reviewed in [3]. However, these formulas have a number of general deficiencies which hinder their practical application; they give a poor description of the differential characteristics of neutron albedo for angles of incidence and reflection greater than 75° and are only applicable for limited energy ranges of the incident and reflected neutrons.

The information on differential current number albedo for neutrons from concrete obtained in this work is described by a formula similar to that given in [4, 5]:

TABLE 1. Values of the Coefficients in the Formula Presented in the Paper and of the Coefficients in the Expansion of the Neutron Elastic Scattering Kernel in Powers of the Cosine of the Scattering Angle

Energy groups, MeV	A	B	C	D	b_0	b_1	b_2	b_3	b_4	b_5
14,0—10,5	0,2737	0,3263	0,1939	1,1033	0,0437	—0,00948	—0,124	—0,0571	0,208	0,119
10,5—6,5	0,5555	0,3751	0,1437	1,3891	0,0437	—0,00948	—0,124	—0,0571	0,208	0,119
6,5—4,0	0,1454	0,5065	0,2200	1,1950	0,0556	—0,0520	—0,0417	0,1888	0,293	0,0591
4,0—2,5	0,05609	0,5078	0,2794	0,9502	0,0624	—0,00709	—0,151	0,0517	0,130	0,0247
2,5—1,4	0,1654	0,5150	0,2115	1,1876	0,104	0,0315	0,0548	0,0363	0,0794	0,008261
1,4—0,8	0,0382	0,5096	0,2561	0,8472	0,205	0,0505	0,114	0,0822	0,0192	—0,0201
0,8—0,4	0,0351	0,5516	0,3544	0,9352	0,250	0,198	0,190	0,0458	—0,0117	—
0,4—0,2	0,1094	0,4531	0,1114	0,9325	0,259	—0,198	—0,0547	—0,0187	0,0421	—
0,2—0,1	0,1877	0,4459	0,1201	1,0220	0,219	0,0219	—0,0152	—0,0121	0,00926	—
$1 \cdot 10^{-1}$—$4,65 \cdot 10^{-2}$	0,1548	0,4515	0,1366	1,0130	0,215	0,0268	—0,00265	—	—	—
$4,65 \cdot 10^{-2}$—$2,15 \cdot 10^{-2}$	0,1815	0,4360	0,1394	0,9890	0,223	0,0269	—0,016	—	—	—
$2,15 \cdot 10^{-2}$—$1 \cdot 10^{-2}$	0,1753	0,4232	0,1514	0,9293	0,218	0,0270	—0,0047	—	—	—
$1 \cdot 10^{-2}$—$4,65 \cdot 10^{-4}$	0,1489	0,4241	0,1551	0,9361	0,225	0,0277	0,0014	—	—	—
$4,65 \cdot 10^{-3}$—$2,15 \cdot 10^{-3}$	0,1727	0,4130	0,1544	0,9639	0,232	0,0282	0,0014	—	—	—
$2,15 \cdot 10^{-3}$—$1 \cdot 10^{-3}$	0,1309	0,4210	0,1572	0,9526	0,236	0,0284	0,0014	—	—	—
$1 \cdot 10^{-3}$—$4,65 \cdot 10^{-3}$	0,08707	0,3984	0,1856	0,8315	0,236	0,0285	0,0014	—	—	—
$4,65 \cdot 10^{-4}$—$4,65 \cdot 10^{-5}$	0,1478	0,3928	0,1499	1,0668	0,236	0,0284	0,0015	—	—	—
$4,65 \cdot 10^{-5}$—$4,65 \cdot 10^{-6}$	0,2531	0,2734	0,1403	0,9693	0,236	0,0284	0,0015	—	—	—
$4,65 \cdot 10^{-6}$—$1 \cdot 10^{-6}$	1,1931	0,1330	0,1620	0,8136	0,236	0,0284	0,0015	—	—	—

$$a_{\mathrm{C}}(E_0,\ \theta_0,\ \theta,\ \varphi) = \frac{A(E_0)\sum_{i=0}^{5} b_i \mu_s^i + B(E_0)[H(\mu)H(\mu_0)-1] + C(E_0)(|\mu_s|+\mu_s)}{1+[D(E_0)\,\mu_0/\mu]},$$

where μ_0, μ, and μ_s are respectively the cosines of the angles of incidence, reflection, and scattering; $H(\mu) = (0.5773 +\mu)/(0.5773 +\mu\sqrt{1-\alpha})$ is the Chandrasekhar function; $\alpha = 0.6$; b_i are the coefficients of the expansion of the scattering kernel in powers of the cosine of the scattering angle, the values of which are given in Table 1; $A(E_0)$, $B(E_0)$, $C(E_0)$, and $D(E_0)$ are coefficients which depend on the energy of the incident neutrons and which are calculated by the method of least squares on the basis of the neutron albedo characteristics calculated in this work (see Table 1).

The error in the description of the differential albedo characteristics by means of the formula presented is no more than 25%; this completely meets practical requirements.

LITERATURE CITED

1. E. M. Vaisman et al., in: Topics of Papers at the All-Union Scientific Conference on Shielding against Ionizing Radiation at Nuclear Installations [in Russian], Izd. MIFI, Moscow (1974), p. 42.
2. V. F. Khokhlov and V. D. Tkachev, Idem, p. 78.
3. T. A. Germogenova et al., Neutron Albedo [in Russian], Atomizdat, Moscow (1973).
4. B. A. Efimenko et al., in: Problems of Radiation Dosimetry and Shielding [in Russian], No. 13, Atomizdat, Moscow (1973), p. 15.
5. V. G. Zolotukhin et al., in: Topics of Papers at the All-Union Scientific Conference on Shielding against Ionizing Radiation of Nuclear Installations [in Russian], Izd. MIFI, Moscow (1974), p. 16.

TRITIUM CONTENT IN LIQUID MEDIA AND IN AIR OF WORKING LOCATIONS AT NUCLEAR POWER STATIONS

Yu. P. Abolmasov

UDC 621.039.58:621.311.2

Tritium concentration was measured with Tricarb-3380 and SBS-1 scintillation spectrometers using standard scintillators of toluol and dioxane. The measurement error depended on sample activity but was no more than 20%.

TABLE 1. Maximum Tritium Concentrations in Various Media at Nuclear Power Stations of Various Kinds

Power station and reactor	Type of reactor	Power, MW		Q, mCi/liter			Q, pCi/liter
		electric	thermal	coolant	recirculating water	discharge water*	working area air†
Novo-Voronezh I	VVÉR	210	760	3,0	3,0	to 0,1	85
Novo-Voronezh II	VVÉR	365	1400	10	3,0	to 0,1	64
Novo-Voronezh III	VVÉR	440	1375	520	to 10	to 1,0	180
Novo-Voronezh IV	VVÉR	440	1450	340	to 10	to 1,0	Background
Kolsk I	VVÉR	440	1450	31 ‡	2,5	2,5	—
Beloyarsk I	Uranium–graphite	100	286	29	to 10	0,26	Background
LAÉS I	PBMK	1000	3200	0,48	0,3	0,27	10
VK-50	Boiling water	35	150	4,0	—	0,053	—
SM-2	Research	—	75	160	—	—	—
MIR	Channel, research	—	270	27	—	—	—

*Concentration before discharge.
†Samples collected with visible leakage of vapor from technical equipment present.
‡During the three months after beginning of operation.

All liquid samples were thoroughly cleansed chemically of radioactive isotopes which interfered with the measurement or identification of tritium. In measurements using a liqiud scintillator, special vessels of potassium-free glass were used to reduce the background from the natural isotope ^{40}K. Air from working locations was sampled for tritium dioxide by bubbling the air through distilled water and by deposition of atmospheric moisture on cooled metal surfaces.

The tritium concentration Q depends on a large number of technical and physical parameters of the nuclear power station: reactor power, core design, existence of impurities in core and coolant that lead to the formation of tritium, amount of coolant leakage, mode of reactor operation, etc. Therefore the concentrations of tritium both in the coolant and in the liquid and gaseous discharges from a nuclear power station are subject to changes in time. Because of this, Table 1 presents the maximum values of the measured concentrations (more than 1000) over the entire period of investigation (1973-1975).

ANALYTIC REPRESENTATION OF ION
ENERGY LOSS IN STOPPING BY NUCLEI

V. A. Zybin and V. A. Rykov

UDC 539.101

The absence of a simple analytic form for the energy dependence of the specific energy loss in stopping by nuclei in the Lindhard theory [1-3] causes difficulty in making the calculations. A formula was proposed [4] for the calculations but one with parameters which changed for various energy intervals, which also presents some inconvenience.

However, one can select such a function which represents the dependence of specific energy loss in stopping by nuclei over the entire energy range in which the condition $v < v_1 = Z_1^{1/2}e^2/\hbar$ is satisfied. The function has the form

$$\left(\frac{d\varepsilon}{d\rho}\right)_n = \frac{a\varepsilon^{1/4}}{b+\varepsilon}$$

(1)

($a = 0.77$, $b = 1.1$, ε and ρ are dimensionless values of energy and range),

$$\varepsilon = E \frac{a_{TF}M_2}{Z_1Z_2e^2(M_1+M_2)};$$

$$\rho = R4\pi a_{TF}^2 N \frac{M_1M_2}{M_1+M_2},$$

where E is energy; R is the ion range in the target material; N is the number of atoms per unit volume; Z_1, Z_2, and M_1, M_2 are the atomic numbers and masses of ion and target atom respectively; $a_{TF} = 0.8853(Z_1^{2/3} + Z_2^{2/3})^{1/2}$.

For the range of ε from 0.01 to 40, the results obtained from Eq. (1) agree within 5% with the Lindhard data for the Thomas — Fermi interatomic interaction potential shown graphically in [1]. For the range $40 \leq \varepsilon \leq 300$, Eq. (1) gives practically the same results as the equation

$$\left(\frac{d\varepsilon}{d\rho}\right)_n = \frac{\ln 1.249\varepsilon}{2\varepsilon},$$

(2)

proposed in [2] for the same range of ε.

One can use the expression

$$d\rho = d\varepsilon \left[\left(\frac{d\varepsilon}{d\rho}\right)_n + \left(\frac{d\varepsilon}{d\rho}\right)_e\right]^{-1},$$

(3)

to calculate the range where $(d\varepsilon/d\rho)_e$ is the energy loss in stopping by electrons, which is represented in the Lindhard model by

$$\left(\frac{d\varepsilon}{d\rho}\right)_e = k\varepsilon^{1/2},$$

$$k = \frac{0.0793 Z_1^{2/3},\ Z_2^{1/2}\,(1+M_2/M_1)^{3/2}}{(Z_1^{2/3}+Z_2^{2/3})^{3/4}\,M_2^{1/2}}. \tag{4}$$

Substitution of Eqs. (1) and (4) in Eq. (3) makes possible the calculation of particle range by numerical methods.

LITERATURE CITED

1. J. Lindhard, M. Scharff, and H. Schiott, Kgl. Danske Vid. Selskab. Mat-fys. Medd., 33, No. 14 (1963).
2. J. Lindhard, V. Nielsen, and M. Scharff, ibid, 36, No. 10 (1968).
3. J. Lindhard and M. Scharff, Phys. Rev., 124, 128 (1961).
4. V. V. Yudin, Dokl. Akad. Nauk SSSR, 207, 325 (1972).

847

COMECON NEWS

THE INTERATOMINSTRUMENT EXHIBITION

V. A. Dolinin

This exhibition was held April 15-24, 1976, in Sofia, and consisted of numerous units for nuclear engineering made and supplied by members of the International Economic Organization for Nuclear Instrumentation, INTERATOMINSTRUMENT.

The exhibits of all participants shared a common display arranged by types of instrument, which allowed Bulgarian specialists to compare similar instruments and to obtain a full picture of the available units widely used in the participating countries.

The Soviet Union demonstrated 10 instruments at the exhibition:

The TOR-3 γ-ray thickness gauge for measuring the thickness of sheet material, tube walls, and vessels made of carbon steel with access from one side only;

The UR-8M radioisotope servo level gauge for continuous automatic remote monitoring and measurement of liquid levels in closed or open vessels;

The NR-IIN static-charge neutralizer for eliminating static charges from materials;

The SRP68-03 geological-prospecting scintillation counter for detecting radioactive ores from the γ emission;

The UZB2-03 equipment (Katran) for monitoring contamination on the hands, legs, and face masks, especially for β-emitting substances in radiochemical laboratories in industrial organizations;

The DRGZ-02 dosemeter (Argun') for measuring x- and γ-ray dose rates;

The BDBSZ-1eM basic detector unit (Vorya) for γ-ray and for charged-particle recording and spectrometry, in the following energy ranges: α rays 1-10 MeV, β rays 0.05-3 MeV, and γ rays 0.03-3 MeV;

The FRAD-1 two-channel x-ray analyzer for rapid qualitative and quantitative analysis of elements from calcium to uranium (Z of 20-92) from the K or L series in media of complex composition;

The UIM2-1eM ratemeter for measuring mean count rates and indicating any excess over present values from standardized units for detecting α, β, and γ rays and also neutrons; and

The IDMD-1 clinical dosemeter for monitoring radiation dose in radiotherapy (Krug). The instrument measures the narrow-beam exposure dose for x rays and γ rays in the dose range 1-1000 R and dose rates in the range 1-1000 R/min at quantum energies from 10 to 1250 keV in radiological examinations.

Seven of the instruments were sold. The Katran system and the TOR-3 were bought for the Kozlodui Nuclear Power Station.

Other participants in the exhibition, apart from the USSR, were the following members of the Interatominstrument organization: Élektroimpek (Bulgaria), The Gamma and Metrimpek Organizations (Hungary), Messlektronik (German Democratic Republic), and KOVO (Czechoslovakia), who demonstrated more than 100 units, which ranged from radiation detectors to laboratory equipment for work with radioactive materials.

The exhibition proved of considerable value to Bulgarian scientists. Every day there were more than 1000 visitors. At a press conference organized by the Institute of Atomic Research, there were about 20 journalists from various sections of the press, film industry, and television.

The exhibition in Sofia was a success, and many of the instruments were sold, while the requests for licences were made for some of them.

INTERNATIONAL SYMPOSIUM ON
RADIOACTIVELY TAGGED ORGANIC COMPOUNDS

A. K. Zille

This Symposium was held May 11-15, 1976, in Marianske Lazne (Czechoslovakia), which provided for contacts between workers in COMECON member countries in the areas of tagged organic compounds generally, but especially methods of synthesis, separation, purification, and analysis. The symposium was attended by 69 representatives of COMECON members, as well as representatives of the COMECON Secretariat and a representative of the International Atomic Energy Agency.

The symposium involved two sections: Section I dealt with the synthesis of radioisotope-tagged organic compounds, while Section II dealt with physical and physicochemical methods of separation, purification, and analysis for such compounds, as well as with isotope exchange.

The participants discussed the current state of the art and the trends in research on methods of producing such compounds, and also on methods of analysis, separation, purification, and stability testing, with emphasis on rules for naming such compounds, in addition to extensive exchange of experience on various branches of experimental research and use of laboratory equipment.

Particular attention was given to research on the conditions employed in reductions used to make tritium-labeled compounds and also to the enzymatic synthesis of compounds labeled with ^{14}C and tritium.

Some papers dealt with the production of complicated compounds used in biology and biochemistry (steroids, nucleic-acid components, antibiotics, antigens, peptides, pesticides, and so on). Advances were reported in the production of compounds of high specific activity with good chemical and radiochemical purity. The discussions showed that the participants were extremely interested in exchanging information on this branch of applied radiation work, and that the contacts could improve the rate of advance in new methods of making tagged compounds, while providing also for an extended range of such compounds as produced in COMECON member countries.

During the symposium, there was a discussion on developing the notation for tagged organic compounds. It was emphasized that joint studies on this topic should be made on the basis of the recommendations of the Standing Commission of COMECON on nuclear power research, in conjunction with recommendations from the International Union of Pure and Applied Chemistry, and also methods generally adopted throughout the world for naming tagged organic compounds.

The symposium was held at a very high scientific level, and it has considerable importance for researches in COMECON member countries, which will undoubtedly provide favorable conditions for further international division of labor and cooperation in the production of tagged organic compounds.

During the symposium, there were extensive discussions between the interested parties on specialization in the production of tagged compounds, and the results of these discussions will be considered in September 1976 at a meeting of representatives of COMECON members concerned with isotope production.

COLLABORATION NOTEBOOK

The 9th meeting of the Committee of the Scientific Council on Processing Irradiated Nuclear Power-Station Fuel was combined with the conference of specialists on handling spent fuel rods in the period April 5-9, 1976, in Prague (Czechoslovakia).

A report was presented on the activities of the Committee during 1971-1975, especially as regards organization of multilateral collaboration between COMECON member countries in the reprocessing of nuclear power-station rods, together with suggestions on the main lines of collaboration up to 1990. The Council considers that the main efforts of researchers in COMECON member countries in this period should be directed to the following: transportation of spent fuel rods; development and improvement of nondestructive methods of determining fissile-material contents in spent fuel rods; improvements in technology and equipment for recovering nuclear fuel from rods from water-cooled and water-moderated power reactors; definition of economic means of processing fuel rods from fast reactors; and development of methods and instruments for remote monitoring of processes and process management in radiochemical production.

It was pointed out that it would be desirable to collaborate with the International Atomic Energy Agency in the drawing up of standards on the transportation of irradiated nuclear power-station fuel.

The Council and the Conference dealt with the current state of researchers in Poland, the USSR, and Czechoslovakia on fuel processing. Advances were reported in the design of equipment for continuous dissolution of fuel rods, filtering equipment, and methods of preparing solutions for filtration by means of flocculating agents.

The Council also considered and adopted suggestions from the delegations from the German Democratic Republic, the USSR, and Czechoslovakia that comparisons should be made of determinations of components in solutions from spent nuclear fuel.

The Council also discussed reports from conferences on the processing of spent fuel rods from fast reactors, transportation of spent nuclear fuel, and nondestructive methods of determining fissile material content, as well as summaries presented by the delegations on researches in 1975, specifications drawn up for various stages in working plans for 1976-1980, and the draft program for the 4th Symposium of COMECON Member Countries on Researches in Processing Irradiated Fuel.

The 7th Meeting of the Radiation Safety Council was held May 18-21, 1976, in Siofok (Hungary). The Council discussed and agreed recommendations on dosimetric monitoring in areas around nuclear power stations, specifications for environmental protection in the case of emergencies at nuclear power stations containing water-cooled and water-moderated reactors, and recommendations on the basic measures to be taken after an emergency arising from loss of the coolant.

The meeting also considered surveys of papers presented at the Conference on Radiation Safety in the Operation of Nuclear Power Stations, which was held September 8-13, 1975, in Czechoslovakia. The Council considered suggestions and recommendations following from the papers at that conference, and agreed to include various topics in the plan.

During this meeting, there was also a meeting of specialists on the research program for 1976 of recommendations on the evaluation of radioactive effluents from nuclear power stations entering the Danube, and also recommendations on the use of coastal waters in the Baltic as coolants in nuclear power stations.

CONFERENCES AND MEETINGS

ALL-UNION CONFERENCE ON WATER TREATMENT
IN NUCLEAR POWER STATIONS

L. M. Voronin, V. M. Gordina,
and V. A. Mamet

Proper means of water treatment and effluent processing are essential to reliable and safe operation of major nuclear-power equipment, as well as the radiation background in power-station buildings and the effects of nuclear power stations on the environment. This important current topic was considered at an All-Union conference entitled Organization of Water Processing, Combating Deposition and Corrosion, and Chemical and Radiochemical Monitoring of Nuclear Power Stations, which was held from March 30 to April 2, 1976 at the Kola Nuclear Power Station.

The conference was organized by the State Atomic Energy Commission in conjunction with the principal research sections of the Ministry of Energy, and it involved over 200 specialists from 50 organizations, including the Novyy Voronezh, Kola, Leningrad, Armenian, Kursk, and Beloyarsk Power Stations, the Bilibinsk Atomic Energy Center, the Kurchatov Institute of Atomic Energy, Moscow Power Institute, Dzerzhinskii High-Temperatures Institute, and so on. In all there were 50 papers, which included survey papers and communications on processes in chemical technology at the Novyy Voronezh, Beloyarsk, Kola, and Leningrad Power Stations, the Bilibinsk Center, and papers on water handling in two-loop and one-loop power stations, as well as the organization of water treatment in foreign power stations.

Much interest was aroused by papers dealing with corrosion of equipment, deposition, and decontamination.

The major problems in organizing water treatment for nuclear power stations have involved solving various technical problems during reactor operation:

1. Incorporation of boron regulation systems into water-cooled and water-moderated power reactors, with the development of means of maintaining the optimum chemical composition in the coolant under these conditions;

2. Ways of optimizing the water treatment in single-loop nuclear power stations and in the second loops in water-cooled and water-moderated reactors; and

3. Methods of processing radioactive effluents, process automation, methods of decontamination of major equipment, etc.

The Conference observed that research institutes in various branches of the industry, nuclear power stations, design and construction organizations, and technical colleges should devote considerable attention to water treatment, since this would advance the solution of various major problems and provide for more reliable operation of existing nuclear power stations.

Considerable advances have been made in improving water treatment, choosing constructional materials, organizing chemical monitoring, and effluent treatment and equipment decontamination, but certain weak spots were pointed out in some papers, particularly the inadequate coordination between different organizations. Contributions to the discussions emphasized the need for somebody to coordinate the efforts of organizations in the various ministries to handle future problems in water treatment, with systematic research and dissemination of experience in the operation of existing power stations. The need for automatic chemical monitoring in nuclear power stations has now become acute, especially as regards water treatment, together with automatic control systems for maintaining water quality. Proper account must be taken of working conditions in choosing constructional materials for systems and units in power stations, while materials of different classes

must be compatible. Several papers discussed possible methods of providing proper water treatment, such as the use of hydrogen peroxide and chelating agents, thermal regeneration of ion-exchange materials in boron control, treatment of filters containing heat-resistant absorbents, and automation in water treatment systems. The conference formulated suggestions designed to improve research results and design studies, while reducing the periods needed to complete design work and also measures to improve the reliability and economic aspects of existing and future nuclear power stations.

INTERNATIONAL CONFERENCE ON ELEMENTARY
INTERACTIONS AT LOW ENERGIES

P. S. Isaev

This conference was held on March 10-12, 1976, in Novosibirsk and was organized by the Joint Nuclear Research Institute and the Institute of Mathematics, Siberian Division, Academy of Sciences of the USSR, to discuss some major topics in elementary particle interactions at energies up to 2-3 GeV, together with lines of advance in research in this area in the near future. The President of the Organizing Committee was D. V. Shirkov, Associate Member of the Academy of Sciences of the USSR. The conference was attended by about 60 scientists from the Soviet Union, the Joint Nuclear Research Institute, and socialist and capitalist countries.

One of the most important topics is the derivation of equations to describe the partial waves for the scattering amplitudes for elementary particles, with emphasis on analytical features in the various Riemann sheets (papers by A. N. Vall, Yu. V. Parfenov, and I. I. Orlov, Irkutsk University, M. Müller-Proisker, German Democratic Republic, M. Blažek, Czechoslovakia, and E. Radescu, Romania). C. Bessise and P. Mery (France) discussed the use of the Padé approximation in calculating large scattering phases, together with various detailed mathematical aspects of the Padé method. These papers produced a lively discussion.

Much attention was also given to $\pi - \pi$ interactions; an excellent model for π-meson interaction with hadrons may be based on the small pion mass in conjunction with chiral symmetry in the limit of zero mass for the pion; this was discussed in papers by V. N. Pervushin (Joint Nuclear Research Institute) and V. I. Dend'el (Institute of Theoretical Physics, Academy of Sciences of the Ukrainian SSR, Kiev). Pervushin's paper was essentially a survey of studies recently performed at the Joint Nuclear Research Institute. Papers by R. Wit (Poland) and S. A. Bunyatov (Joint Nuclear Research Institute) dealt with experimental analysis of pion — nucleon scattering and the one-pion threshold generation in pion — nucleon collisions. In the latter paper, interaction radii were given for the pion — pion system that differ substantially from those predicted in the theory of chiral symmetry. It would appear that existing theoretical processing methods should be substantially modified in the threshold region as the experimental data are refined.

Some interesting communications were also made on the electromagnetic interactions of hadrons, electromagnetic hadron generation, and the joint analysis of hadron and electromagnetic data.

A survey by G. Höller (Federal German Republic) reported recent researches on the coupling between the strong interaction in a pion — nucleon system and the electromagnetic form factors for nucleons. Dispersion analysis of the experimental data indicates a marked deviation from the universal vector theory for the subthreshold behavior of the amplitudes, which in turn results in anomalies in the behavior of the nucleon form factors at low energies. Papers by N. N. Achasov, A. A. Kozhevnikov, and G. N. Shestakov (Novosibirsk) dealt with effects that produce electromagnetic mixing for vector mesons. S. B. Gerasimov (Joint Nuclear Research Institute) described a quark-parton model with different types of interaction for the strange and nonstrange quarks, which has some interesting consequences. A separate session was concerned with the discussion of electromagnetic form factors for pions and nucleons. The paper by V. M. Budnev and V. V. Serebryakov (Novosibirsk) dealt with effects rising from inelastic contributions. If one assumes the existence of a new vector that explains the behavior of the inelastic form factor, then the behavior of the pion form factor

should show anomalies. There are hopes that new measurements of the π-meson form factor made in Novosibirsk (Institute of Nuclear Physics, Siberian Division, Academy of Sciences of the USSR) might throw light on this situation after processing.

Another paper by G. Höller (Federal German Republic), which was a logical continuation of the previous one, also dealt with the possibility of introducing new vector particles, which are required to describe the known energy behavior of nucleon form factors. An unexpected result is the marked deviation from vector-meson universality. The paper by T. D. Blokhintseva (Joint Nuclear Research Institute) dealt with data on the radii of isovector pion form factors as derived from experiments on electromagnetic generation in pion — nucleon collisions performed at the Joint Nuclear Research Institute. The results agree within the errors of measurement with the data derived from direct measurements on other reactions.

P. S. Baranov and L. V. Fil'kov (Physics Institute, Academy of Sciences, Moscow) reported recent experimental data on γ-ray scattering at nucleons in the energy range 80-110 MeV, with a theoretical interpretation based on the bootstrap approach within the framework of dispersion relations.

K. Levin (German Democratic Republic) presented a critical analysis of the dynamics of radiative capture of low-energy neutrons by protons. The closing session was concerned with papers by J. Lukersky (Poland) on the rigorous description of unstable particles and A. B. Govorkov (Joint Nuclear Research Institute) on the latest experimental data on the J/ψ particles. A point to be emphasized particularly here as regards particles with new quantum numbers (charm and color) is that the interaction problems have much in common with those in the physics of elementary particles at low energies, i.e., with the topics considered at this conference.

The scientific interests of all participants were similar, which led to a lively discussion on all the papers, which increased the value of the conference considerably and served to demonstrate some promising research lines. The conference was attended by many young physicists from Novosibirsk and Irkutsk.

The conference was the third one held in Siberia on this topic (the first two were held in Irkutsk). It was accepted as desirable to organize similar conferences regularly in Siberia.

INTERNATIONAL CONFERENCE ON
HORIZONS IN SCIENCE 1976

V. I. Asvrin

This conference was held January 19-22, 1976, in Coral Gables (Florida), which was organized by the Theoretical Research Center at the University of Miami and which dealt with new theoretical approaches in high-energy physics, as well as recent experiments, particularly on neutrinos and colliding electron — positron beams. The following major topics were dealt with in the papers:

1. The quark model for elementary particles: quark symmetry and weak interactions, and quantum chromodynamics; mode of coupling of quarks in particles, infrared singularities, and the unobservability of quarks; and hadron states of quarks coupled into balls. 2. The properties of new resonant states. 3. Research on reactions produced by neutrinos. 4. A gauge scheme for electrochromodynamics. 5. The theory of soliton states. 6. The theory of magnetic charge and the scope for magnetic charge observation by experiment. 7. Hadron interaction at high energies.

A survey by M. Gell-Mann dealt with a possible theory for the strong and weak interactions (quantum chromodynamics). In this scheme, quarks of spin 1/2 can have three different colors and n_f values for another quantum number, to which the name taste has been given, while gluons have spin 1 and belong to color octets. Asymptotic freedom occurs in this theory only if $n_f < 33/2$ and the mass of each quark is sufficiently large.

Vector-type models are the most logical ones in this approach, which are constructed by analogy with electromagnetic interaction and which contain vector and axial interactions of particles differing in mass. The quarks in such models are unobservable and are coupled by some hypothetical infrared mechanism. They have no anomalous divergence. A possible symmetry group for the weak interaction is $G_W = SU_2 \otimes U_1$.

A new heavy lepton E and the corresponding neutrinos are introduced in order to provide a detailed scheme for the weak interactions, and all leptons are grouped into left- and right-handed sets of six:

$$\begin{pmatrix} \nu_e & \nu_\mu & N_E \\ e & \mu & E \end{pmatrix}_L \quad \begin{pmatrix} \nu_e & N_\mu & N_E \\ E & \mu & e \end{pmatrix}_R.$$

Similarly, left- and right-handed quarks are introduced for the strong interactions:

$$\begin{pmatrix} u & c & t \\ d & s & b \end{pmatrix}_L \quad \begin{pmatrix} t & c & u \\ d' & s' & b \end{pmatrix}_R,$$

where c is a quark having the new quantum number charm.

The paper by P. Minkowski showed that the introduction of a right-handed current of the new heavy quarks in this scheme tends to emphasize transitions with $\Delta I = 1/2$ by comparison with ones corresponding to $\Delta I = 3/2$, and the neutrino acquires a small mass as a result of the interaction: $m_{\nu_e} = 1/30$ eV, while $m_{\nu_\mu} = 1/10$ eV. The experimental evidence on lepton transition indicates that neutral currents may exist. Research on radiative transitions between quarks allows one to estimate the quark mass ratio. In particular, $m_c/m_s \approx 16$ for a charmed quark.

S. Glashow pointed out that wave fields may contain additional phases which may result in violation of CP invariance within the framework of this scheme. Also, the scheme contains not merely one Cabibbo angle but several angles of this type. Possible methods of deriving these angles from experiment were pointed out.

J. Pati presented a different approach to particle structure and the description of the weak interaction. The gluons in the model have a nonzero mass, and the quarks are not infrared-coupled. Here in principle it is possible for observable colored quark states to be formed, but these are unlikely. Quarks and protons are not stable in this scheme.

Much interest was aroused by the discussion of the properties in the family of J/ψ resonant states (ψ, ψ', ψ'', χ, P_c, X) as found in various laboratories; M. Oberlach reported the latest data on the mass and width for the highest state ψ'': $M_{\psi''} = (4,414 \pm 0.007)$ GeV, $\Gamma_{\psi''} = (33 \pm 10)$ MeV, and $\Gamma_{el} = (440 \pm 140)$ eV. The paper also presented data on the 3γ decays of ψ and ψ'. 17 instances have been observed of $\psi \rightarrow [X(2.78) \rightarrow 2\gamma]\gamma$ decay. Also, ψ decays in the $p\bar{p}\pi^0$ system have been observed (six cases) and also in the $p\bar{p}\gamma$ system (two cases) on the Stanford linear accelerator.

Gilman's paper contained a detailed survey of the experimental data on the probabilities of the various decays in the group of ψ resonances. The basic conclusion was that all the data correspond to the charm scheme in these states. There is a marked conflict between certain types of ψ decay and the concept of vector dominance. In addition, the paper discussed the search for particles with open charm or new leptons in the 4 GeV region, where sharp structures occur, on which the data are currently being refined.

B. Lee discussed a new interesting experiment on the external proton beam at the Fermi National Accelerator Laboratory in Batavia, in which electron—positron pairs of high mass are produced in pBe collisions. There appears to be a narrow resonance of mass about 6 GeV (11 cases, resolution about 90 MeV, cross-section about $5 \cdot 10^{-36}$ cm^2/nucleon, probability of absence of peak about 2%). Pairs of masses 7, 8, and 10 GeV approximately have also been observed (27 cases in the range 5-10 GeV).

In addition, a ν_μ beam has been used with a bubble chamber in the same laboratory and has revealed four cases of simultaneous production of μ^- along with e^+ and K^0 and hadron systems. The evidence may be explained as due to the production of a D meson, which is a particle with open charm, which then decays to $e^+\bar{\nu}_e$ and K^0. The data and the previous evidence do not conflict with the conclusion that a charmed particle is produced if the probability of decay via the K_s + hadron channel is about 10%, while the mass lies in the range 1.8-2.0 GeV.

A. Mann discussed deep inelastic processes in neutrino and antineutrino beams. The experiments revealed appreciable deviations from the theoretical predictions derived from the elementary particle model in which there are massless free quark-partons. The deviations are called y anomalies and amount to a uniform y distribution of the observed events in an antineutrino beam, which does not correspond with the theoretical prediction of a low probability for values of y around 1. The anomaly makes itself felt in the region of low

values of the transferred momentum, or more precisely low x, where the difference in mass of a heavy quark from zero is important.

The corresponding correction term can be estimated within the framework of the colored-gluon model, as was demonstrated by papers by D. Politzer and A. de Ruhula. In particular, it was found that correction for the nonzero quark mass results in appreciable violation of the self-modeling (or scale) feature of the deep inelastic processes. However, the latter is approximately restored if the scale variable x is replaced by the new variable

$$\xi = x + \frac{m_c^2 - x^2 m_p^2}{2 M E_\nu y}.$$

The condition for restoration of scale invariance gives an estimate for the mass of a charmed quark as $m_c \approx$ 2 GeV.

Therefore, experiments on ψ resonances and neutrino interactions can give very valuable information on elementary particle theory. This gives particular importance to experiments in the various laboratories throughout the world, particularly the Serpukhov accelerator.

One of the sessions at the conference dealt with theoretical and experimental researches on the hypothetical magnetic charge. P. Dirac dealt with the current state of the theory of magnetic monopoles, and also the history of the theory. Magnetic charge arises naturally on account of the symmetry of Maxwell's equations for vacuum with respect to interchange of the magnetic and electric fields, provided that the electromagnetic field is quantized. Introduction of magnetic charge requires the concept of a string joining the charge to an infinitely remote point, where a magnetic charge of opposite sign would lie. However, instead of a mathematical line one requires an extended string of finite thickness in order to avoid singularities in the equations, with the magnetic matter distributed continuously within the string. In that case, a monopole is simply the end of the string. Papers by P. Price and R. Ross surveyed the experimental evidence from searches for magnetic charge, which so far have proved unsuccessful.

Some papers contained results on high-energy hadron interactions, where particular attention was given to schemes compatible with the increase in the total cross sections at infinitely high energies. T. Wu demonstrated that there is class of diagrams within the framework of a certain gauge field theory that corresponds to the contribution of the vacuum singularity, and which on summation defines the path lying above unity for zero momentum transfer. If this path is used in the optical model, one gets the maximum possible increase in the total cross sections.

L. D. Solov'ev reported that data from the Institute of High-Energy Physics on polarization in pp and p$\bar{\text{p}}$ scattering conflict with the Regge poles model, but may have a natural explanation in the rapid (Fruassar) growth model, which provides a good description of the Serpukhov effect and other data on the total and differential cross sections. This indicates the importance of high-energy polarization experiments.

A. Martain discussed a generalization of the limiting-fragmentation theorem to the case of increasing total cross sections; he showed that the set of all physical values for the variable s includes a sequence s_N such that

$$\lim_{N \to \infty} \frac{d\sigma/dt \,(s_N, \, t)}{d\sigma/dt \,(s_N, \, 0)} = f\left(t \, \frac{\sigma_{tot}^2}{\sigma_{el}}\right).$$

The papers presented at this conference in Coral Gables indicate that high-energy physics research is now penetrating into the elementary particles, with research on the internal structures of various particles from a unified viewpoint. The papers will undoubtedly be of considerable interest to physicists, while the new experimental evidence to be expected in the near future from the accelerators at CERN, the Institute of High-Energy Physics, Stanford, and Batavia should play a decisive part in research in this area.

The conference papers will be published as a collected volume.

CONFERENCE ON THE PRODUCTION OF PARTICLES
WITH NEW QUANTUM NUMBERS

A. D. Dolgov

Some major discoveries have recently been made in high-energy physics that indicate that there is a new family of elementary particles; related topics form the center of attention in all major accelerator laboratories throughout the world. Experimental data on new phenomena in elementary-particle physics were discussed at this conference held in Madison (USA) on April 22-24, 1976. The conference was attended by over 200 participants from the USA (the Stanford Linear Accelerator SLAC and the Fermi National Accelerator Laboratory FNAL), from the Federal German Republic (the DESY electron synchrotron), the USSR (The Institute of Theoretical and Experimental Physics and the Institute of High-Energy Physics), and CERN.

The topics discussed at the conference can be divided into four groups: new phenomena in e^+e^- annihilation, photogeneration, hadron reactions, and neutrino reactions. Numerous results were reported at the conference, so we consider only the most important here.

O. Lynch (SLAC) dealt with searches for new narrow (ψ-type) resonances in e^+e^- annihilation; no new peaks in the range 3.5-4 GeV were found, nor at 6 and 7 GeV. These data cast doubt on the existence of the resonance recently observed by Lederman's group at FNAL. More precisely, if this resonance exists and is narrow, the above data would imply that the lepton width Γ_{ee} is less than 100 eV, whereas if it is broad, the ratio Γ_{ee}/Γ_{tot} is less than 10^{-5}. The first value is less by an order of magnitude than the lepton width for analogous mesons of lower mass, while the second would result in particularly large values for the production of the new resonance in hadron reactions.

The same group also presented data on behavior of the cross section in the range 3.8-4.4 GeV. It was asserted that there is a broad resonance with m =4.4 GeV and Γ=40 MeV, and perhaps several (3-5 ?) others. The latter, however, do not exceed two standard deviations. The only definite results is that there is a sharp increase in the cross section from 3.99 to 4.03 GeV. The theoretical interpretation of this stepout is unclear.

G. Goldhaber (SLAC) dealt with the properties of intermediate levels (γ mesons) observed in decay of the ψ(3, 7) meson. A new (fourth) state of mass 3.45 GeV has been discovered in $\psi \rightarrow \psi\gamma\gamma$ decay. The angular distributions in $\psi' \rightarrow \chi\gamma$ decays have been recorded. The first direct measurements on the B$(\psi' \rightarrow \gamma\chi_{3.41})$ = (8 ± 4)% partial width have also been performed. Revised data were also presented on the product of the partial widths B$(\psi' \rightarrow \chi\gamma)$ B$(\chi \rightarrow$ hadrons).

The results from this group cast doubt on the existence of the η(2, 8) resonance. In any case, if it exists, the decay width for pp should be small. From the theoretical viewpoint, it would appear most natural to interpret the new mesons as bound states of charmed quarks, but the new data do not fit completely within that scheme.

In this connection, interest attaches to a statement made in the paper by W. Braunschweig (DESY) that decays of resonances in the region 3.9-4.4 GeV to ψ bosons + hadrons do not exceed 2%.

Photoproduction of ψ was also reported in a paper by O. Anderson (SLAC). The first results were presented on the scattering cross sections for ψ at nucleons in relation to atomic number: $\sigma_{\psi N}$(E =20 GeV) =2.7 ± 0.8 mb, which is close to the value obtained in the vector-dominance model: $\sigma_{\psi N} \simeq 1$ mb. The results undoubtedly show that ψ is a hadron. Another important result is that the rate of increase in the cross section for photoproduction of ψ increases rapidly with energy. The stepout occurs at 12 GeV. This effect is ascribed to the large contribution to the imaginary part of the photoproduction amplitude from the production of pairs of charged mesons of mass 2 GeV. Further, the production of leptons by γ rays has been observed, the cross section showing threshold-type behavior in the energy range from 8 to 20 GeV.

Some papers dealt with the properties of the leptons produced in hadron reactions. The paper by A. Ader presented arguments in favor of the production of these leptons in pairs, which means that the source cannot be weak decays of new particles.

C. McDonald (CERN) reported the discovery of directly produced photons (i.e., ones not due to the decay of known mesons) in pp collisions. These direct photons might explain the production of direct leptons by an ordinary electromagnetic mechanism.

C. Chen (FNAL) discussed the production of 2 and 3 muons in μN reactions. It was asserted that the measured kinematic distributions can be fitted only to the hypothesis of production and subsequent decay of new long-lived mesons.

Much attention in neutrino experiments is given to the properties of neutral currents. Experimental data were reported (L. Schtutte and P. Wanderer, FNAL) that indicate that parity is not conserved in neutral-current interactions.

Elastic ν_p scattering was discovered simultaneously by two groups (G. Williams and P. Sokolsky, Brookhaven National Laboratory accelerator). The measured cross section is in reasonable agreement with the gauge model.

One of the least understood and therefore most interesting effects is the very large (about 4) mean value for the number of K mesons per e^+ event in reactions of $\nu N \rightarrow \mu^- e^+ \ldots$ type (paper by J. von Krogh, FNAL). No theoretical explanation has been found. The analogous reaction produced by antineutrinos $\bar{\nu} N \rightarrow \mu^+ e^- \ldots$ (D. Sinclair, FNAL) did not produce strange particles. The latter experiment was performed by an international group, which involved the participation of the Institute of Theoretical and Experimental Physics and the Institute of High-Energy Physics (USSR).

New data on the known y anomaly were discussed (T. Ling, FNAL). It would seem that the most natural explanation lies also in the production of new particles.

The paper by A. Mukhin (USSR) dealt with the results from a joint experiment of the Institute of Theoretical and Experimental Physics and the Institute of High-Energy Physics, in which muon pairs were observed in a neutrino beam. The preliminary evidence indicates that the effect is quite large.

On the whole, the papers presented at the conference show clearly that there is a new family of heavy long-lived elementary particles. Although these particles have not been observed directly, i.e., as peaks in the invariant-mass spectrum or as tracks in emulsions, the indirect evidence is extremely impressive, and it would seem that in the near future the particles will be recorded directly.

857

SYMPOSIUM ON APPLICATIONS OF ^{252}Cf

I. K. Shvetsov

This international symposium was organized on the initiative of the French Atomic Energy Commission and was held in two stages. The first was held April 22-24, 1976, in Brussels, and dealt with the use of ^{252}Cf in biology and medicine. The second stage concerned the preparation of sources and application in various areas of science and technology, and it was held April 26-28, 1976, in Saclet (France). There were no representatives of the USSR at the first stage, but the summaries indicate that the papers were of considerable practical and scientific interest. The second stage was attended by B. F. Myasoedov, N. D. Tyufyakov, and I. K. Shvetsov from the USSR; in all, there were 51 papers from various countries at the symposium: the USA, France, Britain, the Federal German Republic, etc.

The meetings were held sequentially for the following sections: 1) production of californium and source preparation, 2) uses in the nuclear industry, 3) research uses, 4) neutron radiography, and 5) uses in geology and other areas.

Several papers were read at the plenary session, in which particular attention was devoted to dosimetry and radiation-field measurement for californium sources. D. J. Mevissen (professor at Chicago and Brussels Universities) indicated the good results from using ^{252}Cf in medicine and biology, while R. Morgan (USA) described the californium production program in the USA.

The maximum output of californium could be 5 g/yr, but the production of such amounts has been delayed by the lack of market demand. It is planned to produce 2 g in 1976.

In the first section, californium production was discussed in two papers: L. King (USA) and Yu. Zamyatnin et al. (USSR).

L. King gave data on the accumulation of transplutonium elements, including ^{257}Fm, in the Oak Ridge TPU system from 1967 to 1976. The total amounts, for instance, of ^{244}Cm and ^{252}Cf constitute 1745 and 2678 mg, respectively.

The scheme presented for isolating and purifying the transplutonium elements involved using D2EGFA and CAO as extractants, with ion exchange at the refinement stage. The performance was improved by the use of a chloride medium.

Zamyatnin et al. considered irradiation conditions for initial material in the SM-2 reactor, with emphasis of the accumulation of californium. A major difference of the isolation scheme from that used at Oak Ridge was the use of nitric acid solutions at all stages. The amount of californium produced is reckoned in tens of mg.

Subsequent papers dealt with preparation of californium sources: A. Bologne et al. (USA), V. Zinkovskii et al. (USSR), and I. Shvetsov et al. (USSR).

Californium sources for various purposes are made in the main by the following methods (A. Bologne):

1. For medical purposes, from wire consisting of a cermet of palladium with Cf_2O_3, which is enclosed in a platinum — irridium sheath of final diameter 0.3 mm. The wire is cut into pieces of the required size, which are encapsulated in a double sheath;

2. For geology and physics research, from Cf_2O_3 as tablets enclosed in platinum or stainless-steel sheaths. If platinum is used, the sealing is provided by soldering with gold. Zinkovskii et al. (USSR) and I. K. Shvetsov et al. (USSR) propose to make neutron sources by sorbing californium on a porous material, which is subsequently encapsulated.

Since 1968, the laboratory at Savanna River has made about 3000 neutron sources for various purposes, for which about 750 mg of ^{252}Cf was used. Techniques for producing californium sources for industrial purposes are currently being developed, which involve the use of wire containing 2, 20, or 200 μg of californium per cm.

A. Bologne stated that five automatic loading systems for patient treatment have now been built in various countries.

Several papers dealt with the resistance of californium sources to shock loads, vibration, changes in pressure and temperature, etc.

N. D. Tyufyakov (USSR) and S. A. Prescott (USA) described neutron multipliers based on californium giving thermal neutron fluxes of (2-3) $\cdot 10^8$ neutrons/cm^2 $\cdot$ sec. Prescott indicated that such multipliers have been made for sale.

The papers concerned with californium in the nuclear industry presented results on uses at all stages in the fuel cycle, including prospecting for uranium, dressing, fuel production, and processing of irradiated fuel. Appropriate analytical schemes have been developed, for instance, in the USA, and it is stated that the discrepancies on the amount of fissile material in a fuel as found by the supplier and the user constitute only 0.12% or less.

Most of the papers at the third section dealt with californium sources used in instruction: teaching students how to handle such sources and discussion of results.

The papers on neutron radiography indicated that californium sources are of value in nondestructive testing and that researches in this area should be extended.

Workers from the USA presented a paper on neutron radiography applied in aircraft engineering. The test equipment can be used in two styles: as a stationary system or transportable on vehicles. The equipment contains a californium source of up to 10 mg, which has been used in monitoring turbine blades, fuel tanks, and so on.

L. Bennett (Canada) gave a description of a transportable equipment for neutron radiography containing a californium source of up to 2 mg. The tests were performed with a source of 1 mg of californium placed in a remote-controlled head.

Other papers presented at this section related to the determination of interfaces between liquid and solid phases with californium sources, detection of the boundaries of petroleum-bearing beds, and analysis of geological specimens via (n, γ) reactions. In the cases, the sources contained from 1-2 up to 15 μg of ^{252}Cf.

Most of the papers at the fifth section dealt with the use of californium sources for activation analysis, as in the analysis of ores, steel, cement, and coal. Many papers on this topic were presented by workers from France and the USA.

At the end of the symposium, there were visits to the Medical Neutron Source Preparation Laboratory at Fontenay-aux-Roses, the Triton reactor, and external-beam neutron — radiography systems.

SEMINAR ON COMPUTER SIMULATION OF
RADIATION-INDUCED AND OTHER DEFECTS

Yu. V. Trushin

The first seminar on computer simulation of defects was held at Kalinin Polytechnic Institute in Leningrad, March 16-17, 1976; it served to familiarize the participants with major studies in this area. Over 50 participants represented 25 research institutes and higher teaching institutions from 18 cities in the USSR.

The seminar opened with a survey paper on problems in the simulation of radiation damage in crystals (V. V. Kirsanov, Institute of Nuclear Physics, Academy of Sciences of the Kazakh SSR). We give below brief summaries of representative papers.

The Institute of Technical Physics, Academy of Sciences of the Ukrainian SSR, has calculated spectra for the primary ejected atoms produced by neutrons, protons, γ rays, and ions. The results are based on elastic and inelastic nuclear models: the optical model and the intermediate-state one (V. A. Yamnitskii).

The Nuclear Physics Research Institute at Tomsk Polytechnic Institute has considered the effects of primary electron channeling in a pair-collision model, and also the channeling of positrons, protons, and other particles, which affects the distribution of the radiation parameters and the spectra of the radiation-induced defects. The calculations for electrons in Si have been confirmed by experiment (S. A. Vorob'ev).

At Kalinin Polytechnic Institute, Monte Carlo calculations have been performed on the energy and angular distribution for electrons transmitted or backscattered by a metal plate. The distance given by the successive-collision model for the depth for the maximum absorbed energy is less by an order of magnitude than that found from the curve calculated by the enlarged-collision method (A. I. Mel'ker). .

Leningrad Polytechnic Institute has also devised a method of simulating the radiation damage produced by neutrons and high-energy protons by means of electron accelerators. The simulation consists in irradiating the components with γ rays of minimum energy above 20 MeV. This method of simulation has been confirmed by experiment by comparing the effects of protons and high-energy γ rays on the characteristics of silicon (B. F. Kosmach).

V. G. Chudinov (Institute of Metal Physics, Urals Scientific Center, Academy of Sciences of the USSR) has calculated the diffusion of heat energy from a cascade region in the continuum approximation for metals and insulators; it was found that melting begins at a temperature around half the melting point in a metal, with the production of a vacancy loop. This results in stepwise change in various physical properties. In the case of insulators, melting occurs in most of the tracks even at zero temperature.

The Kurchatov Institute of Atomic Energy has written programs and performed researches on simulation of the production and annealing of defects in cascades, with calculations on the spectra of primary ejected atoms under neutron irradiation, and also has simulated some radiation-induced creep mechanisms (Yu. R. Kevorkyan).

É. Ya. Mikhlin (Power Physics Institute) and V. V. Nelaev (Institute of Nuclear Power, Academy of Sciences of the Belorussian SSR) have performed model calculations on the recombination zone for Frenkel pairs in α-Fe with or without hydrostatic compression. Compression (strain $\varepsilon = 10^{-3}$) increases the recombination zone by about a factor 3. This means that: 1) There exist types of strain that can accelerate the recombination rate, and 2) these may include ones that provide an increase more than reported above.

The Institute of Applied Mechanics, Academy of Sciences of the Ukrainian SSR, has written a program to handle dynamic aspects of atomic collisions, derived the minimum in the potential energy, and determined the equilibrium configurations of defects (vacancies, interstitial atoms, complexes), as well as the energy

characteristics in simulation of radiation damage in binary crystals of metallic alloy type, and also inter-metallides and interstitial phases. Three pair-interaction potentials were used: $A - A$, $A - B$, and $B - B$. Studies have been made of the effects of size and mass difference between the A and B atoms on the propagation of focusons and crowdions, as well as on relaxation processes, which is particularly important for interstitial phases (V. V. Ogorovnikov).

The Institute of Physics, Academy of Sciences of the Georgian SSR, has calculated the total scattering cross section for cold neutrons at vacancies and surrounding displaced atoms in relation to neutron wavelength λ in the range from 2 to 12 Å (V. L. Svetlik).

Other papers dealt with simulation results for various defects.

The Institute of Metal Physics, Urals Scientific Center, Academy of Sciences of the USSR, has written ALGOL programs for the BESM-6 to calculate the energy and geometrical characteristics of point defects in metals. It is possible to incorporate thermal vibration. A single potential can be used to derive the energy of formation for vacancies in copper $E_v^F = 0.978$ eV, the migration energy $E_v^m = 1.005$ eV, the divacancy binding energy $E_B = 0.3$ eV, and the energy of formation of a Frenkel pair $E_F = 4.2$ eV. The temperature dependence of E_v^F has been derived over the range 0–400°K (I. E. Podchinenov).

The Institute of Solid-State Physics, Academy of Sciences of the USSR, has simulated the thermally activated motion of dislocations interacting with randomly disposed obstacles. Models for simple dislocation complexes have also been discussed (S. I. Zaitsev).

The Institute of Nuclear Physics, Academy of Sciences of the Kazakh SSR, has developed two computer models for simulating dislocation glide in response to stress on the basis of opposition from defects of various extents and sizes (V. V. Kirsanov).

The Institute of Technical Physics, Academy of Sciences of the Ukrainian SSR, has examined simulation of coherent twin boundaries, incoherent twin boundaries (i.e., ones containing screw twin dislocations), and complete screw dislocations in bcc crystals. Results have been obtained for the state of stress, energies of atoms at boundaries, energies near dislocation cores, and the sizes, energies, and structures of cores in twinning dislocations. It is found that the complex spatial splitting of the core characteristic of complete screw dislocations is absent (V. S. Boiko).

The Institute of Metal Physics, Urals Scientific Center, Academy of Sciences of the USSR, has examined a lattice-gas model to determine the structure, width, free surface energy, and mobility for interphase boundaries of (111) and (100) orientation in fcc crystals in relation to temperature and the driving force of the phase transition. Crystal growth mechanisms and kinetics have been considered for a one-component two-phase system. It has been found on examining the equilibrium, in particular, that the width of the interphase boundary in an fcc metal crystal in contact with its own melt is 4-5 times the interatomic distance, whereas a crystal — vapor interphase boundary is atomically sharp (V. O. Esin).

The Physics and Mathemetics Section, Bashkir Branch, Academy of Sciences of the USSR, has calculated the atomic configuration in a wedge dislocation-type microcrack in a bcc crystal having an overall Burgers vector equal to twice the lattice parameter. It has been found that the separation in the crack exceeds the radius of action of the interatomic forces, so the crack surface can be considered as a free one (Sh. Kh. Khannanov).

Other discussions at the seminar concerned exchange of programs and other information, as well as topics for future meetings. The next ones will be held in June 1976 and in January-February 1977 in Leningrad.

861

SCIENTIFIC AND TECHNICAL EXCHANGE

VISIT OF AN ERDA DELEGATION TO THE USSR

E. F. Arifmetchikov

This delegation from the Energy Research and Development Agency visited the USSR from May 22 to June 5, 1976 and was headed by the Deputy Director Richard W. Roberts. The delegation was welcomed by the President of the Soviet Section of the Soviet — American Joint Commission on Collaboration in the Peaceful Use of Atomic Energy, A. M. Petros'yants, who is also the President of the State Commission on Atomic Energy of the USSR, the Minister of Power Plant Construction of the USSR, V. V. Krotov, and the Deputy Minister for Power and Electrification of the USSR, N. D. Mal'tsev. The delegation visited the Kurchatov Institute of Atomic Energy, the Power-Physics Institute in Obninsk, the Lenin Nuclear-Reactor Research Institute in Dmitrovgrad, the Leningrad, Novyy Voronezh, and Beloyarsk Nuclear Power Stations, the Power Station with the BN-350 reactor at the city of Shevchenko, and the Izhor plant in Leningrad. The American workers were interested in the organization and coordination of research on nuclear power in the USSR, the safety supervision system for nuclear power-plant operation, the proportion of nuclear power in the future energy balance of the country, and researches in the USSR on the use of natural energy sources (geothermal, solar, wind, tides, etc.). In turn, Dr. Roberts acquainted Soviet workers with some of the ERDA plans on the development of nuclear power in the USA. It is proposed that the ERDA budget in 1977 should be 7 billion dollars (at present 4 billion dollars), with half intended for research. The short-term plans of ERDA are designed to increase the extraction of coal (from 600 million tons to 1 billion tons in 1985) and to develop nuclear power. The oil output will remain at the previous level in this period. The long-term ERDA plans (after the year 2000) involve the use of fast reactors in nuclear power stations, together with solar and thermonuclear energy. ERDA has drawn up a program terminating in 1982-1983 for estimating the reserves of uranium in the USA, for which purpose 40-50 million dollars has been set aside, and also a program of research on fuel cycles, nuclear-fuel reprocessing, and radioactive-waste storage. The last will be assigned 60 million dollars in the coming year. There will also be a considerable increase in the budget for research on utilization of solar energy. While about 13 million dollars have been spent so far for this purpose, it is proposed that 150-200 million dollars should be spent in 1977-1978. The program for developing fast reactors has been altered and more closely defined. When the Clinch fast reactor is commissioned in 1983, a 3-yr checkout period will be employed instead of the 5-yr one previously proposed. In 1986, a large prototype (precommercial) breeder reactor will be commissioned, and 3 years later the first commercial fast reactor (one of a continuing series). However, up to 1995, fast reactors will not play any considerable part in the energy supplies of the USA. It was pointed out that the main problem in nuclear power in the USA at the present time (in particular, programs for building fast reactors) are not ones of engineering but of public opinion on the topic.

BOOK REVIEWS

Yu. A. Egorov, V. P. Mashkovich, Yu. V. Pankrat'ev,

A. P. Suvorov, and S. G. Tsipin

RADIATION SAFETY AND NUCLEAR POWER STATION SHIELDING*

Reviewed by N. G. Gusev

Between 1963 and 1974, Atomizdat produced six issues under the name Physics of Reactor Shielding. These contained mainly papers on theoretical and experimental researches on shielding from penetrating and neutron radiations from nuclear reactors.

The new series is of narrower coverage in that particular attention is given to radiation safety and shielding from penetrating radiations in nuclear power stations.

The book consists of five sections. It contains original papers relating mainly to theoretical and experimental researches on shielding from penetrating radiations, with only one section containing papers on radiation safety in nuclear power stations.

Much of the space is given to papers read at the 1st All-Union Conference on Ionizing-Radiation Shielding in Nuclear —Engineering Systems, which was held in Moscow in December 1974.

The first section deals with the theory of radiation transmission and methods of shielding calculation: The radiation-transport equation is solved, with estimation of the accuracy of the solutions, and also a description of the computation program.

The second section deals with measurements on shielding, shielding constants, and transmission of radiation by inhomogeneous media.

The third section deals with some aspects of radiation safety and shielding at the Lenin Nuclear Power Station in Leningrad and at the Novyy Voronezh Nuclear Power Station, and also for power stations with fast-neutron gas-cooled reactors. The detailed studies performed directly at nuclear power stations are of particular value.

The fourth section deals with testing of shielding materials, including measurement of gas release from some shielding materials under irradiation, and also criteria for the radiation stability of concretes.

The fifth section deals with spectrometric and dosimetric methods of examining radiation sources and radiation fields. Unfortunately, the topic of radiation safety in nuclear power stations is dealt with inadequately in this volume.

It would be desirable in future issues to combine the traditional type of paper on shielding from penetrating radiation with papers on aspects such as the radiation characteristics of sources (particularly coolant systems), the discrepancies between design and actual characteristics, the time course of all features of the radiation environment at a nuclear power station and in the surroundings, reliability aspects of equipment and systems, equipment repair, internal and external radiation doses (individual, group, and population), standards for radioactive wastes from nuclear power stations (gases, aerosols, liquids, and solids), the extent and scope of radiation monitoring, engineering safety at nuclear power stations (including emergency control systems), choice of power-station sites, and environmental protection in relation to nuclear-power stations as a whole.

*Issue 1, Atomizdat, Moscow (1975), 2 rubles 28 kopecks.

Also, more use should be made of the experience of practical workers in the fields of radiation safety and dosimetry at nuclear power stations.

This new series will arouse considerable interest in those concerned with the design of shielding and with the technological and social aspects of radiation safety at nuclear power stations. It is also of consider-able interest to students and graduates in the corresponding areas and to engineers at nuclear power stations.

V. T. Tustanovskii

ACCURACY AND SENSITIVITY ESTIMATION

IN ACTIVATION ANALYSIS

Reviewed by E. M. Filippov

Activation analysis is increasingly being applied, so this book should prove of considerable value.

The volume consists of 15 chapters, five appendices, and a literature list.

Chapters 1-4 deal with the definition of various terms in analysis and with error sources, the distributions of measurement results, random errors in analysis, and the statistical and overall errors in results.

Chapters 6-10 deal with statistical evaluation (confidence estimates) for analysis results, systematic errors, errors arising from signal loss, errors due to radiation monitor drift, and errors due to equipment instability generally.

Chapters 11-15 deal with the effects of irradiation geometry and specimen measurement geometry, accuracy comparisons for activation analysis and other methods, methods of checking measuring equipment, means of calculating working conditions providing minimum analysis error, and sensitivity estimations for activation analysis.

Throughout the book there are practical examples of error and sensitivity estimation for activation — analysis methods.

The general composition of the book is not entirely satisfactory. The volumes of some chapters scarcely exceed small paragraphs. Some of these could have been denoted simply as paragraphs, but the fault is not fundamental.

In general, the book is written at a high scientific level and should be useful to a wide range of scientists concerned with nuclear methods of analysis for various materials.

G. Hammel and D. Okrent

REACTIVITY COEFFICIENTS IN LARGE

FAST-NEUTRON POWER REACTORS (USA, 1970)*

Reviewed by G. M. Pshakin

This book presents an all-round discussion of reactivity effects occurring in large fast power reactors, and also of problems arising in determining such effects during design stages, in addition to the influence of such effects on reactor behavior in emergency situations and transient states.

Chapters 1-3 give nuclear data and computational methods used in calculating reactivity effects. The information on the nuclear data is presented in general form, since the latter become out of date fairly rapidly. The discussions on the uncertainty in the constants, although fairly condensed, give a clear conception of the effects on the calculated reactivities.

Fairly detailed descriptions are given of methods of fitting nonresonant group cross sections for light and heavy elements, and also methods of processing resonant cross sections for heavy elements with allowance for resonance overlap in homogeneous and heterogeneous media, with emphasis on the group approximation.

Chapters 4-6 deal with the sodium and Doppler effects, as well as the effects of displacement of reactor materials. Detailed analyses are presented for the physical processes that cause these effects, and also the relationship to various factors such as neutron spectrum, temperature, core volume, isotope composition, and so on.

Heat transfer and mechanical displacement of elements in the core in response to temperature are considered for transient states; this section contains a large volume of theoretical and experimental evidence, particularly on the sodium cavity effect, but the accuracy of the calculations, in particular on the Doppler effect, has not been evaluated via the measurements on the SEFOR reactor, which at the present time provides the best means of testing methods of calculating the Doppler effect for fast reactors.

Chapters 7-9 deal with the behavior of a fast reactor in transient and emergency states; stability is discussed in relation to negative feedback, which is well illustrated by experimental evidence obtained with the EBR and Rhapsodie reactors.

Chapter 8 deals with prompt-neutron supercritical hazards. The basic characteristics of power surges are derived from simple feedback models. The Bethe — Tait analytical method is discussed, which is used in describing reactor explosions, and a study is made of the role of the Doppler effect in the development of the explosion.

Chapter 9 deals with possible emergency situations that may result in excess reactivity.

The book deals largely with sodium-cooled fast reactors, and only the ninth chapter presents some general arguments on reactivity effects in relation to safety in fast reactors with other coolants.

On the whole, the book gives a full and all-round overview of reactivity effects that occur in fast power reactors. A large volume of theoretical and experimental evidence is presented on the errors in assessing these effects. The brevity in certain sections is compensated by the extensive bibliography (438 entries).

The book is of undoubted interest to reactor physicists and engineers concerned with the design of fast reactors, and also to students specializing in this area.

---

*Translated from English, Atomizdat, Moscow (1975), 2 rubles 95 kopecks.

engineering science

continued from back cover

Title	# of Issues	Subscription Price
Metallurgist *Metallurg*	12	$225.00
Metal Science and Heat Treatment *Metallovedenie i termicheskaya obrabotka metallov*	12	$215.00
Polymer Mechanics *Mekhanika polimerov*	6	$195.00
Problems of Information Transmission *Problemy peredachi informatsii*	4	$175.00
Programming and Computer Software *Programmirovanie*	6	$95.00
Protection of Metals *Zashchita metallov*	6	$195.00
Radiophysics and Quantum Electronics (Formerly Soviet Radiophysics) *Izvestiya VUZ. radiofizika*	12	$225.00
Refractories *Ogneupory*	12	$195.00
Soil Mechanics and Foundation Engineering *Osnovaniya; fundamenty i mekhanika gruntov*	6	$195.00
Soviet Applied Mechanics *Prikladnaya mekhanika*	12	$225.00
Soviet Atomic Energy *Atomnaya energiya*	12 (2 vols./yr. 6 issues ea.)	$235.00
Soviet Journal of Glass Physics and Chemistry *Fizika i khimiya stekla*	6	$ 95.00
Soviet Journal of Nondestructive Testing (Formerly Defectoscopy) *Defektoskopiya*	6	$225.00
Soviet Materials Science *Fiziko-khimicheskaya mekhanika materialov*	6	$195.00
Soviet Microelectronics *Mikroélektronika*	6	$135.00
Soviet Mining Science *Fiziko-tekhnicheskie problemy razrabotki poleznykh iskopaemykh*	6	$225.00
Soviet Powder Metallurgy and Metal Ceramics *Poroshkovaya metallurgiya*	12	$245.00
Strength of Materials *Problemy prochnosti*	12	$295.00
Theoretical Foundations of Chemical Engineering *Teoreticheskie osnovy khimicheskoi tekhnologii*	6	$195.00
Water Resources *Vodnye Resursy*	6	$190.00

SEND FOR YOUR FREE EXAMINATION COPIES

Back volumes are available. For further information, please contact the Publishers.

breaking the language barrier

WITH COVER-TO-COVER
ENGLISH TRANSLATIONS
OF SOVIET JOURNALS

in
engineering
science

SEND FOR YOUR
FREE EXAMINATION COPIES

Back volumes are available.
For further information,
please contact the Publishers.

Title	# of Issues	Subscription Price
Automation and Remote Control *Avtomatika i telemekhanika*	24	$260.00
Biomedical Engineering *Meditsinskaya tekhnika*	6	$195.00
Chemical and Petroleum Engineering *Khimicheskoe i neftyanoe mashinostroenie*	12	$275.00
Chemistry and Technology of Fuels and Oils *Khimiya i tekhnologiya topliv i masel*	12	$275.00
Combustion, Explosion, and Shock Waves *Fizika goreniya i vzryva*	6	$195.00
Cosmic Research (Formerly Artificial Earth Satellites) *Kosmicheskie issledovaniya*	6	$215.00
Cybernetics *Kibernetika*	6	$195.00
Doklady Chemical Technology *Doklady Akademii Nauk SSSR*	2	$65.00
Fibre Chemistry *Khimicheskie volokna*	6	$175.00
Fluid Dynamics *Izvestiya Akademii Nauk SSSR mekhanika zhidkosti i gaza*	6	$225.00
Functional Analysis and Its Applications *Funktsional'nyi analiz i ego prilozheniya*	4	$150.00
Glass and Ceramics *Steklo i keramika*	12	$245.00
High Temperature *Teplofizika vysokikh temperatur*	6	$195.00
Industrial Laboratory *Zavodskaya laboratoriya*	12	$215.00
Inorganic Materials *Izvestiya Akademii Nauk SSSR, Seriya neorganicheskie materialy*	12	$275.00
Instruments and Experimental Techniques *Pribory i tekhnika éksperimenta*	12	$265.00
Journal of Applied Mechanics and Technical Physics *Zhurnal prikladnoi mekhaniki i tekhnicheskoi fiziki*	6	$225.00
Journal of Engineering Physics *Inzhenerno-fizicheskii zhurnal*	12 (2 vols./yr. 6 issues ea.)	$225.00
Magnetohydrodynamics *Magnitnaya gidrodinamika*	4	$175.00
Measurement Techniques *Izmeritel'naya tekhnika*	12	$195.00